Design of a High-Pressure CO_2 Reduction Reactor System

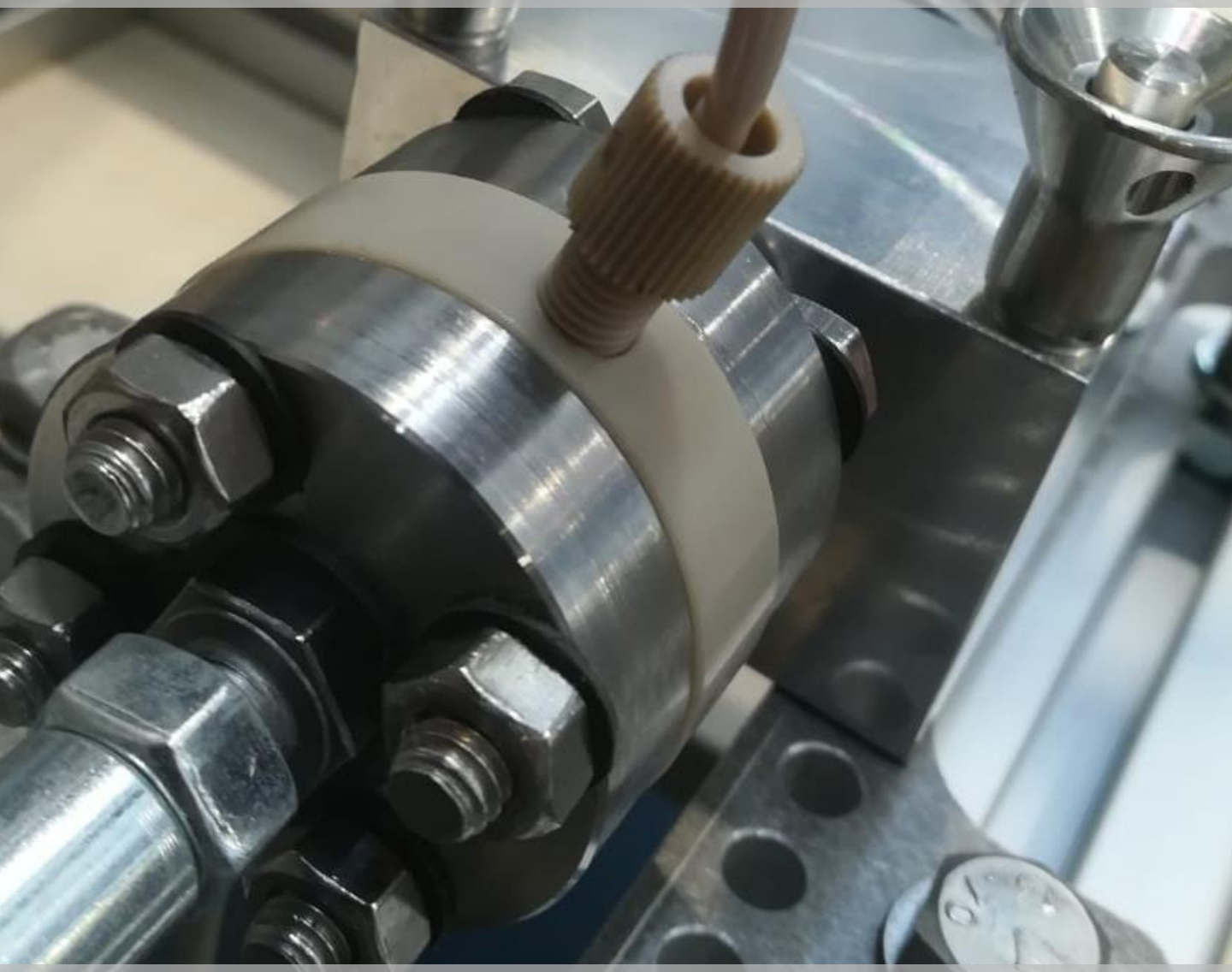

Q. C. G. Wols

TU Delft

Design of a High-Pressure CO_2 Reduction Reactor System

by

Q.C.G. Wols

to obtain the degree of Master of Science
at the Delft University of Technology,
to be defended publicly on Tuesday September 22, 2020 at 9:00 AM.

Student number:	4219112	
Thesis committee:	Prof. dr. ir. W. de Jong,	TU Delft
	Dr. R. Kortlever,	TU Delft, supervisor
	Dr. T. E. Burdyny,	TU Delft
	Dr. A. Morrison,	TU Delft, supervisor

An electronic version of this thesis is available at http://repository.tudelft.nl/.

TU Delft

Abstract

In the last decade, many initiatives have been undertaken by governments, companies and other institutions to reduce the output and concentration of CO_2 in the atmosphere. The current non-emitting energy sources with highest potential are solar and wind energy. Unfortunately, these energy sources vary in power production, while the demand fluctuates far less. Hence, a solution is needed for crossing the times when there is a mismatch in energy supply and demand. One potential solution is to store excess energy in chemical bonds by using electrochemical CO_2 reduction.

In this thesis, a CO_2 reduction reactor system has been designed that can facilitate new research on CO_2 reduction. The design is based on an extensive literature study on existing reactor designs. With this study, important design parameters have been identified. It was concluded that an important feature of this new reactor should be the ability to perform high pressure experiments with recycled electrolyte. As the electrolyte can be corrosive in some configurations, the reactor should be resistant to these chemicals. To maximize the utilisation of the system, it needs to be easily adaptable, and it should be possible to assemble and disassemble the system fast.

After proposing the design based on these design parameters, calculations have been performed to confirm that it does not yield under the desired operation conditions. After this confirmation, the design has been build. The built reactor was reviewed based on the design parameters and its ability to produce a CO_2 reduction product. It has been confirmed that indeed, the CO_2 reduction reactor system was successful in reducing CO_2. To fully maximize the potential of the design, it is advised to further expand it with components able to efficiently fill and drain the system with electrolyte.

Contents

1

Introduction

CO_2 is a green house gas emitted by several industrial processes, including burning fossil fuels. Last few years the concentration of this gas in the atmosphere has increased. This increase in concentration allows the atmosphere to hold on to more heat, which can, in turn, increase the planet his mean temperature [1]. Unfortunately, this warmer climate can have negative effects on biodiversity and habitable areas for life on earth [2]. That is why there are many initiatives from governments, companies and other institutions to reduce the output and the concentration of CO_2 in the atmosphere. The main measure is to increase taxes on emitting processes and subsidize non-emitting sources of energy [3], to promote the use of green-energy alternatives.

The current non-emitting energy sources with highest potential are solar and wind energy [4]. The costs of these energy sources are dropping steadily. Moreover, new technologies and materials concerning solar and wind energy are under development, which could one day make these energy sources competitive alternatives compared to fossil fuels, as can bee seen in Figure 1.1. However, at this moment, this not yet the case.

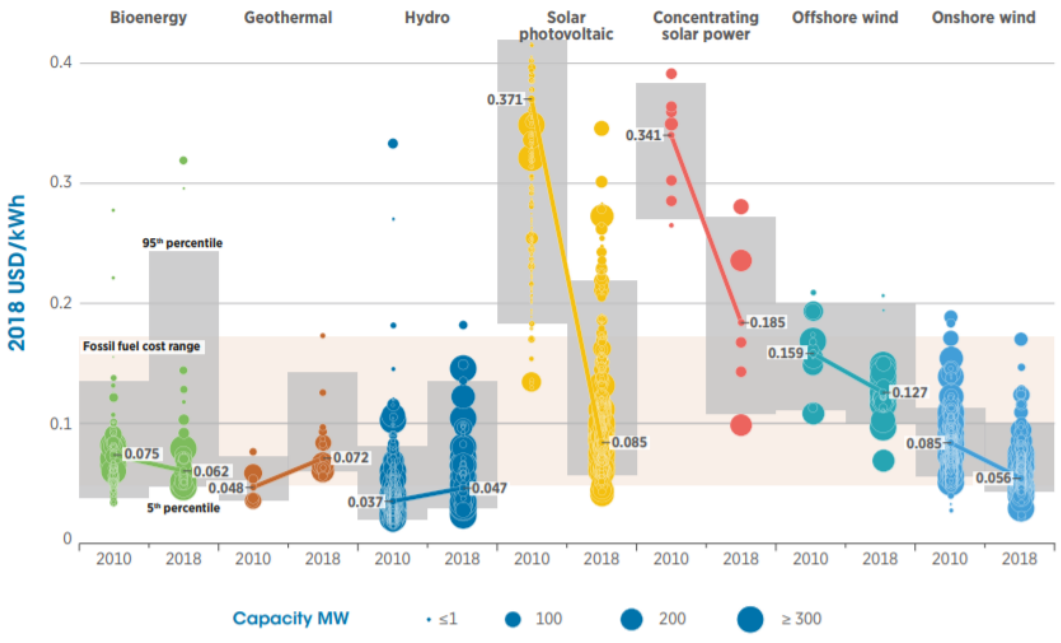

Figure 1.1: Global LCOE of utility-scale renewable power generation technologies, 2010–2018 [5]. The costs per kWh are displayed with the capacity of multiple individual sources in the years 2010 and 2018

The disadvantage of using solar and wind energy, is that these energy sources vary in power production, while the demand fluctuates far less [6] [7]. This means that there are solutions needed for crossing the times when there is a mismatch in energy supply and demand.

Power to gas could potentially provide a solution to this problem. In power to gas systems the surplus in energy during production spikes is stored in the form of chemical bonds. This can be in the form of simple molecules, such as methane, or in more complex molecules, such as ethane or propane [8]. And by using CO_2 as feed, this solution could solve two problems at once: both the high concentration of CO_2 in the atmosphere can be decreased, and the need for energy storage would be solved (see Figure 1.2).

The conversion of CO_2 for power to gas purposes is not trivial: CO_2 is a fully oxidized and thermodynamically stable molecule, so it is not likely to react at ambient conditions. Thermochemical, photochemical and electrochemical methods have been explored for CO_2 conversion [9]:

- **Thermochemical conversion**
  Thermochemical conversion requires high reaction temperatures, high pressures and hydrogen as the reducing agent. This is energetically problematic for implementation in large scale applications.
- **Photochemical conversion**
  Only a few systems have been reported to be photocatalytically active for CO_2 reduction, while the selectivity and production rate of these systems are far too low to be economically viable [9].
- **Electrochemical conversion**
  With electrochemistry, CO_2 can be converted into higher order carbon molecules. The conversion of CO2 into higher order carbon molecules reduces the emission of CO2 and creates a potential valuable products that can be used by the industry or consumers. However, this has not been demonstrated on a large scale [10].

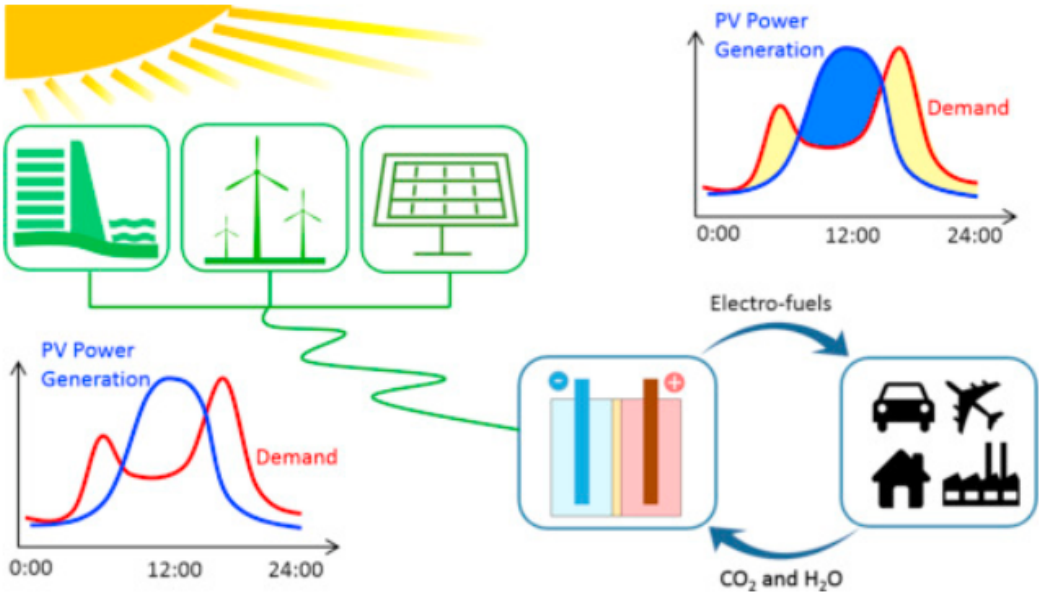

Figure 1.2: An overall schematic of electro-fuel enabled energy storage to migrate the mismatch between renewable energy generation (photovoltaic as an example) and energy demand [9]

Electrochemical conversion of CO_2 has several advantages: the reaction rate can be controlled by the applied current, it has wide scalability due to modular electrolyzer design and it has excellent coupling to intermittent renewable energy sources due to the fast response time of electrochemical systems [11]. These factors can make the technology easily scaled up in production, and have a flexible power consumption and production per unit. This is an advantage when the power source is varying [12].

For electrochemical experiments, there are a lot of different configurations possible in terms of material of electrodes and electrolyte used during CO2 reduction reactions. Each of these combinations have their own reaction characteristics. Moreover, the conditions in the reactor can also change the characteristics of the reaction. Multiple solutions have been worked on to produce certain kinds of chemicals that are suppressed by a mass transfer-limit caused by a low concentration of CO_2 in the electrolyte. High pressure is a solution that does not have plenty of work on it [13].

Because there are so many combinations and conditions yet to be tried, much is still unknown about the potential of applying electrochemistry in the reduction of CO_2. Additional Experiments at elevated pressures and at higher current densities are still needed for the full picture. Higher pressures and current densities could ,in turn, be beneficial for the financial feasibility of this type of reactor [14]

To explore this field of science, many experiments must be done to map all the variables of these reactions. However, experimenting with high pressure fluids is no easy task, and the reactors that are currently in use have complex designs and many components. A new reactor system that allows researchers to conduct experiments faster and safely is therefore essential.

The goal of this thesis is to design an easily adaptable reactor, which can provide a systematic approach for testing different electrode and electrolyte combinations. Before designing the reactor, an extensive literature study is carried out to see what is important for the design and look at the present reactors designs for additional parameters. The design parameters will be based on this study, which is provided in chapter 2. In chapter 3, these design parameters are further discussed, after which the design is presented in chapter 4. Finally, experimental work performed with the reactor in is presented chapter 5, followed by the Results and Discussion of the experiments in chapter 6. The report ends with the important conclusions and possible opportunities for further research.

2

Literature Review

In this chapter, the literature on CO_2 reduction is reviewed to gain insight in important design parameters for the reactor system. It is necessary to review CO_2 reduction experiments, electrolysis reactors, high pressure fluid properties, identification methods, electrolysis mechanics and safety measures, in order to design an elevated pressure CO_2 reduction reaction reactor system.

2.1. Electrochemical CO_2 reduction reaction

When designing a reactor, it is important to know what reaction(s) must take place and how to influence the process in the reactor. In a typical CO_2 electrolyzer, water is oxidized to molecular oxygen and protons at the anode, whereas CO_2 is reduced at the cathode. The reaction is an electrochemical process that can lead to a wide range of CO_2-derived products. The redox potentials of the reaction pathways of these different CO_2-derived products are similar, which makes the selective production of desired chemicals challenging. An overview of different reaction pathways with their products and standard potentials is provided in table 2.1.

Table 2.1: Formal Potentials (E^0) Associated with the Electrochemical CO_2 reduction reactions and Oxygen Evolution Reaction referenced against a reversible hydrogen electrode [15]

Electrode	Reaction	E^0
Cathode	$CO_2 + 2H^+ + 2e^- \rightarrow CO + H_2O$	-0,106
	$CO_2 + 2H^+ + 2e^- \rightarrow HCOOH$	-0,250
	$CO_2 + 4H^+ + 4e^- \rightarrow HCOH + H_2O$	-0,070
	$CO_2 + 6H^+ + 6e^- \rightarrow CH_3OH + H_2O$	0,016
	$CO_2 + 8H^+ + 8e^- \rightarrow CH_4 + 2H_2O$	0,169
	$CO_2 + 8H^+ + 12e^- \rightarrow C_2H_4 + 2H_2O$	0,064
	$2H^+ + 2e^- \rightarrow H_2$	0,000
Anode	$2H_2O - 4e^- \rightarrow O_2 + 4H^+$	1,230

The situation becomes even more difficult in an aqueous CO_2 electrolyzer, due to the severe side reactions of hydrogen evolution occurring at a similar potential as the desired reaction(s). These unwanted side reaction can make the technology economically invalid [16]. This competition can be avoided by using electrodes that require high over-potentials and increasing the molar fraction of carbon dioxide in the mixture [17].

High over potentials usually mean high inefficiencies, including broad product distributions at the cathode, competitive hydrogen evolution reaction from proton reduction and reduced efficiencies (equation 2.1). To achieve a reactor with high faradeic efficiency, an optimal ratio must be found between these losses and the production rate by combining the right electrode with corresponding over potential [15].

$$FE = \frac{Moles_{produced}}{Moles_{theoretical}} = \frac{Moles_{produced}}{\frac{I*t}{N_{electrons}*F}} \tag{2.1}$$

FE is the faradeic efficiency, I is the current, t is the time in seconds and F is the Faraday constant.

2.1.1. Mass transport of CO_2

The transport of CO_2 molecules to the electrode surface is essential for a CO_2 reduction reaction [17]. In figure 2.1, a model is shown of CO_2 transport in a CO_2 reduction reaction. It can be seen that multiple factors play a role in CO_2 transport [18]:

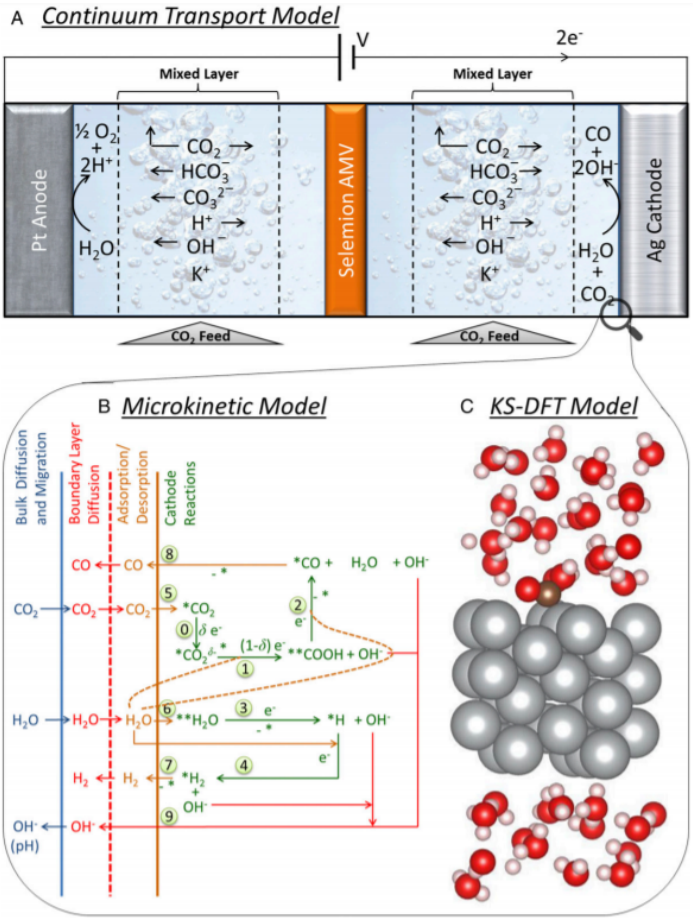

Figure 2.1: Model for species transport and reaction in a 1D electrochemical cell for CO_2 reduction [18].

- **Convection** is depended on flow velocity and patterns.
- **Bulk and Boundary layer Diffusion** Dependent on the temperature and the change in concentration of CO_2. The change in concentration is due to the consumption of CO_2 in the reaction, which makes the concentration near the electrode lower. This is according to Fick's first law and the Stokes–Einstein equation. These are displayed in equation 2.2 and 2.3.
- **Adsorption** relies on the temperature, gas, liquid or dissolved solid to a surface and the concentration of the substance. The Langmuir equation gives the relation between concentration of the substance and the fractional occupancy of the adsorption sites. The rate constants are dependent on the gas, liquid or dissolved solid to a surface and the temperature. The relation is given in 2.4.
- **Desorption** also relies on the temperature, gas, liquid or dissolved solid to a surface and the concentration of the substance. The rate constants and the kinetic order are dependent on the gas, liquid or dissolved solid to a surface and the temperature. The general desorption rate is given in equation 2.5.

$$J = -\nabla\varphi D \tag{2.2}$$

J is the diffusion flux, D is the diffusion coefficient, φ is the concentration.

$$D = \frac{K_B T}{6\pi\phi r} \tag{2.3}$$

K_B is the Boltzmann's constant, T is the absolute temperature, ϕ is the viscosity of the medium and r is the radius of the spherical particle.

$$\theta = \frac{KC}{1 + KC} \tag{2.4}$$

θ is fractional occupancy of the adsorption sites, K is the associated equilibrium constant and C is the concentration of the substance.

$$R = rC^x \tag{2.5}$$

R is the rate of desorption ,r is the rate constant for desorption, C is the concentration of the adsorbed material, and x is the kinetic order of desorption.

In order to maximize utilisation of the electrode surface for CO_2 reduction, the migration, diffusion, adsorption of CO_2 and the desorption of CO_2 reduction products must be maximized. Ideally, the electrode's surface is fully covered with CO_2, but it can be expected that there other chemicals present.

The modified CO_2 surface coverage of the electrode is given in equation 2.6. This equation applies when there is competition between multiple substances. It can be seen that a high concentration of CO_2 is beneficial for CO_2 surface coverage and a high concentration of products and electrolyte is disadvantageous for CO_2 surface coverage.

$$\theta_{CO_2} = \frac{K_{CO_2} C_{CO_2}}{1 + K_{CO_2} C_{CO_2} + K_{products} C_{products} + K_{electrolyte} C_{electrolyte}} \tag{2.6}$$

θ_x is fractional occupancy of substance x of the adsorption sites, K_x is the associated equilibrium constant of substance x and C_x is the concentration of substance x.

Increasing CO_2 pressure leads to an increase in the maximum concentration of CO_2. This is beneficial for the mass-transport of CO_2. In some reactors, increased CO_2 mass-transport by increased CO_2 pressure increases the faradeic efficiency of the desired products. However, this relation does not seem to be straight forward. Some reactors show an increasing faradeic efficiency asymptotically nearing 100% by increasing the CO_2 pressure [13] [19] [20]. Others have a maximum CO_2 reduction reaction faradeic efficiency at a certain pressure of CO_2 [21] [22]. This is highlighted in table 2.2.

The reactors that asymptotically near 100% efficiency usually have a single CO_2 reduction reaction product. The reactors that show a maximum CO_2 reduction reaction efficient at a certain pressure usually have multiple competing CO_2 reduction reaction products. In reactors with multiple carbon products, each product reaches its maximum at a different CO_2 pressure. This shows that the composition and proportions CO_2 reduction reaction products may change with increased mass-transfer(see figure 2.2) or that pressure itself influences the surface catalytic reactions. In most cases hydrogen is suppressed when CO_2 pressure is increased at constant current density.

Table 2.2: Data acquired from figure 2.2 C

Substance	FE at 10 bar	FE at 20 bar	FE at 30 bar	FE at 40 bar	FE at 50 bar
HCOOH	15.4	35.5	58.6	39.8	36.1
H2	15.4	6.5	2.4	2.2	1.9
CO	15.4	32.5	21.0	29.4	24.9
Hydrocarbons	48.3	13.4	14.9	11.7	11.9
Total	94.4	87.9	96.9	83.1	74.8

The reason for the drop in faradeic efficiency of the CO_2 reduction reaction with increase in CO_2 pressure was not provided [21]. Two possible explanations are:

- There is an unknown product being formed that was not accounted for. Should that be the cause, a different chemical other than CO, H2, hydrocarbon, formic acid and alcohols formed according to their product analysis method [21]. Reactions with components of the physical cell due to increased CO_2 pressure are unlikely.
- The analysis method is not suitable to form a quantitative relation between CO_2 pressure and faradeic efficiency. Only gas chromatography was used for determining the amount of hydrocarbons[21]. Some hydrocarbons are liquids at elevated pressures and ambient temperatures. For example, the saturation pressures of ethane and propane at 25^oC is 41.9 bar and 9.5 bar, respectively. The liquid fraction of these chemicals could be missed by their analysis method.

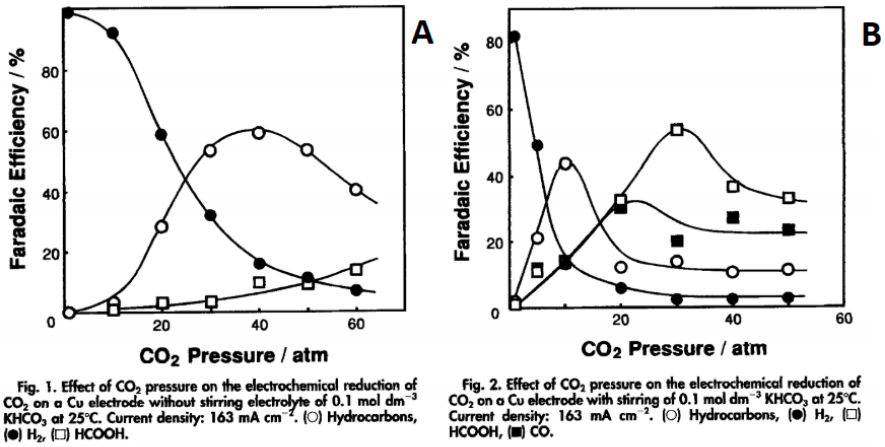

Fig. 1. Effect of CO_2 pressure on the electrochemical reduction of CO_2 on a Cu electrode without stirring electrolyte of 0.1 mol dm^{-3} $KHCO_3$ at 25°C. Current density: 163 mA cm^{-2}. (○) Hydrocarbons, (●) H_2, (□) HCOOH.

Fig. 2. Effect of CO_2 pressure on the electrochemical reduction of CO_2 on a Cu electrode with stirring of 0.1 mol dm^{-3} $KHCO_3$ at 25°C. Current density: 163 mA cm^{-2}. (○) Hydrocarbons, (●) H_2, (□) HCOOH, (■) CO.

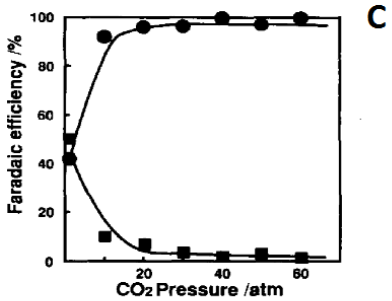

Fig. 1. Effect of CO_2 pressure on the faradaic efficiencies of HCOOH (●) and H_2 (■) formation at Pb electrodes at a current density of 200 mA cm^{-2}.

Figure 2.2: A and B are graphs of the faradeic efficiencies of multiple carbon and hydrogen products in an electrolysis cell with CO_2 pressure as variable [21]. C is a graph of the faradeic efficiencies of a carbon and hydrogen product in an electrolysis cell with CO_2 pressure as variable [13].

2.1.2. The mass transport-limited current

One important characteristic of electrolysis cells is the mass-transport-limited current. For electrolysis, the mass transport-limited current occurs when the mass-transport is insufficient to supply the reacting surface with reactants. A higher limit allows more product to be made in a certain time frame in the same cell. For that reason, cells with a higher mass transport-limited current are, in general, more financially viable than cells with a low mass transport limits. The equation of the mass transport-limited current for porous electrodes, excluding cases where the reactants undergo reactions in the liquid phase (e.g. with a buffer), is shown below [23].

$$I_l = nFA_r uC_0[1 - exp(-\frac{LK_m A_s}{u})] \tag{2.7}$$

Here, n is the number of electrons required for the reaction, F is the Faraday constant, A_r is the cross-sectional area of the porous electrode, u is the superficial velocity, C_0 is the concentration of reactant at the inlet, L is the thickness of the porous electrode, k_m is the mass transport coefficient of the electrode, and A_s is the specific surface area of the electrode [24].

Similar behaviour could be expected for non-porous electrodes. The key difference between the two electrodes is that in one situation the liquid flows trough the medium and in the other it flows over the medium. However, on a smaller scale, these scenarios are not that different. In both cases its a charged catalyst surface with a mass transport of reactants.

When the current is increased beyond the mass-transport-limited current of the system with both these types of electrodes, the faradeic efficiency of hydrogen production will increase. This phenomenon can be seen in figure 2.3. Increasing the current density beyond 200 mA/cm^2 in this configuration decreases the efficiency of HCOOH and increases the efficiency of hydrogen production. Because of the logarithmic scale of the X-axis of the graph, the mass transport-limited current is clearly visible.

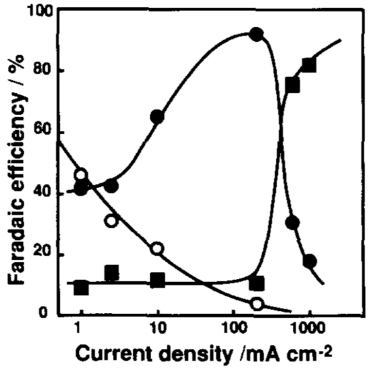

Fig. 4. Effect of current density on faradaic efficiencies of HCOOH (●), CO (○) and H_2 (■) formation under 20 atm of CO_2 at In electrodes.

Figure 2.3: A graph of the faradeic efficiencies of carbon and hydrogen products in an electrolysis cell with current density as variable [13].

2.1.3. Electrode materials for CO_2 reduction reactions

The material of the electrode is a catalyst that influences both the mass-transport-limited current and faradeic efficiency. Each material and their different structures have their own characteristics. The most important tailored properties of electrode materials are catalytic properties, conductivity, corrosion resistance, hardness, current load, form, and size [25].

The common electrode materials consists of metals, metal oxides and carbon based materials. In modern day experiments, composites, surface treatments and different crystal structures are also being investigated for their characteristics [23].

Good materials for CO_2 reduction electrodes are catalysts that selectively and efficiently reduce CO_2 at high current densities. In table 2.3 several high performing materials that produce formic acid can be seen. One of the fundamental challenges in catalyst development is to suppress H+ reduction to H2 without compromising CO_2 reduction [26].

Some materials for CO_2 reduction are susceptible to structural changes. For example, the difference between Pb foil and electro deposited Pb electrode improved the FE at −1.1 V from 20% to $> 90\%$ [27].

Table 2.3 shows that, when designing a CO_2 reduction reactor to support a wide variety of electrode combinations, different challenges may arise. Designing a reactor to hold a copper electrode or a carbon paper electrode is different because of the material properties. Copper can be bought in multiple thicknesses, but carbon paper only available in small thicknesses. Lastly, an important property of

Table 2.3: Examples of electrochemical CO_2 reduction reaction that produc formic acid or formate with different electrocatalysts and electrolytes [26]

Electrocatalyst	Electrolyte	Major products Faradaic efficiency, [%]
[Cu(cyclam)](ClO4)2 complex	DMF/H2O (97:3 v/v)	HCOOH (90%)
Gas-diffusion layer/CNT/Ir complex/polyethylene glycol	0.5 m LiClO4/0.1 m NaHCO3/1% v/vMeCN	HCOO− (83%)
Pd-polyaniline/CNTs	0.1 m KHCO3	HCOO− (83%)
SnOx/Sn	0.1 m KHCO3	HCOO− (71.6%)
Nanostructured Sn	0.1 m NaHCO3	HCOO− (93.6%)
Sn	Ion liquids/H2O/MeCN	HCOOH (92.0%)
Pb		HCOOH (91.6%)
Pd NPs	0.5 m NaHCO3	HCOO− (88%)
Bi nanoflakes	0.1 m KHCO3	HCOO− (79.5%)
Bi/BiOCl	0.5 m KHCO3	HCOO− (92%)
Cu pillars	0.1 m KHCO3	HCOOH (28.7%)
Cu nanofoam	0.5 m KHCO3	HCOOH (37%)
Ag–Sn alloy	0.5 m NaHCO3	HCOOH (80%)
PdxPt(100−x)/C	0.1 m KH2PO4/0.1 m K2HPO4	HCOOH (88%)
SnO2 porous nanowires	0.1 m KHCO3	HCOO− (80%)
Mesoporous SnO2 nanosheets/carbonpaper	0.5 m NaHCO3	HCOO− (87%)
Pb2O	0.5 m KHCO3/NaHCO3	HCOOH (60%/50%)
Co3O4 atomic layers	0.1 m KHCO3	HCOO− (64.3%)
Partially oxidized Co atomic layers	0.1 m Na2SO4	HCOO− (90.1%)
PEI-NCNTs/glassy carbon	0.1 m KHCO3	HCOO− (85%)
N-doped graphene/carbon paper	0.5 m KHCO3	HCOO− (73%)
Boron-doped graphene	0.1 m KHCO3	HCOO− (66%)
N-doped nanodiamond/Si	0.5 m NaHCO3	HCOO− (13.6%) CH3COO− (77.6%)

the electrode material and structure is the durability. As mentioned before, there are lot of possible electrode options. Nevertheless, if the initially good electrodes do not maintain their performance for long, they will not be suitable for industry purposes [28][29]. Figure 2.4 shows the potential surface area loss of an Pt electrode as a function of cycles and time at various potentials. From this example, one can conclude that experimenting in the lab and operating in the industries frequently at high over potentials can have significant effects on the electrode. Therefore it is important to keep track of the history of a certain electrode.

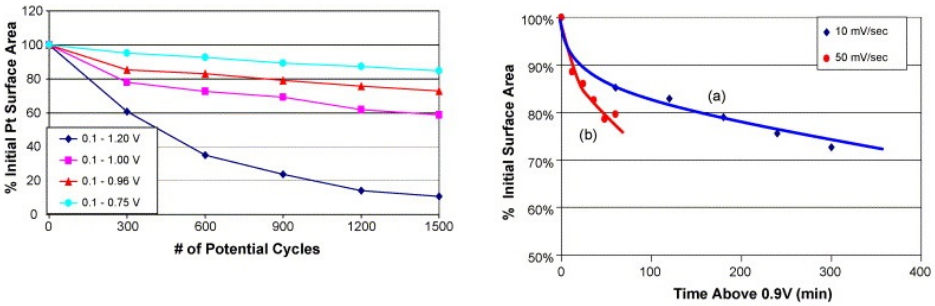

Figure 2.4: Potential effect on catalyst surface area loss [28].

Another example of a degradation factor is the the pH of the electrolyte with the corrosion of graphite electrodes. Graphite electrodes degrade the fastest at a neutral pH, because corrosion of graphite anodes is the result the amount of oxygen evolved per unit time and the activity of the anodic oxygen [30].

2.1.4. The CO_2 reaction and the research reactor design

In this section, the three key factors influencing the rate of the CO_2 reduction reactions are discussed. The amount of current that goes through the reactor, the mass-transport of the reactor and the electrode materials. This section shows that the influence of all three factor can not be predicted by other experiments done at different mass-transport, current densities or electrode materials.

A design for a research reactor therefor must be able to facilitate the possibility to vary all three of these factors. This comes down to a design that can operate at a variety of CO_2 pressures, can facilitate different current densities and can house different electrode materials.

2.2. Electrolysis cell configuration

The electrochemical CO_2 reduction reaction happens in a reactor cell. Electrochemical cells generate electric energy from chemical reactions (in Galvanic cells) or provide electrical energy to supply a reaction (in electrolysis cells). This section will focus on the characteristics relevant to the design of the electrolysis cells that facilitates the CO_2 reduction reaction by supplying electrical energy.

First, the standard electrolysis cell configuration is discussed to set a basis for these type of reactors. Then the mechanics of cell efficiency will be discussed to gain insight in the factors influencing the cell's performance. Afterwards, the different components of the electrochemical cell will be discussed. Lastly, several alterations to the standard cell will be discussed to see what effect these alterations have on the performance of the cell.

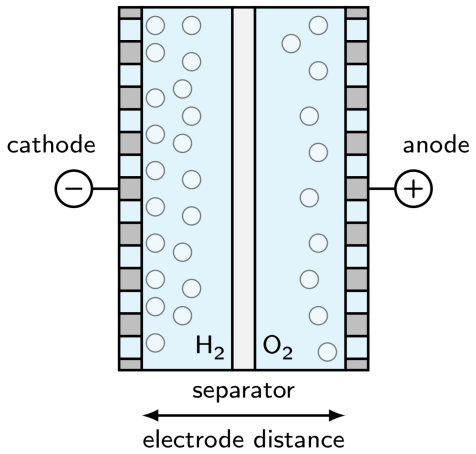

Figure 2.5: A schematic display of a standard electrolysis cell [31]

2.2.1. Standard set up

The standard electrolysis cell design consists of two electrodes submerged in electrolyte and a membrane or separator. This is called a membrane configuration. This membrane is used to separate the products from the anode and cathode, which is important to prevent oxidation of the desired product. An example of an electrolysis cell that produces hydrogen is displayed in figure 2.5.

2.2.2. Cell efficiency

The energy efficiency of the cell is described as the ratio between the energy that is used (for supplying the current of the reaction) and the change in energy of the product that is created. The product that is created has an increased higher heating value compared to feed. The total energy value of the product can be seen as the total produced increase in higher heating value. This ratio can be seen in equation 2.8.

$$\eta_{cell} = \frac{\Delta HHV_{Product}}{E_{cell} * I * t} \tag{2.8}$$

Here η_x is the efficiency of x, ΔHHV_x is the change in higher heating value of x, E_x is the electric potential of x, I is the current and t is time.

The cell efficiency can also be described as the ratio between the reversible cell voltage and the actual cell voltage. This relation can be seen in equation 2.9. The difference in the reversible and actual cell voltages can be explained by viewing equation 2.10. The cell resistance is dissected in equation 2.11.

$$\eta_{cell} = \frac{E_{rev}}{E_{cell}} \tag{2.9}$$

$$E_{cell} = E_{rev} + \eta_{anode} + \eta_{cathode} + I * R_{cell} \tag{2.10}$$

$$R_{cell} = R_{circuit} + R_{electrolyte} + R_{membrane} + R_{bubbles} \tag{2.11}$$

In 2.9, 2.10 and 2.11 η_x is the efficiency of x, E_x is the electric potential of x, I is the current and R_x is the electrical resistance of x.

The four resistances mentioned in equation 2.11 ($R_{circuit}$, $R_{electrolyte}$, $R_{membrane}$ and $R_{bubbles}$) are dependent on the characteristics of the cell and the characteristics of the fluid inside the cell. When designing for maximum efficiency, all of the sources of resistance have to be considered. Both the resistance of the electrolyte, the circuit and the membrane are heavily dependent on the electrical resistance of the used material, the cross-sectional area and the distance which the current has to travel trough the medium [32]. This is in accordance to Ohm's law (equation 2.12).

$$R = \frac{I * l}{A * \kappa} \tag{2.12}$$

Here R is the electrical resistance, I is the current, l is the length of the current path, A is the area of the cross section of the current path and κ is the electrical conductivity of the medium.

The bubble resistance is also heavily dependent on the conductivity of the substance. The conductivity of the gas is usually insignificant when compared to the conductivity of electrolyte. As a result, they can be considered as pockets of non-conducting space. However, bubbles are not stationary and the volume varies depending on the pressure of the system, the solubility and the amount of gas that is present in the system. And not only the electrolyte is less conductive due to the forming of bubbles: the surface of the electrodes is also reduced by bubbles on the surface of the electrode. This will increase the actual current density of the electrode [32] [33].

2.2.3. Single Cell

One of the alternative configurations of an electrolysis cell is the single cell configuration. In this setup, the membrane is left out of the design. The products of the anode and the cathode will mix if no other obstruction is present. A schematic representation of such a setup is depicted in figure 2.6.

The mixing of products can result in dangerous scenarios. For example, if someone operates a single cell hydrogen electrolyser and the products would gather in the head space of the cell, an explosion could happen due to auto-ignition. So, due to major safety hazards, the cell should be used with products that will not auto-ignite, only be used for limited time duration or diluted(ventilated) in such a way that the concentrations stay below the explosion limits [35].

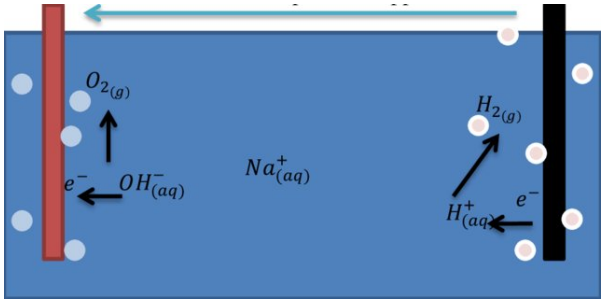

Figure 2.6: Single cell water electrolysis, showing formation of hydrogen gas at cathode and oxygen gas at anode [34]

2.2.4. Zero gap cell

The zero gap design reduces the distance between the electrodes, so it reaches the same thickness as that of the membrane. A schematic representation of such a setup is depicted in figure 2.7. According to equations 2.11 and 2.12, the cell resistance will be reduced by reducing the distance between the electrodes. This will be a benefit for cells that operate at large currents, according to equation 2.10.

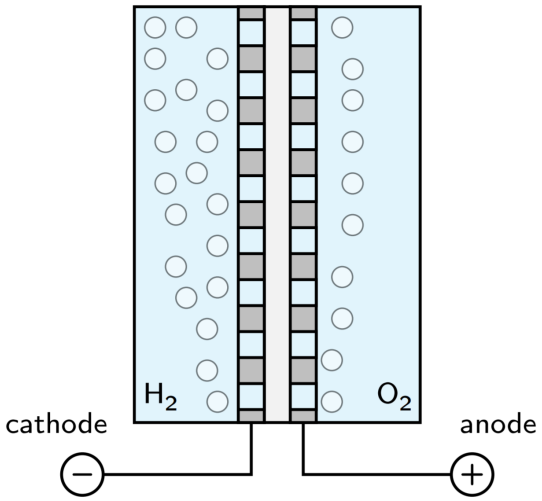

Figure 2.7: A zero-gap assembly where the electrodes are directly pressed onto the separator [31]

Since the current does not have to travel through the bulk of the electrolyte, the reduced conductivity due to the bubbles does not negatively influence the current pathway and therefor the resistance of the cell. However, the bubbles may still negatively influence the surface of the reactor.

2.2.5. Cell configuration of the research reactor

The different configurations have their own characteristics in the product separation and their own specific influence on cell efficiency. In research, energy efficiency is not the key design parameter, but the reliability of the results is. This means that product separation is more important to focus on when selecting a configuration for the reactor. Products of the anode and cathode side can react and influence the result of the experiment.

This means the relevant choice for the configuration is one chamber or two chambers separated by a membrane. The choice between a membrane configuration and a zero gap configuration is less relevant, since it only affects energy efficiency. The choice between them should therefore rely on practicality. In addition, the increase in energy efficiency by using a zero gap configuration can be calculated using equations 2.9 to 2.11.

In conclusion, each reactor configuration has its advantages and drawbacks. To explore the possibilities of CO_2 reduction reactions, each configuration can provide new pieces of knowledge to improve

the reactor designs. It is the researcher's duty to choose the right type of reactor that is able to facilitate the research in the best way [36].

2.3. Electrolytes used in CO_2 reduction reactions

This section will look into the electrolytes used for CO_2 reduction reactors in the literature. Electrolytes provide the solution with additional conductivity, which is a key factor in the cell performance. A low resistance is essential to achieve a high efficiency. This is further discussed in subsection 2.2.2. The choice of electrolyte during the design of an industrial electrolysis cell is therefore important.

Formic acid and formate are CO_2 reduction products that are commonly found in literature. Carbonate salts are often as electrolyte in the production of formic acid and formate. The combinations of several electrocatalysts, electrolytes and their main product are displayed in table 2.3.

It can be seen in table 2.3 that the Pb_2O electrocatalyst is tested with two kinds of electrolyte. A solution of 0.5M of $NaHCO_3$ and $KHCO_3$ were used with a faradeic efficiency of about 50% and 60% respectively [37]. At this molar concentration $NaHCO_3$ has a conductivity of $28800\mu mhos$ and $KHCO_3$ has a conductivity of $42000\mu mhos$ [38]. The difference in conductivity seems to be the driving factor between the different faradeic efficiencies with a common molar concentration. This is in accordance to Ohm's law, that is described in equation 2.12.

Chemicals with high conductivity that are commonly used are hydrochloric, hydrobromic, hydroiodic, nitric and sulfuric acid. The maximum conductivity of these acids lie between the $20 - 40\%_{wt}$ in a aqueous solution [38].

2.3.1. Non-aqueous solvents

A non-aqueous solvent can solve the issue of the low solubility of CO_2 and the unwanted hydrogen evolution reaction. At ambient pressure, di-methylformamide has the best CO_2 solubility, which is 20 times greater than that of water. However, at elevated pressures, cyclohexanone has the best solubility [39].

The products created in these non-aqueous solvents will be different, as there is no water present. Due to the lack of water, CO is the main product with all electrode materials[40]. An overview of electrode materials with their aqueous and non-aqueous products is provided in table 2.4

Table 2.4: Electrode materials with their aqueous and non-aqueous (photo)electrichemical main product

Electrode Material	Aqueous Product	Non-Aqueous Product
Ln	HCOO- [41]	CO [42]
Cu	HCOO- [43]	CO [44]
Ag	CO [45]	CO [46]
p-InP	MeOH [47]	CO [48]

2.3.2. Electrolytes and the reactor design

Most of the electrolytes and some of the solvents are highly corrosive in large concentrations. These larger concentrations are important for cell efficiency. The increased conductivity of the electrolyte decreases the the cell resistance.

Again achieving high cell efficiency is not a key design feature, because the effect of decreased conductivity on efficiency can be calculated with equations 2.9 to 2.11. However it is important to research the effect of the corrosive electrolytes and solvents on the process and key components that facilitate the reaction. The reactor design therefore must be able to handle corrosive chemicals.

2.4. Membranes

This section will look into the role of membranes in the CO_2 reduction reaction and concludes how that effects the reactor design. Membranes are the thin layer that separate the two sides of the standard electrolysis cells. This layer is semipermeable to avoid unwanted reactions between products of the anode and cathode side, and allows certain molecules or ions to pass through it by diffusion or occasionally by more specialized processes of facilitated diffusion, passive transport or active transport [49].

Transport of certain molecules or ions between the two sides is essential to facilitate the electrochemical reactions. For example, in PEM water electrolysis, the membrane allows the protons needed for the reduction reaction to transport itself form one side to another while keeping the hydrogen and oxygen separate [49]. The half reactions of water electrolysis is displayed below in equations 2.13 en 2.14.

$$2H_2O \leftarrow O_2 + 4H^+ + 4e^- \tag{2.13}$$

$$4H^+ + 4e^- \leftarrow H_2 \tag{2.14}$$

Another important aspect of the membrane material is the electrical conductivity. To have a functioning cell, the membrane must be conductive. Most membrane materials have a conductivity relatively low compared to the conductivity of the electrolytes [23]. However, membranes in real life are not ideal. When designing and experimenting with reactors that have these membranes, one must take into account that things like the delamination of layers, product crossover and pH imbalances can happen during operation. A comparison of relevant design aspects is displayed in table 2.5 [50].

Table 2.5: Advantages and Disadvantages of Bipolar Membranes (BPMs) and Cation Exchange Membranes (CEMs) for CO_2 Electrolysis [50].

Membrane	BPM	CEM
Advantages	+ maintains constant pH	+ low price
	+ low product crossover	+ low potential drop
	+ low electrolyte contamination	+ easy manufacturing
	+ acidification and basification	+ high stability/lifetime
Disadvantages	- high price	- high product crossover
	- complex manufacturing	- high electrolyte contamination
	- short lifetime	- acidic anolyte
	- low stability in strong bases	- pH imbalance
	- delamination of layers	
	- limits on high ion concentrations	

2.5. Existing CO_2 reduction reactors

After reviewing the different configurations and possibilities for individual parts for the reactors, this section will take a brief look at these reactors, to identify their properties and to learn about design choices that have been made. This section will be mainly focused on high pressure cells. As mentioned high pressure can increase mass-transport of CO_2 and the mass-transport is a key research variable of the reaction. By reviewing these reactors, insight for the design parameters can be gained.

A distinction is made by dedicating individual subsections for certain configurations or properties of cells:

- Single container high pressure reactors
- Reactor in autoclave
- High pressure cells with recycled electrolyte
- Reactor with gas diffusion electrodes
- Reactors in the Process and Energy department of TU Delft

2.5.1. Single container high pressure reactors

For high pressure CO_2 reduction, single vessel reactors with no in and out flow of electrolyte seem to be common. Most of the reactors do have in and out flow of gas. This provides the possibility to flush out air, and replace it with high pressure CO_2 instead. They also let the CO_2 that is being consumed in the reaction be replaced, and allow gaseous products to be sampled. Example reactors can be seen in figure 2.8.

Some of these reactors have a stirring bar or stirrer. This is added to the cell to ensure that the chamber is well mixed and it avoids CO_2 depleted electrolyte around the electrodes. This is beneficial for the efficiency of the cell [51] [52].

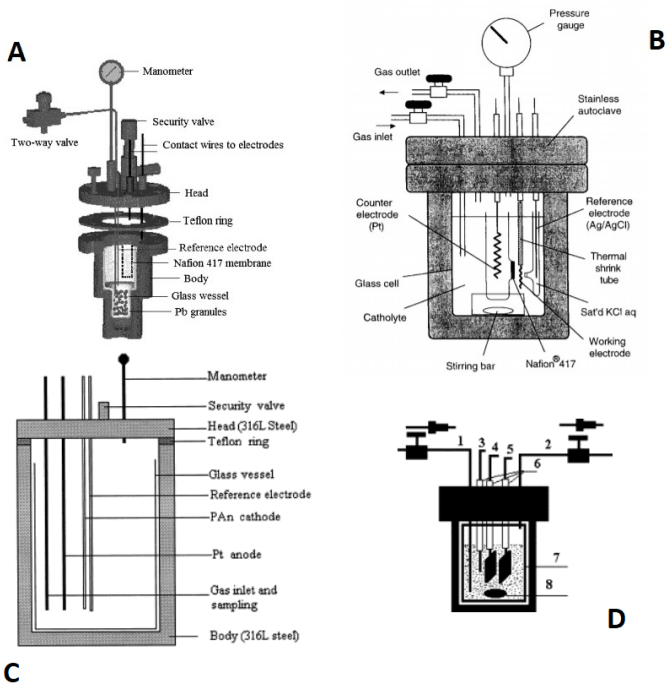

Figure 2.8: A: A fixed-bed reactor with Pb-granule electrodes [53]. B: A stainless steel autoclave with a electrolysis cell in it [51]. C: A high-pressure cell with a polyaniline electrode in in methanol [54]. D: Structure of the high-pressure electrolysis cell: (1) gas inlet; (2) gas outlet; (3) quasi-reference electrode (Pt wire); (4) cathode (Cu plank); (5) anode (Pt plank); (6) Teflon packing; (7) Teflon; (8) stirrer [52].

The reactors are expected to be good for experiments that will approach the theoretical maximum efficiency of the reaction. However, it will be hard to do prolonged tests with these setups and test for industrial feasibility. For industrial purposes, a continuous flow of electrolyte and production configuration is favoured [14]. These single container reactor designs cannot provide that.

2.5.2. Reactor in high pressure vessel

The setup in figure 2.9 is an H-cell configuration inside a high pressure container. High pressure cells are expensive and not readily available to buy, but ambient pressure experimental setups are relatively cheap and readily available. If there is a high pressure vessel available that can fit in these commercially available cells, it may be a good solution for high pressure experiments.

The difference between the reactors of the previous section and the cell of figure 2.9 is the pressure containment. This configuration should have the same possibilities and drawbacks of the high pressure single cell configuration.

2.5.3. High pressure cells with recycled electrolyte

In this section, two high pressure cells with recycled electrolyte design are reviewed. The reactors and the schematic setups are displayed in figure 2.10. Both reactors produce formate at comparable rates,

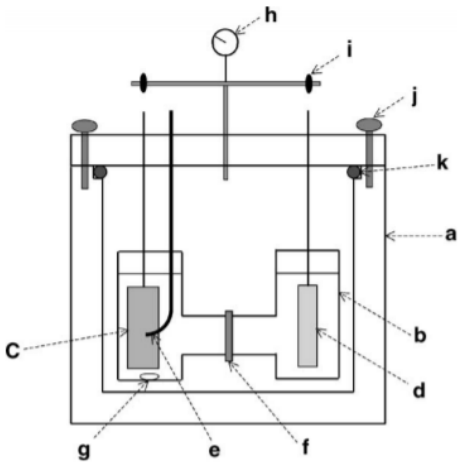

Figure 2.9: tainless steel high pressure vessel with an H-type glass cell: (a) SUS-316 stainless steel high pressure vessel; (b) H-type glass cell; (c) Cu cathode; (d) Pt anode; (e) Ag Q.R.E.; (f) ion exchange membrane; (g) magnetic stirrer bar; (h) manometer; (i) high pressure valve; (j) screw; (k) o-ring [55]

similar geometry and efficiencies. Also, both reactor have supported recent experiments (in the last two years). Their characteristics are displayed in table 2.6 [56] [50].

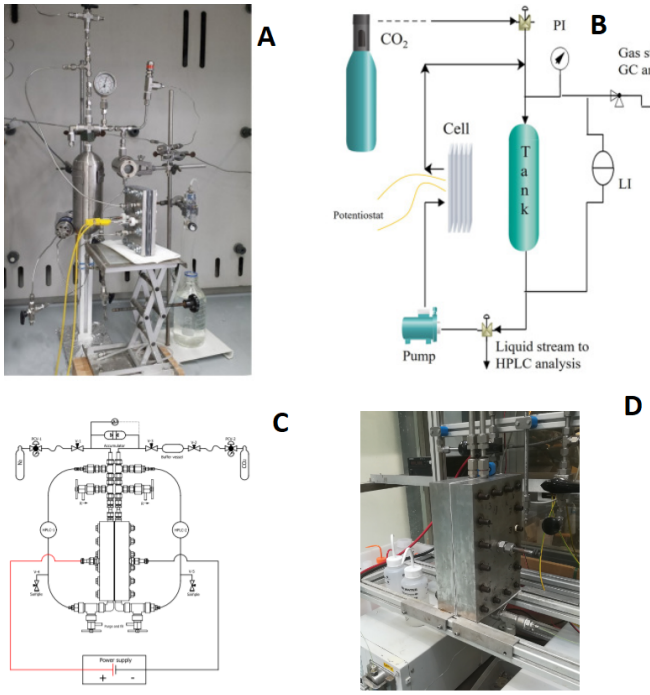

Figure 2.10: A is the picture and B is the schematic of a high pressure CO_2 reduction system [56]. C is the schematic and D is the picture of an other high pressure CO_2 reduction system [50].

Both reactors seem capable of testing many different kinds of CO_2 reduction experiments. However, the maximum operation time is different. This may be due to the size of the tank/ volume of the buffer. A bigger tank may provide the option to experiment longer, but the concentration will change more slowly with a similar production rate. Also, both reactors require several bolts to keep the reactor stack together. This may pose an inconvenience when the reactor needs to be assembled or disassembled for different experiments.

Table 2.6: Comparison of CO_2 Electrolysis to Formic Acid/Formate in Continuous Flow Electrolyzers

Condtition	ref [56]	ref [50]
Max opperating pressure [bar]	30	50
Cathode material	Sn plate	Sn plate
Anode material	$Ti/IrO_2 - Ta_2O$	Ir-MMO
Geometric surface area of cathode [cm^2]	9	80
Flow rate/area of cathode [$mL/min * cm^2$]	3.3	0.125
Cell voltage [V]	6.5	3.5
Current Density [mA/cm^2]	50	30
Faraday efficiency of formic acid [%]	82.5	90
Formic acid production rate [$mmol/m^2 * s$]	2.1	2
max operation time [h]	60	0.33

2.5.4. Reactor with gas diffusion electrodes

A schematic setup of a continuous flow reactor is displayed in figure 2.11. 4 flows pass through the reactor. The reactor uses Cu and Pb diffusion electrodes to separate the gas and liquid products [57] [58].

What is interesting about this configuration, is that this reactor setup can run at high current densities with a high Faradeic efficiency. The highest Faradeic efficiency it achieved for producing CO was 69% with a Cu particle catalyst at a current density of 400 mA/cm^2 [58].

The 4 flows are separated by 3 membranes. To keep these membranes from tearing apart, the flows must have similar pressures. Research on mass transport by increasing pressure with this configuration therefore requires pressure control of all flows. Researching the effect of mass-transport with this configuration is less optimal, because of the required control. The required control will make the design more complicated.

In the schematic representation, a lot of layers are forming the reaction stack, but the supporting components are not included. This makes this configuration the most complicated to realise, which is important to take into account during the design of a new reactor.

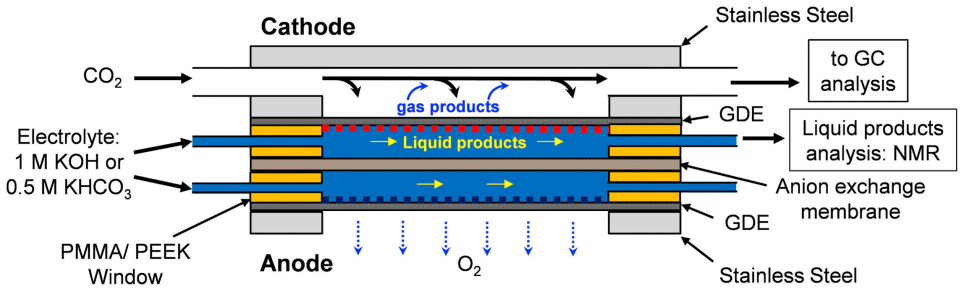

Figure 2.11: Schematic representation of the electrochemical flow cell [58]

2.5.5. Survey of existing reactors in the Process and Energy department of TU Delft

Besides the reactor designs that have been described in literature, there are also some reactors in storage and in use at the TU Delft that performed CO_2 reductions reactions. This section will take a brief look at these reactors, to identify their properties, to learn about design choices that have been made and find out if the designs could be used or adapted.

Reactor 1

The first reactor is shown in figure 2.12. This reactor appears to be a high pressure CO_2 reduction reactor with in- and outlets. It can be seen that there is a large amount of materials and bolts used in this design. If someone wants to assemble or disassemble the reactor, it would require a lot of time

and effort. The coating may have been applied for a electrical insulation or as a chemical barrier. This was presumably done to prevent a short circuit through the bolts of the reactor and avoid oxidation of the metal parts. It can be a good solution to avoid short circuit and unwanted oxidation.

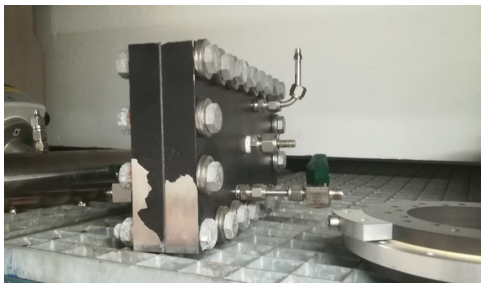

Figure 2.12: A photo taken of a high pressure electrolysis cell at the TU Delft.

Reactor 2

The second reactor is shown in figure 2.13. This reactor does not seem to be designed for high pressure applications. The reactor stack seems to be separate from the plates, nuts and bolts holding it together. There appears to be a lack of order. There are a number of threads sticking out of of the stack, there is corrosion on the threads and residue all over the setup. These things point to a possible lack of safety. The operator could be harmed due to the chemical residues. The setup also seems to be unstable. This could pose a major hazard when combined with the questionable structural design. There are a lot of tubes and wires attached to the stack that could tip the stack. This could damage the stack and cause failures. By looking at the amount of residue, this could already have occurred several times.

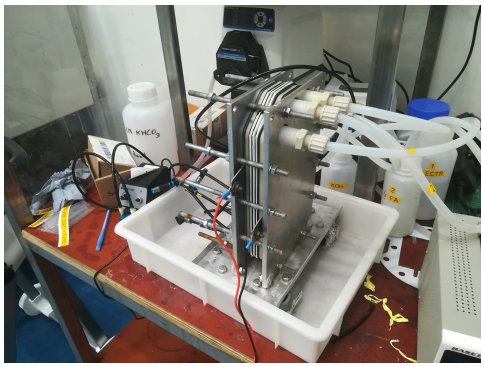

Figure 2.13: A photo taken of a electrolysis cell at the TU Delft

2.5.6. Practical aspects of the reactor design and experiments

Each configuration has a unique downside. A lot of the flow reactor designs use thick steel plates with a lot of bolts going through them, the single chamber reactors do not have recycling electrolyte and the Gas diffusion reactor have many components and are difficult to pressurise in comparison to other configurations.

The high pressure stack with recycled electrolyte configuration have the most potential for a reactor that can facilitates the most important research variables. The only downside of the existing reactor designs is that they require a lot of material and a big amount of components. A new design that bypasses these inconveniences will be best suited to facilitate the research of CO_2 reduction reactions.

2.6. Techno-Economics of CO_2 reduction

This section reviews the Techno-Economics of CO_2 reduction. The ultimate goal of the electrochemical field is not knowledge itself, but the ability to better peoples lives by giving them products more cheaply and mitigating CO_2 emissions. Making the technology economically viable is an important aspect of this. To know what is needed to make the technology economically viable can also help predict the direction of future research and requirements of the reactor design.

Some researchers have raised those questions regarding the potential of CO_2 reduction to mitigate CO_2 emissions at an appreciable level, and whether the process can be performed in an economically feasible way, which would make it competitive compared to traditional chemical manufacturing processes [59].

In general, an efficient CO_2 electrolyzer which is economically competitive, requires [60] :

- Highly active, stable, and selective catalysts
- Durability with minimal ohmic resistance
- High mass transport properties under reacting conditions

The current density was found to be a minor factor in the economics of electrolyzers, with only requiring a lower limit of approximately 250−300 mA/cm^2. For example: in a model used to simulate the economic case of ethanol, a decrease in current density to 100 mA/cm^2 resulted in a NPV decrease of 42 million, while an increase to 500 mA/cm^2 only gave an extra 8 million [11]. Several of the experiments done in literature have already achieved these current densities with decent efficiencies [45] [61] [62] [13], but the stability is still an issue [29].

As a result, the economics of the CO_2 reduction are quite promising, especially when combining these factors with the problem of the fluctuating output intensities of renewable energy sources (as discussed in chapter 1). Therefore, with the requirements given in this section, the electrochemical reduction of CO_2 could compete with the current production methods in the future. One of the requirements of the reactor's design (the ability to test different cathode catalysts at different mass-transport conditions) was already raised in previous sections of the literature study. No new requirements where obtained in this part of the review.

2.7. Formaldehyde case study

As mentioned before, many products can be produced by CO_2 reduction reactions. To gain extra insights on designing a CO_2 reduction reactor, a formaldehyde case study was done. First, the specific reaction mechanisms of producing formaldehyde are reviewed. Afterwards, the possible cathode materials and the interaction of formaldehyde with different relevant substances is discussed.

2.7.1. The reaction mechanisms of formaldehyde CO_2 reduction

In this subsection, the focus is on the specific reaction mechanisms of CO_2 reduction into formaldehyde. The electrochemical conversion of carbon dioxide into formaldehyde consists of two stages at the cathode side. In the first stage, carbon dioxide is converted into formic acid. In the second stage, formic acid is converted into formaldehyde and water. Formaldehyde is not formed directly [63]. The reaction equations can be seen below.

$$CO_2 + 2H^+ + 2e^- \rightarrow HCOOH \tag{2.15}$$

$$HCOOH + 2H^+ + 2e^- \rightarrow HCHO + H_2O \tag{2.16}$$

At the anode side, water is converted into oxygen to provide the protons to form formaldehyde at the cathode side. The reaction equations can be seen below.

$$2H_2O \rightarrow O_2 + 4e^- + 4H^+ \tag{2.17}$$

The importance and effects of mass-transport are discussed in section 2.1. There was not literature found that researched this factors in a electrochemical setting. It would be interesting to see what the mass-transport effects of formate or formic acid are on the production of formaldehyde.

2.7.2. The suitable electrodes for producing formaldehyde

As mentioned before, a cathode is needed for the carbon dioxide reduction reaction to take place. For the production of formaldehyde, several electrodes have been tested, but the most promising appears to be boron doped diamond and glassy carbon. Their formaldehyde conversion rate could be related to the presence of carbon atoms that have sh^3 bonds [63]. The generated products and the corresponding Faradaic efficiencies per electrode material are displayed in figure 2.14.

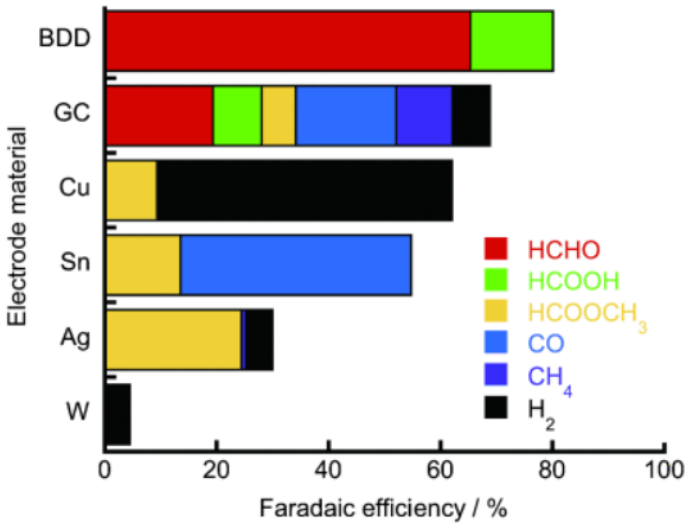

Figure 2.14: Faradaic efficiency of the products generated by the electrochemical reduction of CO_2 using various electrodes in a $MeOH$ electrolyte. The electrochemical reduction was performed at $-1.5\ Vvs.Ag/Ag^+$ using a platinum counter electrode in a two□compartment cell $(100\ mL)$ separated by Nafion for $1\ h$ at room temperature and atmospheric pressure [63]

The main differences that can be seen from figure 2.14 is that boron doped diamond (BDD) has a higher Faradaic efficiency for forming both formaldehyde and formic acid. It should be mentioned that these performances are for a methanolic electrolyte.

Moreover, boron doped diamond produces fewer byproducts. So, the two electrode materials that produce formaldehyde are boron doped diamond and glassy carbon. Boron doped diamond only has formic acid as by product, but the presence of formic acid seems inevitable as it its an intermediate product of formaldehyde. However, glassy carbon produces several byproducts:

- Methyl-formate
- Carbon-monoxide
- Methane
- Hydrogen

2.7.3. Formaldehyde in aqueous solutions

One important characteristic of formaldehyde is the high reactivity. As a result, it is commonly handled in aqueous and/or methanolic solutions [64]. Furthermore, methanol is also formed in the Cannizzaro reaction in aqueous solutions of formaldehyde. Therefore, it is often necessary to consider ternary formaldehyde-water-methanol mixtures [65]. This implies that these reactions need to be considered when studying the reduction of CO_2 into formaldehyde.

In aqueous solution, formaldehyde forms different adducts with the solution. The two most prominent ones are methylene glycol ($HOCH_2OH$) and poly(oxymethylene) glycols ($HO(CH_2O)_iH, i > 1$) [64]. The chemical reactions of these two adducts are displayed below.

$$CH_2O + H_2O \rightleftharpoons HOCH_2OH \tag{2.18}$$

$$HO(CH_2O)_{i-1}H + HOCH_2OH \rightleftharpoons HO(CH_2O)_iH + H_2O \tag{2.19}$$

The reactions and equilibrium distribution of the adducts in the solution have a major influence on the chemical-reaction-kinetics and transport properties of the mixture. Therefore, the reactions and equilibrium distribution have to be taken into account for any thermodynamic model of these systems [64].

The molar fraction of formaldehyde in a steady state aqueous solution is low compared to molar fractions of the glycols it forms with water. So when one wants to measure the amount of formaldehyde in the system, the amount of glycols have to be measured as well when equilibrium is reached.

besides forming adducts with water, formaldehyde can react with OH^- molecules. In aqueous solutions OH^- molecules are present. The Cannizzaro reaction is the base-induced disproportionation of two molecules of a non-enolizable aldehyde to give a primary alcohol and a carboxylic acid [66]. Formaldehyde is such an aldehyde that can react with a base solution to to form methanol and formate in a higher order reaction [67]. The reaction is displayed in equation 2.20.

$$2CH_20 + OH^- \rightarrow CH_3OH + HCOO^- \tag{2.20}$$

In aqueous solutions during electrolysis there is often oxygen present. This is especially true in single cell configurations. A micro kinetic model was used to calculate the normalized oxidation rate of formaldehyde in a oxygen saturated aqueous solution at 50 bars of pressure and room temperature [68]. The result of the calculations was a reaction rate of less than $1 * 10^-6$. This result suggest that oxidation can be assumed to be an insignificant factor. The micro kinetic model can be found in the appendices(D.6).

2.7.4. Formaldehyde in methanolic solutions

One of the solvents which can be used for CO_2 reduction reactions is methanol. Just as in the aqueous solution, formaldehyde forms adduct with the methanolic solution. The main adducts are hemiformal (HOC_2OCH_3) and ploy(oxymethylene) hemiformals ($HO(CH_2O)_iCH_3$, $i > 1$). The chemical reactions of these two adducts are displayed below.

$$CH_2O + CH_3OH \rightleftharpoons HOCH_2OCH_3 \tag{2.21}$$

$$HO(CH_2O)_{i-1}CH_3 + HOCH_2OCH_3 \rightleftharpoons HO(CH_2O)_iCH_3 + CH_3OH \tag{2.22}$$

These side reactions have to be taken into account when making any thermodynamic model containing these substance (similar to the reactions in the aqueous solution). This is also the case when determining the composition of the products made in a reactor [65].

2.7.5. ternary formaldehyde-water-methanol mixtures

As mentioned before, due to methanol being formed in a chemical reaction in aqueous solutions of formaldehyde, it is necessary to consider ternary formaldehyde-water-methanol mixtures [65]. However, no other mention of this reaction was found in the literature of aqueous formaldehyde solutions. The reactions in a ternary mixture that have been found are shown in figure 2.15. The only reaction that formed methanol out of formaldehyde and water that was found, was a hydrogenation reaction of formaldehyde on am ice surface [69]. The hydrogenation reaction equations are shown below.

$$H_2CO + H \rightarrow CH_3O \tag{2.23}$$

$$CH_3O + H \rightarrow CH_3OH \tag{2.24}$$

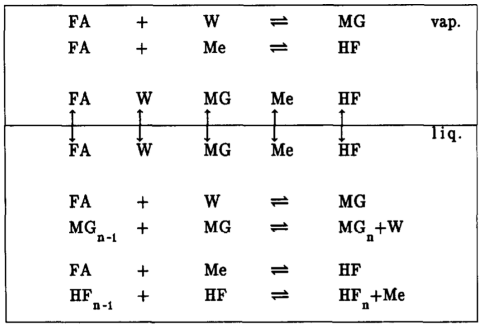

Figure 2.15: Vapor-liquid equilibrium in a water-methanol-formaldehyde mixture [70]

2.7.6. Reactor design for a formaldehyde CO_2 reduction reactor

This case study showed that over time the products change in composition and thermodynamic characteristics. In the rest of the literature this phenomenon was not described in a CO_2 reduction reactor. The design of a formaldehyde producing CO_2 reduction reactor must take into account the possible change in thermodynamic characteristics. The adducts can for example have a great influence on the reactor's performance, by influencing the following factors:

- **Analysis of the reactor's performance**
  The analysis the reactor's performance is also much dependent on the adducts. For example, if the product is reduced by forming adducts and the efficiency is calculated without consideration, the resulting efficiency is too low. Previous sections already showed the possibility that there are both gaseous and liquid products. This section shows that analysing the performance requires a appreciate identification method. To look this aspect for design a review was done of identification methods in section 2.9.
- **mass transport**
  Additionally to the surface coverage of products discussed in subsection 2.1.1, the surface of the electrode may become covered with the formed adducts. If the loss in CO_2 coverage is significant, this will decrease the performance and must be taken into account when discussing the result of experiments.
- **Viscosity of the mixture**
  Changes in product or adduct concentration can change the mixture's viscosity. When the viscosity becomes higher than expected, a desired mass flow may not be achieved.

2.8. Water-gas interaction

As seen in subsection 2.7.2, it is possible that different kinds of molecules other than the desired product are produced by the reaction. This section looks into the interaction of the relevant molecules that are produced by and fed to the reactor in aqueous solutions, according to the reactions in subsection 2.2.2. This will provide insight on how the fluids in the system behave for designing the designing the reactor system.

2.8.1. Carbon dioxide

CO_2 that is present as feed will be dissolved in the electrolyte. It can be seen in figure 2.16 that the solubility has a linear behaviour until a pressure of 50 bar. After that point, the slope of the solubility decreases in magnitude.

Dissolved CO_2 in water forms carbonic acid. The hydration equilibrium constant at room temperature is $[\mathrm{H_2CO_3}]/[CO2] \approx 1.7 \times 10^{-3}$. Hence, the majority of CO_2 molecules remain unreacted after equilibrium. The reaction rate ($0.039s^{-}1$) is relatively slow, so this will only be relevant for longer experiments. Orthocarbonic acid is formed as well, but in minor quantities [71], so it will be neglected in this thesis.

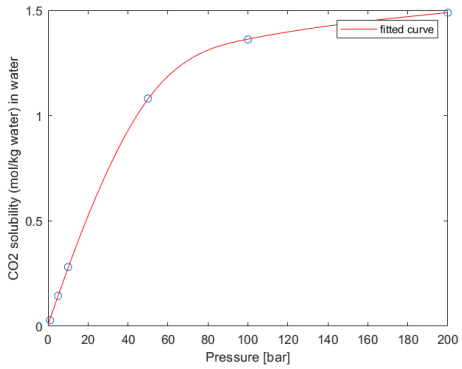

Figure 2.16: A graph of the solubility of CO_2 as function of pressure [72]

2.8.2. Carbon monoxide

CO can be the main product in some CO_2 reduction reactions, but when using a glassy carbon electrode it is a byproduct. The solubility does not follow the same behaviour as CO_2. It can be seen that the solubility of carbon monoxide is increasing linear with increased pressure. The graph can be seen in figure 2.17.

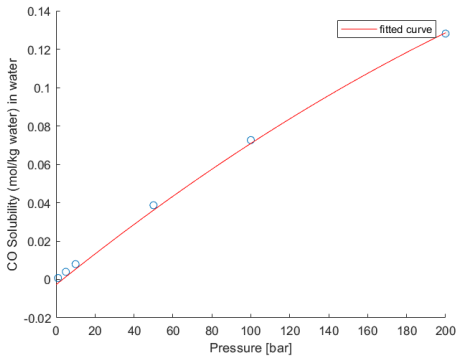

Figure 2.17: A graph of the solubility of CO as function of pressure [73].

Water and carbon monoxide can form CO_2 and hydrogen via an exothermic water shift reaction. The reaction is displayed in equation 2.25. However, the temperatures needed for this reaction is much higher than ambient, and no data could be found on reactions with liquid water 2.25. It is therefore assumed that the reaction is negligible.

$$CO + H_2O \rightleftharpoons CO_2 + H_2 \tag{2.25}$$

2.8.3. Oxygen

Oxygen is produced as byproduct in every reaction. The solubility of oxygen in water can be seen in figure 2.18. The concentration of oxygen in the electrolyte is assumed to have no direct influence on the performance, because oxidation of water is impossible and oxidation of products is assumed to be low due to the low performance temperature (ambient temperature).

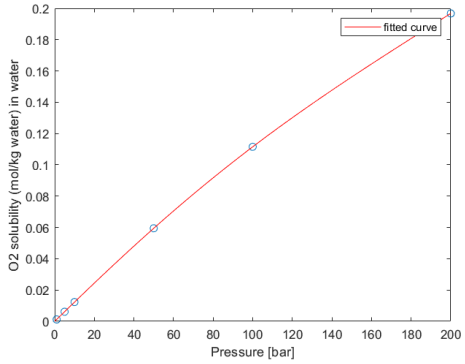

Figure 2.18: A graph of the solubility of O2 as function of pressure [74].

2.8.4. Hydrogen

In certain conditions, hydrogen is produced in significant amounts. The solubility of hydrogen in water can be seen in figure 2.19. Just as oxygen, the concentration of hydrogen in the water is assumed to have no influence on the performance of the cell. It can be seen in the figure that the solubility is relatively minuscule and linear as function of pressure. When hydrogen is produced, bubbles seem imminent.

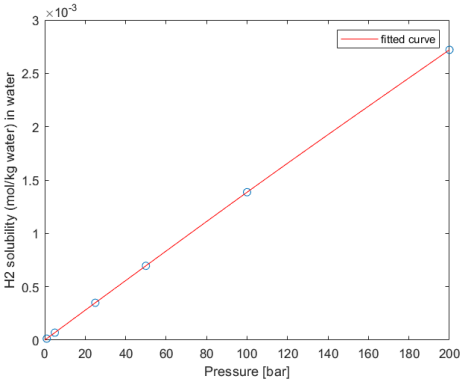

Figure 2.19: A graph of the solubility of H2 as function of pressure [75].

2.8.5. Methane

Just as the other gasses (except for CO_2), the solubility increases linearly with pressure in the 1-100 bar range. This can be seen in figure 2.20. There are no known reactions between water and methane at ambient temperatures.

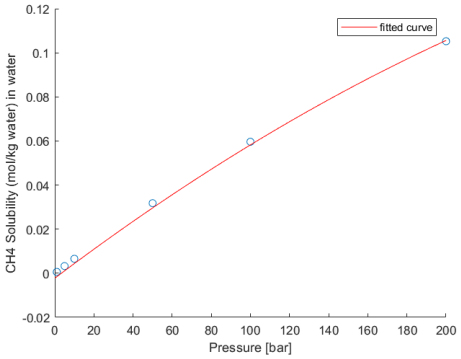

Figure 2.20: A graph of the solubility of CH4 as function of pressure [76].

2.8.6. Water-gas interaction and reactor design

Knowing how molecules in the reactor behave is essential for the design of a reactor system. Molecules that are discussed in this section have limited presence at ambient conditions in the electrolyte, but these molecules have an increased presence in the electrolyte at higher pressures. When the reduction reaction in a reactor with high pressure condition has gaseous products, a significant part of the product can be dissolved in the electrolyte. If the designed setup or analysis method did not account for dissolved products, the analysis will not be accurate.

2.9. Identifying substances

A important result of the research on CO_2 reactions is the efficiency of the reaction. To determine the efficiency of the reaction, the present chemicals in the electrolyte must be identified.This section will look into different identification methods to see if it will impact the design. Only the available methods at the TU Delft in the Process and Energy department will be discussed.

2.9.1. Chromatography

Chromatography is a technique used to separate a mixtures based on the chemical's ability to adhere to two different substances. The mixture is dissolved in a carrier fluid called the mobile phase, which carries the chemicals through a structure holding another material, called the stationary phase.The separation of the mixture is based on the differential partitioning between the mobile and stationary substance [77].

There are two main types of chromatography: gas and liquid. Since the CO_2 reduction reactors produce both gasses and liquids with potential (by)products in them, the setup must have both types to gain a full analysis of the process. However, the mixture must be separable based on the individual chemical's characteristics for it to give a reliable analysis [77].

2.9.2. Absorption spectroscopy

In absorption spectroscopy, the mixture is exposed to a certain kind of radiation. The response of the mixture could provide information on the composition. There are tree main types of emission spectroscopy: ultraviolet-visible (UV-VIS), Infra red (IR) and nuclear magnetic resonance (NMR). UV-VIS and IR absorption spectroscopy are similar: both use light to determine the concentration of chemicals in a mixture. The effectiveness of the methods depends largely on the spectra of the chemicals and the characteristics of the spectroscopy device itself.

The main difference between these two techniques is the radiation wavelength that is used. UV-VIS absorption uses high energy wavelengths between approx. 200 - 1000 nm, which is able to excite

electrons to higher electronic energy bands. IR spectroscopy generally uses 2.5 - 25 µm wavelengths and is able to map rotational and vibrational electronic structures of a molecule [78].

The main criteria for accurate measurements of mixtures is that each individual compound has enough of its own unique peaks at various wave-numbers. If multiple peaks of several chemicals overlap at multiple wave numbers, and neither compound has a distinguished peak, it could be difficult to accurately determine the composition of the mixture [78].

The IR spectra of CO_2, formic acid, formate and formaldehyde were compared in an ideal case, to see if the method is plausible to give accurate results. The spectra aligned among each other can be seen in figure 2.21. The dashed lines represent the wavelength of characteristic peaks of the compounds. Some dashed lines intersect one unique peak of one of the substances, but others have multiple intersections with substance. To easily and accurately analyse the mixture, enough measurements at wavelengths with unique peaks are needed. In this case, unique peaks are limited, which would not make IR spectroscopy a favourable characterization technique.

However, as mentioned in subsection 2.7.2 and in section 2.7 there could be more kinds of chemicals involved, which makes an accurate determination of the concentration more difficult. The electrolyte itself could have an effect on the measurements as well. It could be said that for an accurate measurement, multiple analysis techniques or calibration tests are needed. Moreover,if there are more compounds involved, more calibration tests with mixtures are needed to give an accurate measurement of the process.

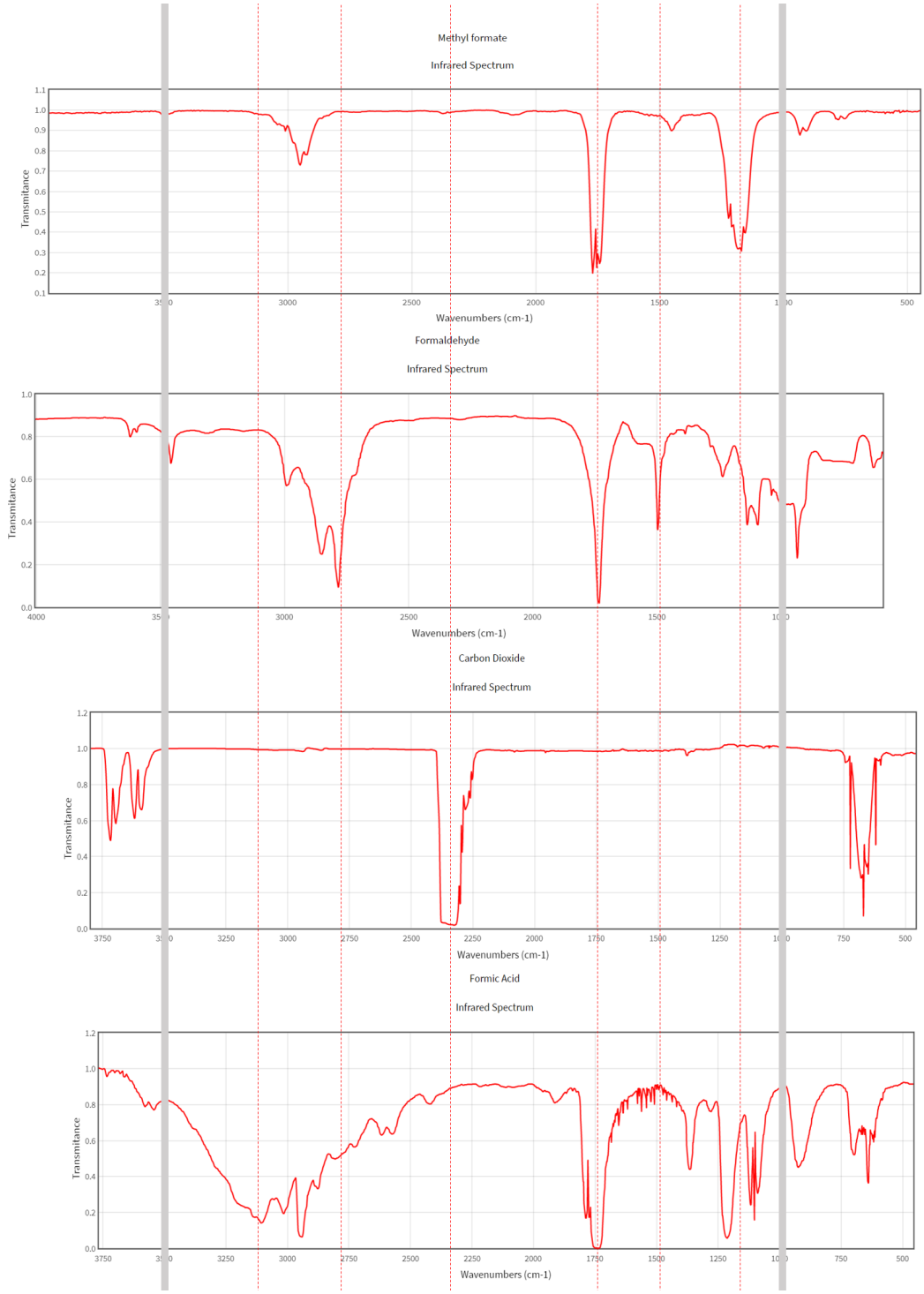

Figure 2.21: A collection of IR absorption graphs of different chemicals with dashed lines through their unique peaks obtained from the NIST archive.

2.9.3. Mass spectroscopy

A mass spectrometer ionizes the compounds in a mixture and separates them by accelerating them using a electric or magnetic field. Afterwards, the charge to mass ratio is measured for the different compounds, which are plotted into a mass spectrum [79].

The ability to distinguish one chemical from another is based on the difference in the unique mass to charge ratio. It can be seen in figure 2.22 that methanol has several peaks around the $32m/z$. This implies that chemicals with similar molar masses could be hard to distinguish. In the case of a formaldehyde reactor, this could prove a challenge to obtain accurate results, as the molar masses of the involved chemicals are relatively similar. Calibration tests seem to be needed if one looks at table 2.7.

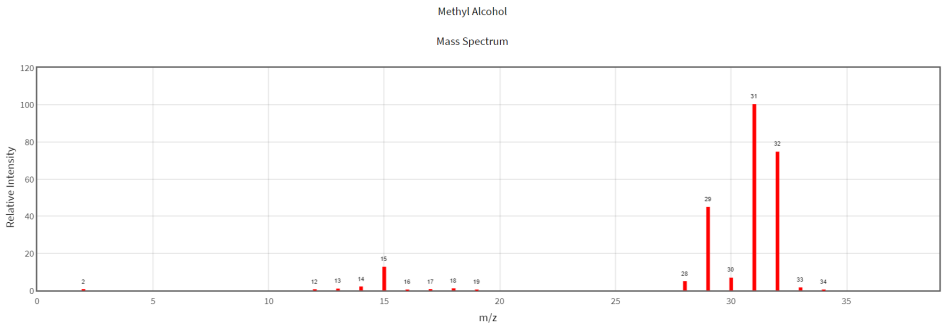

Figure 2.22: A graph of the mass spectrum of methanol taken from the NIST archive.

Table 2.7

Chemical	Molar Mass [g/mol]
Formic Acid	46.03
Formate	45.02
CO_2	44.01
Methanol	32.04
Oxygen	32.00
Formaldehyde	30.03
Water	18.02

2.9.4. Identification and reactor system design

To facilitate these different types of analysis in design, one must look at the products, the amount of different chemicals and the reaction conditions. For example, analysing a high pressure reaction with both multiple gaseous and liquid product will require a different setup than analysing a ambient pressure reaction with a single liquid product.

The design therefor must focus on adaptability to facilitate the different setups. Designing for every scenario will make the analysis part of the design large and unnecessarily complicated when doing reactions that have few products in single phase.

2.10. Conclusion

A literature study has been performed to gain insight in important design parameters for the design of a CO_2 reduction reactor system. From this study, it can be concluded that a CO_2 reduction reactor should be able to facilitate the following aspects of an electrochemical reaction:

- Variation in Mass-transport
- Variation in current-density
- Different electrode materials
- Different cell configurations
- Corrosive electrolytes
- Handling a variety of products and possible byproducts
- Different analysis methods

One specific design that could include all of these aspects would be useful. Therefore, the goal of this thesis is to design a reactor system that is able to facilitate all of the above, or that could be adapted to include functionalities later on if any of these aspects are missing. The parameters below will lead to a system design that will achieve this:

- **Variable mass-transport** - Mass-transport is a key research topic, so being able to have a varying transport facilitates the research.
- **Chemically resistant** - Electrolytes and products can be corrosive, so its important that the design can resist these chemicals
- **Adaptable** - A lot of different configurations and additional components to measure and facilitate the process are possible, so limiting the design to one specific configuration and set of component is limiting for the utility of the design.
- **Easy handling** - Current designs require a lot of material and have many components, so a design that bypasses these disadvantages is an improvement on the current situation.

3

Design Parameters

This chapter will discus the design parameters of the CO_2 reduction reactor system design. The bulk of the parameters will be based on the conclusion of the literature review. The rest of the parameters are based on general needs of the environment in which the reactor will be placed.

3.1. High pressure

The first requirement is that the system must be able to operate at high pressures. Mass-transport research is an important topic. Mass-transport in the system is influenced by concentration of CO_2 and the temperature. For that reason, the reactor system will be designed for increased pressures, to increase the concentration and mass-transport of CO_2.

The pressure of the gas piping in the lab can reach 40 bars of pressure. The gas bottles can be acquired at 100 bar when they are full. The system should be designed to handle 100 bars of internal pressure. This ensures that the system can handle lab pressures with an acceptable safety margin.

3.2. Chemical resistance

As seen with CO_2 reduction reactors, the electrolytes can be corrosive. So when selecting reactor materials, it is important to be aware of the possibility that the reactor could be damaged in case of choosing the wrong materials.

Moreover, the potential products (like formaldehyde and formic acid) in high concentrations can be very reactive substances. For that reason, it is essential that both the products and possible electrolytes are taken into account when selecting reactor materials .

3.3. Adaptable

In an electrolysis cell, there are a lot configurations possible and supporting components that can be added. To maximise the utility of the design, it need to be adaptable to support different kinds of experiments.

3.4. Fast assembly and disassembly

To gain good insight in a CO_2 reduction reaction, a lot of experiments are needed. All these experiments need to be safe and reliable. By focusing on a design that uses very little parts and parts that do not require extra tools to assemble, productivity of the researchers can be greatly improved.

3.5. Location

Because there could potentially be dangerous chemicals present in the reactor, the setup must be able to operate in both a fume hood and outside the lab. The fume hood at the TU Delft can provide multiple high pressure gasses including CO_2. Outside the lab environment, gas bottles are available as well.

Currently, there are many ongoing experiments at the department where the intended fume hood is located. This means it is inevitable that one fume hood must house several experiments. This can lead to major space restrictions and requires caution with loose parts of the setup. Consequently, the setup and reactor must occupy as little space as possible, and loose bits must be avoided in the design. This is also the case when operating outside the lab.

3.6. Safety

Last, but not least, is the safety aspect of the design. This parameter did not came forth from the literature study, but it a very important one. Despite the great potentials of the technology, if it is harming or killing everyone near it who is trying to operate it, it will not have a bright future. Jokes a side, as engineers there is the the moral obligation to take the effects of what the devices we design have on the world.

The high pressure fluid that is potentially corrosive is important to control, otherwise it could do damage to people and/or other equipment. So preventing leaks and mechanical reliability are essential for providing safety. Also, minimizing the hazard when a failure does occur is important. When both the chance of an accident happening and the potential damage is minimized, the associated risks will be minimal.

The pressure equipment directive was used to as guide for the safety of the design. It can be found in appendix E.

Table 3.1: Caption missing. And nice table, just put a bit more space between the items on the list so you can see which ”reasoning” points go with which ” choice” points.

Component	Design choice	Reasoning
Reactor	Stack Configuration	- simple to design, easy to upscale, eligible for different configurations and convenient for small scale experiments
	PEEK reaction chamber	- Simple design due to non-conductivity
	Stainless steel electrode casing	- Simple design due to conductivity
	Female fittings	- Reliable and simple manufacturing
	Kalrez or EPDM O-ring seals	- Good corrosion resistance
	Ring terminal electrical contacts	- Stable electrical connection
	Clamp holding the stack together	- Simple, compact, no tools needed and cheap.
	Bolt with star knob for adjusting clamp force	- Simple, compact, no tools needed and cheap.
	Aluminium plate frame on beams	- Different configurations possible
	bolts through the reactor	- Option to run and test reactor outside setup
The reservoir	Cylinder with piston configuration	- Variable volume of the reservoir
	Stainless steel thick walled cylinder	- Good dimension, good corrosion resistance and can house different configurations
	PEEK piston	- Good corrosion resistance, material already available and will not scratch the inside of the cylinder
	Kalrez or EPDM O-ring seals	- Good corrosion resistance
	Female fittings in the moving pistion	- Reliable and simple manufacturing
	Addtional piston with alternative fitting	- Reliable and simple manufacturing and ability to test additional design choice
	Aluminium plate frame	- Different configurations possible and supports the use of the moving piston
	Aluminium placement blocks	- Different configurations possible and supports the use of the moving piston
Pump	The GAH series pump of microfluid	- Pump with good qualities
Tubing	IDEX 1/8” PEEK tubing	- Good corrosion resistance,low pressure drops and a wide variety of products
Power supply	Potentiostat	- Option to control the absolute potential of the working electrode
Main Frame	ITEM aluminium profile frame	- Good availability, light weight and easy to adjust and add components

4

The design of the reactor system

To achieve the design parameters as described in chapter 3, a continuous-flow reactor with one chamber will be designed. This will be the most simple configuration to design, it is easy to scale up, eligible for different configurations and convenient for small scale experiments. Minimizing the electrical resistance of the system is not a key design feature.

In this chapter, the different design choices will be discussed. First, the whole setup and tubing will be discussed, then the reactor stack, afterwards the reservoir and lastly the supporting equipment.

4.1. The setup

First to be covered is the setup of the reactor system. The setup must achieve the following key features:

- Supply a flow of electrolyte through the reactor
- Supply a current/potential to the reactor
- Contain pressures of up to 100 bar
- Saturate the electrolyte with CO_2
- Allow for analysis of the electrolyte
- Resist corrosive materials

To achieve these key features, a setup was designed as shown in figure 4.1. It is a system with a reservoir, reactor with power source, pump and a gas bottle. The initial setup will be kept as simple as possible to keep the adaptability of the design.

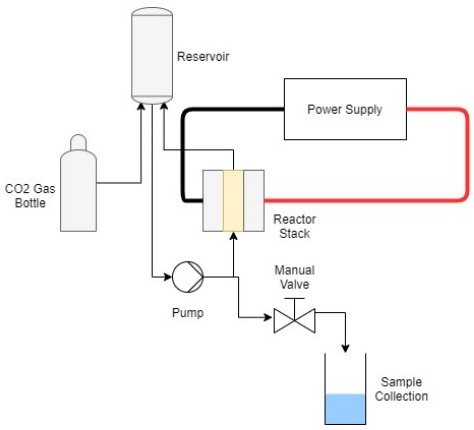

Figure 4.1: A schematic overview of the setup of the reactor system. The setup includes a a reservoir, reactor with power source, pump and a gas bottle.

4.2. The tubing

The first design choice to be made is what kind of tubing is used to connect the different parts of setup. IDEX tubes will be the supplier for the tubing. The reasons for choosing this brand are as follows:

- They have a wide range of PEEK components that can resist high pressures and corrosive chemicals.
- Most of the fittings that they have in their stock can be tightened by hand, which is good for fast assembly and disassembly.
- There are tools available to quickly adapt the tubing.
- All their components are pressure rated and have indications on the amount of usages. This is good for the reliability and safety.

4.3. The reactor

The reactor stack is the first component to be discussed. The reactor is designed as a stack of 3 pieces. The three pieces consist of two electrode holding pieces (electrode casings) and one reactor chamber. This choice allows one of the pieces to be quickly replaced if there is a need to. The stack can be seen in figure 4.2.

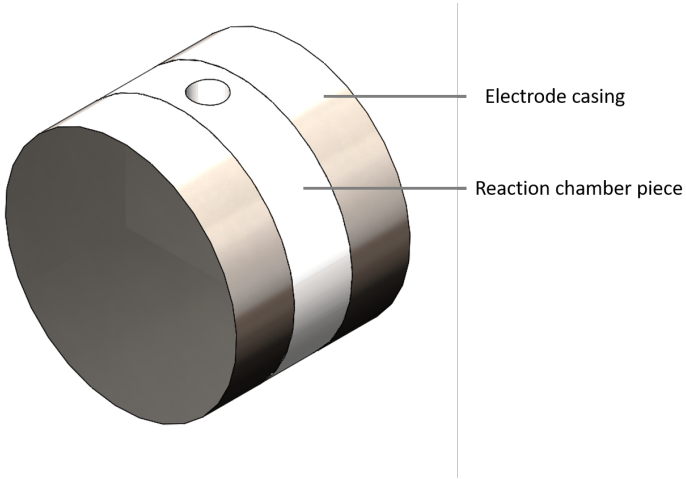

Figure 4.2: A closed stack of the CO2 reduction reactor rendered in Solid Works.

In the design, there is a focus on a reactor diameter as small as practically possible. A large reactor would be desirable to mimic industrial conditions closer, but the high pressures in the large reactor will lead to large forces. This requires more material and is more hazardous. However, going very small will require special tools and equipment which is not desirable for the adaptability. A diameter of 40 mm was settled on due to local manufacturing ability.

4.3.1. The reactor chamber piece

The first piece of the reactor stack that will be discussed is the reactor chamber. The reactor will contain a single chamber. The chamber has to have two electrode surfaces and it should be able to contain high pressure corrosive liquids and gasses. A cylindrical shape is ideal for the high pressure containment because of the ratio of the perimeter and surface of a circle.

The two circular surfaces at both ends of the cylinder can house the electrodes due to their flat shape. Another benefit of the cylindrical shape is the ease of manufacturing compared to a cornered shape.

The outside shape of the reaction chamber will be circular. The two main reasons behind this choice were the ability to have custom thickness of the chamber and the possibility to quickly manufacture different chamber designs from a single piece of cylindrical staff.

The in- and outlets of the reactor are to be placed on either sides of the cylinder. This minimises the radius of reaction chamber and is easily manufactured. The reaction chamber with the electrode placements can be seen in figure 4.3. To gain insight on the flow pattern in the reactor, a model was made. It was found that the flow of electrolyte can influence the mass transfer parameters of the reactor (as discussed in section 2.1.1). The flow patterns in this reactor design are not ideal (see model presented in appendix F), but are regarded as acceptable.

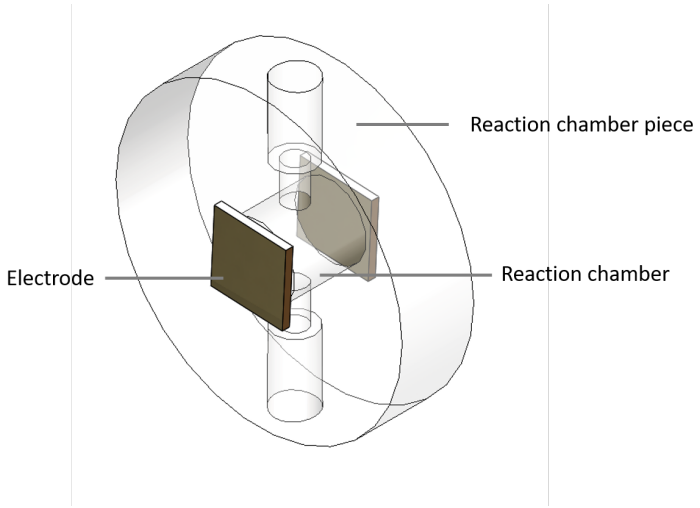

Figure 4.3: A render of the reactor chamber for the CO2 reduction reactor with two electrodes attached to the chamber.

Due to the stacking configuration, the reaction chamber itself must not conduct electricity. If it does conduct, it will cause a short circuit in the reactor. There are 2 possible solutions:

- **Require the material to be non-conductive** - This option would rule out several material options, but make the design more simple.
- **Insulate the material if it is conductive** - This option would allow more choice in material and would not require corrosion resistance of the material, but it will make the design more complicated by adding the layer. The added layer must adhere to the insulating material and must be corrosion resistant, electrically insulating and stand up to repeated assembly.

The non-conductive option was selected. This design choice will have less risk of failure and is more easily tested. To choose the proper material, CES EduPack 2019 was used. All materials in the data base were filtered on their resistance to acids, alkali and organic solvents. The filtered materials where plotted in a graph with price on the x-axis and mechanical strength on the y-axis (figure 4.4).

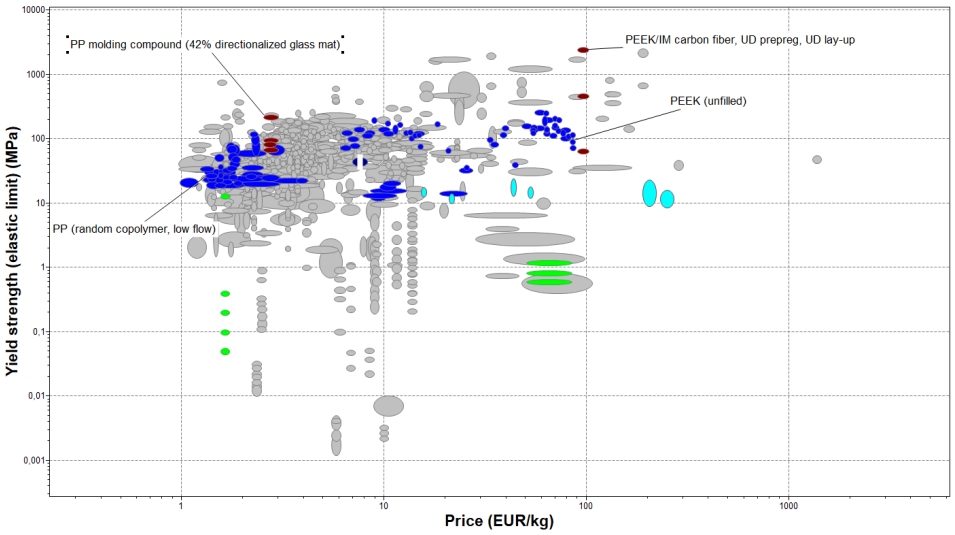

Figure 4.4: A graph displaying materials plotted using CES EduPack in a graph with their price on the X-axis and their yield strength on the Y-axis. Materials indicated in grey did not pass the durability filter mentioned in the report. The materials that have been named, are the most promising and materials around these materials are variants of these named materials.

In the graph, four materials are highlighted. These show one variant of PEEK and PP and one of their fiber reinforced variants. These were the materials which have been considered. The reinforced variants are however not suitable for this application, because the manufacturing with these materials is more complex and the adaptability would be less. The added complexity is against the design goals.

It can be seen in figure 4.4, that both PP and PEEK have good resistance to these potential electrolytes and products. PEEK is far more expensive, but it is a stronger material. Because the amount of material volume needed for the reactor is low and a stronger material is more preferable, PEEK was selected as material for the reactor chamber.

To measure the absolute potential of the electrodes, a reference electrode is needed. The reference electrode needs to be in contact with electrolyte near the working electrodes. An additional hole with a fitting port was added to the reactor chamber. The hole is perpendicular to the inlet and outlet holes. A transparent version of the final reactor chamber design can be seen in figure 4.5 and the technical drawing can be found in appendix G, figure G.8.

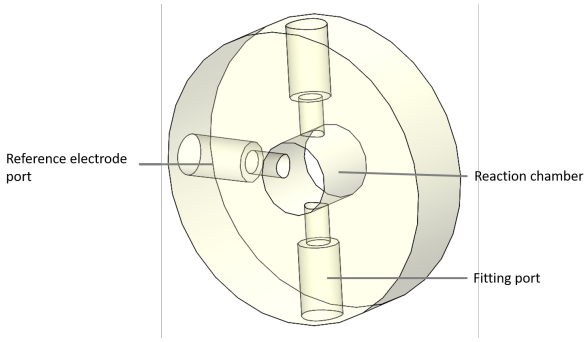

Figure 4.5: A transparent version of the reactor chamber made in SolidWorks.

4.3.2. The electrode casing

The second piece of the stack that is treated is the electrode casing. The electrodes need to have an electric potential and they should be in contact with the electrolyte inside the reaction chamber, in order to initiate the desired electrochemical reaction. As mentioned before in section 2.7.3, the electrolytes and products are likely to be relatively reactive. This means that the material that holds the electrodes in place must be able to get current to the electrodes, and it should be resistant to corrosive chemicals. The casing will be made out of an conductive material to have simple design.

To select the right material, a graph was made with filtered materials. The program used was CES EduPack 2019. The materials were first filtered on their resistance to acids, alkali and organic solvents and their electrical conductivity. Then, the materials were plotted with price on the X-axis and yield strength on the Y-axis. The result can be seen in figure 4.6.

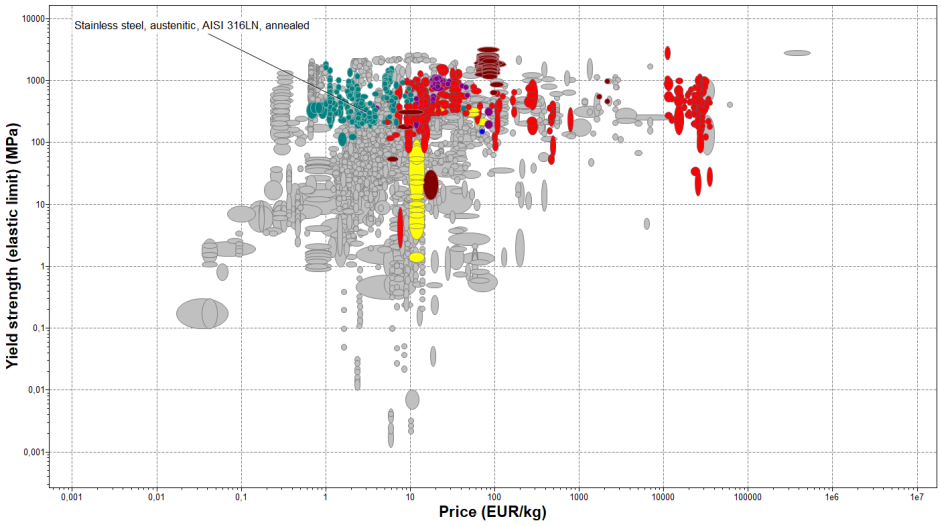

Figure 4.6: A graph displaying materials plotted using CES EduPack in a graph with their price on the X-axis and their yield strength on the Y-axis. Materials indicated in grey did not pass the durability filter mentioned in the report. The Materials named are the most promising and materials around these materials are variants of these named materials.

The stainless steel 316 was the most suitable material. It can be seen that the stainless steel alloys are the cheapest material with a high yield strength that meets the criteria. The alloy has the best corrosion resistance for its price and it is available at a lot of suppliers. The electrode casing will be produced out of a cylindrical bar. By doing so, the same manufacturing benefits apply as with the reaction chamber. All these properties make this alloy choice ideal for keeping the design adaptable, reliable and safe.

A 10x10 mm square pocket of 1.5 mm deep in the middle of the casing will be used to house the electrodes. Most of the metal electrode materials can be acquired commercially in this thickness, and the sheets of material can be cut into size. As a result, the design will have the most flexible pocket. The technical drawing if this part can be found in appendix G figure G.1.

Some of the electrode materials can only be acquired for smaller thicknesses. To secure the psychical contact of the electrode and the casing, a soft/flexible material can be placed between the chamber and the electrode. The contact can also be secure by placing the soft/flexible material in a folded electrode. The solutions are displayed in figure 4.7 and 4.8.

To select the right material, a graph was made including filtered materials. The materials were first filtered on their resistance to acids, alkali and organic solvents and their electrical conductivity. The program used to construct this graph was CES EduPack 2019. The materials were plotted with price on the X-axis and yield strength on the Y-axis. The result can be seen in the figure 4.9.

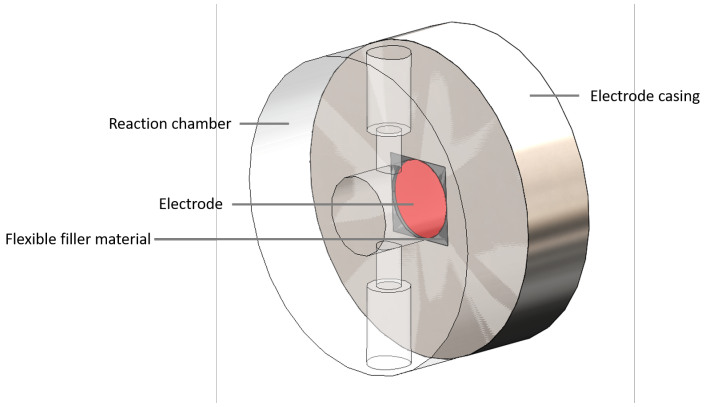

Figure 4.7: The CO2 reduction reactor chamber with a electrode attached to it. The electrode is in its stainless steel casing. Between the chamber and electrode are small black pieces that hold the electrode in place. The electrode is displayed with a red colour for clarity.

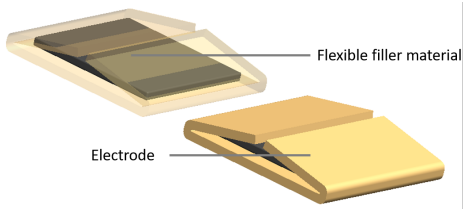

Figure 4.8: A folded electrode configuration.

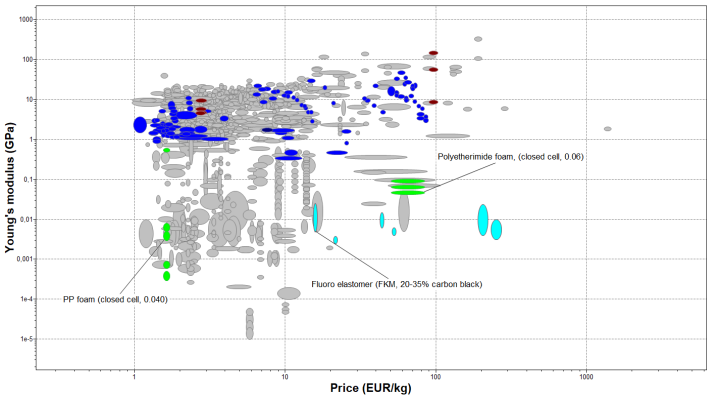

Figure 4.9: A graph displaying materials plotted using CES EduPack in a graph with their price on the X-axis and their Young's modulus on the Y-axis. Materials indicated in grey did not pass the durability filter mentioned in the report. The Materials named are the most promising and materials around these materials are variants of these named materials.

4.3.3. Sealing the reactor stack

The pressed stack will not be leak tight on itself. To achieve the high pressure design parameter, several options were considered for this problem:

- **O-ring** Would require a groove in one of the surfaces of contract and can be bought in many sizes.
- **Gasket** Could be applied without a groove, but would require design and fabrication of a custom gasket.
- **Liquid Gasket** Commercially available for high pressure applications, but it adheres on the surface.
- **Glue** Can create a good sealing, but is practically permanent.

The O-ring solution will be used because this option has the most flexibility and ease in usage. Groove dimension for standard sizes of O-rings are given in the NewDealSeals O-ring Handbook and they are in accordance with the standards given by ERIKS [80] [81]. The standards sizes of NewDealSeals and standards given by ERIKS were check by the script in appendix D.5.

The suitable material for the O-ring is a Kalrez® FFKM polymer or EPDM. Both polymers are known for their excellent resistance to almost all chemical liquids. The Kalrez® has better overall resistance, but is expensive. The default is an EPDM O-ring, and the Kalrez® should be used when highly corrosive chemicals are used.

The O-ring grooves were put into the electrode casings (see figure 4.10). The reasons are the characteristics of the reaction chamber material. PEEK has a lower yield strength than steel, and polymers have aless distinguished elastic region [82]. Applying the grooves in the reaction chamber in the face of the chamber will generate spots with higher stress in the PEEK. In general, it is better to have increased stress in steel instead. This stress can also be avoided by increasing the length of the reaction chamber, but increasing the length will:

- **Use more material** - This will cost more and will negatively affect the adaptability.
- **Increase the cell electrical resistance** - minimizing the cell resistance is not focus of the design, but if it can be avoided it is beneficial for the performance.

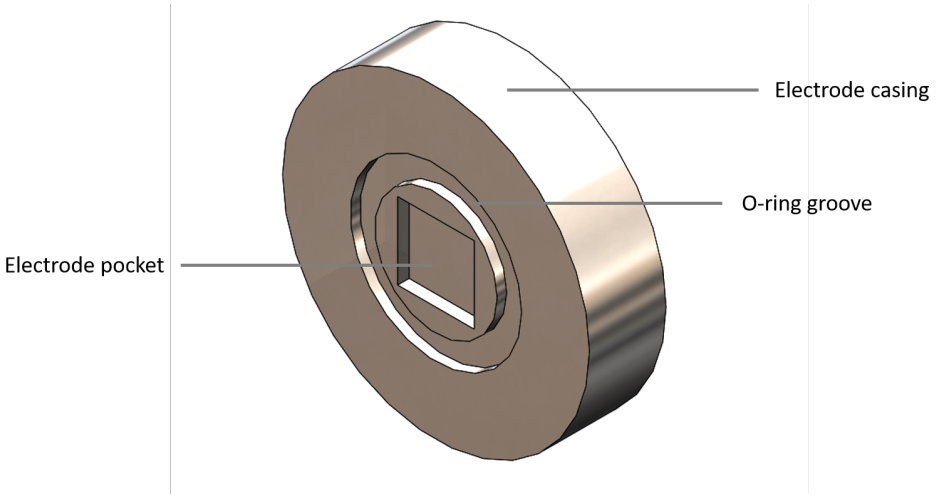

Figure 4.10: An electrode casing for the CO2 reduction stack. The square hole is placing the electrode. The circular groove is for the O-ring. This is rendered in Solid Works.

4.3.4. Current path

Another essential topic is getting current flowing through the stack. The current has to flow trough the electrodes and electrolyte for an reaction to take place. By letting the electrodes rest on the stainless steel casing, current can flow by connecting the two casing units to an power source.

Good electrical contact of the current cycle is essential for stable performance and accurate experiments. Two cables can be connected to the casing by using ring terminals. This will provide a stable connection. The circuit is displayed in figure 4.11.

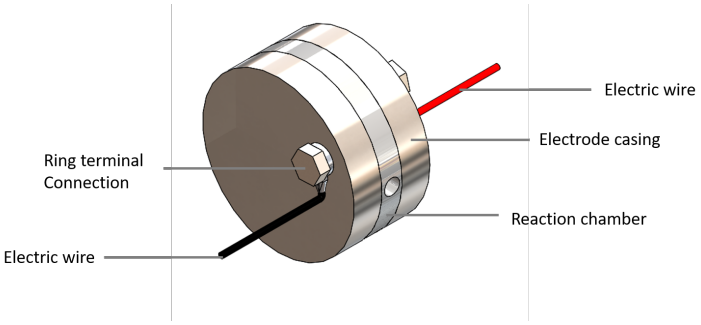

Figure 4.11: A closed stack of the CO2 reduction reactor with electric wiring rendered in Solid Works.

4.3.5. Connections for the tubing

Not only current has to flow through the reactor, but also CO_2 carrying electrolyte. IDEX Fittings will be used to connect the tubing to the reactor. There were two options considered for the fittings to connect the PEEK tubing to the reactor chamber:

- **Female fitting** - Is more easy to manufacture, but requires a require fitting port in the wall of the reactor chamber
- **Male fitting** - Is harder to manufacture and the only way to achieve this is to glue or melt tubing into a hole in the reactor chamber.

The first option will be the most reliable and flexible. IDEX has standards for holes that guarantees a certain amount of operating pressure. The second option's ability to contain pressure is dependent in the quality of the glue layer. Therefore, the first option is preferred. A technical drawing of the port is in appendix G figure G.7.

A flat bottom fitting made of PEEK will be used for this set up. This type of fitting can operate up until 172 bars of pressure which is well withing the specs and look to be the easiest to manufacture. A cross section of the reactor stack with the fitting ports can be seen in figure 4.12

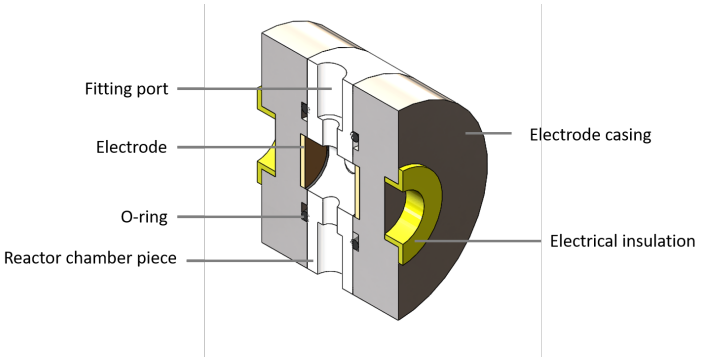

Figure 4.12: A cross section of a 3D model of a CO2 reduction reactor in Solid Works

4.3.6. Securing the stack

The pressure inside the reactor will push the stack apart if nothing prevents it. There are several options to apply a force onto the stack to keep it together. These options are displayed below in a table with their characteristics. The characteristics are:

- **Compactness** - How much volume would it take to incorporate if in the design. The setup must be able to fit in the limited space of the fume hood. Options that take less space are therefor preferable.
- **Necessities** - Tools required to assemble the option in the setup. Avoiding the need of tools will increase the space available and makes the design better adaptable.
- **Manual handling** - Ease of use for the operator in terms of setup and handling during and after assembly.
- **Price** - What is the cost of the option.

For each option commercially available products where examined and compared to each other. All the components were required to be able to exert a minimum force of 1 KN to contain the pressure in the stack and compress the O-rings sealing the stack.

Table 4.1: Multiple options to force the CO2 reduction reactor together with their characteristics relevant for the design choice. The options of this table are described in appendix H

Options	Compactness	Necessities	Manual handling	Price
Single clamp	Good	Tools	Easy	Cheap
Hydraulic Press	Bad	Lever or pump	Hard	Expensive
Clamp	Good	None	Easy	Cheap
Spring clamp	Good	Lever	Hard	Cheap
Linear actuator	Good	Current	Easy	Expensive

A clamp, specifically the heavy pressure rod pusher, model 6842, of AMF, is one option that stood out as the best candidate. This clamp can produce a maximum clamping force of 4 kilo newton. That is well within the requirements. The design setup including the clamp can be seen in figure 4.13.

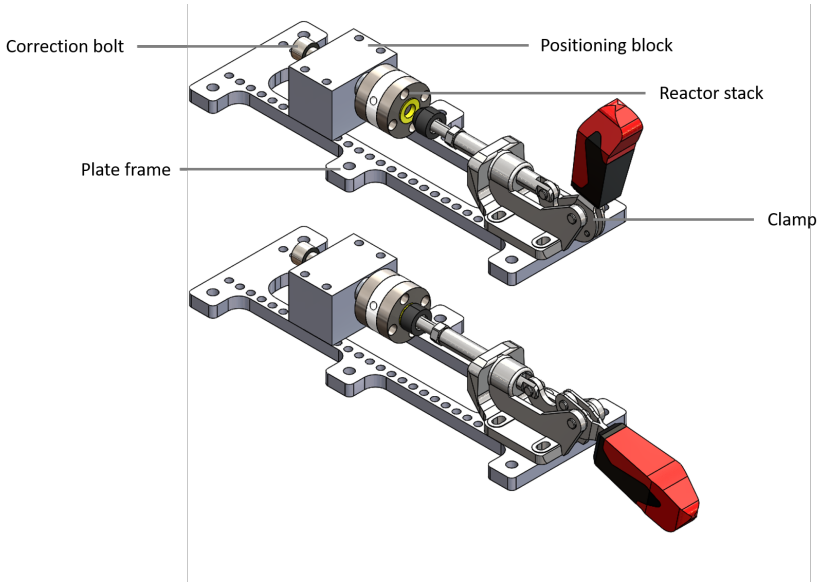

Figure 4.13: The CO2 reduction reactor stack with the clamping setup rendered in Solid Works.

The force that is exerted by the clamp can not be adjusted when it is clamping. That is why a additional correction bolt is added to the design. This bolt can push against the reactor and increase the force applied by the clamp while the clamp is applying force. A star knob will be added to the bolt to avoid the need of tools. The design not including the star knob can be seen figure 4.14 and the technical drawing of the block housing the bolt is in appendix G figure G.2.

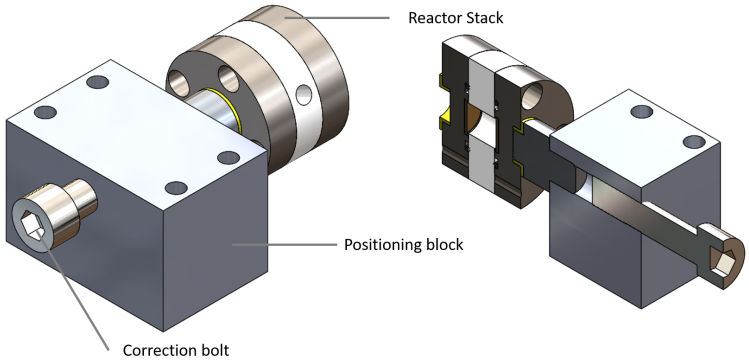

Figure 4.14: on the left is the Block that holds the CO2 reduction reactor in place. In this block a bolt can push against the stack to alter the clamping force. On the right is a cross section of this block. Both are rendered in Solid Works.

To house all the components, a frame was made from a 10 mm aluminium plate cut in shape by a water cutting device. The frame has additional holes to accommodate multiple configurations of the components. The frame has six holes on the outside of the frame that allow it to be bolted on two beams to reinforce it. The technical drawing of the frame that supports the reactor can be found in appendix G figure G.6.

To have the additional option to operate the reactor stack outside the setup and frame ((as part of a contingency plan), four 6 mm bolts were added that go through the reactor stack. These were electrically insulated by sliding bearings from the outside stack pieces.

4.3.7. Stress on the reactor stack

There are several forces applied to the reactor stack. In this subsection the resulting stresses are calculated. This is done to check if the dimension and material choices can withstand the applied forces. The reactor is mainly subject to the forces of the clamp and high pressure electrolyte. The clamp can deliver a force of 4 kilo newton and the inside pressure can go up to 100 bar.

The electrode casing is considered to be a cylinder with a radius of 40 mm. It is assumed that the force is homogeneously spread across the surface and the grooves and holes are not significant. The internal pressure will compress the casing in the same direction as the clamp, but will not increase the tension.

When equation 4.1 is applied the stress in the material is $3.2Mpa$. Stainless steel 316 alloys have yield strengths of $205 - 310MPa$ according to CES Edupack, so the clamping force will not cause yielding. The fatigue strength of the steel at 10^7 cycles is $228 - 252MPa$, so fatigue failure is not likely to occur.

However the pin that pushes against the casing will generate local stress at the pin-casing boundary that will be much greater than the overall stress. To calculate this local stress, equation 4.1 was used but on a circular surface with a diameter of the rod(20 mm). The calculated stress was $12.7Mpa$. That is still well within the yield strength of common steel alloys.

$$\sigma_{compression} = \frac{F}{A} \tag{4.1}$$

Where σ is the tension, F is the applied force perpendicular to the surface A.

The reaction chamber will be seen as a cylinder with an outer diameter of 40mm and a inner diameter of 10mm. Applying equation 4.1 and the maximum clamping force to this surface homogeneously gives

a stress of $3.4Mpa$. PEEK has a yield strength of $87 - 95Mpa$ and a tensill strength of $70.3 - 103MPa$ according to CES EduPack. The compression will not cause a failure.

The internal pressure of the chamber will cause stress as well. Because the outer diameter is 40mm and the inner diameter is 10mm this cylinder is considered to be thick walled container. Equations 4.2 and 4.3 are applied with an internal pressure of 100 bars and a external pressure of 1 bar. The tangential and the radial stress are plotted as function of the radius in figure 4.15.

$$\sigma_{tangential} = \frac{P_i * r_i^2 - P_o * r_o^2}{r_o^2 - r_i^2} + \frac{r_i^2 * r_o^2 (P_i - P_o)}{r^2 (r_o^2 - r_i^2)} \tag{4.2}$$

$$\sigma_{radial} = \frac{P_i * r_i^2 - P_o * r_o^2}{r_o^2 - r_i^2} - \frac{r_i^2 * r_o^2 (P_i - P_o)}{r^2 (r_o^2 - r_i^2)} \tag{4.3}$$

Were P_i is the pressure inside the tube, P_o is the pressure outside the tube, r_i is the inner radius of the tube, r_o is the outer radius of the tube and r is the radius parameter.

In the reactor chamber, three holes are added for the flow of electrolyte and the reference electrode, including thread for a fitting. Due to the orientation of the holes and the tangential stress vector, the stress will concentrate around the holes.

The stress will be maximized at the point where the wall is the thinnest. This maximum stress is also added to the plot in figure 4.15. It is assumed that the stress will homogeneously distributed on the remaining surface. The ratio of the remaining thickness and the original thickness is used to calculate the maximum stress. As can be seen in the graph, the stress near the holes is significantly larger.

The radial tension is presumed not to be influenced by the holes. The radial stress is a compression along the radial direction of the cylinder. This goes all trough the center. Because of the lack of material, the inside can not be pushed to the outside.

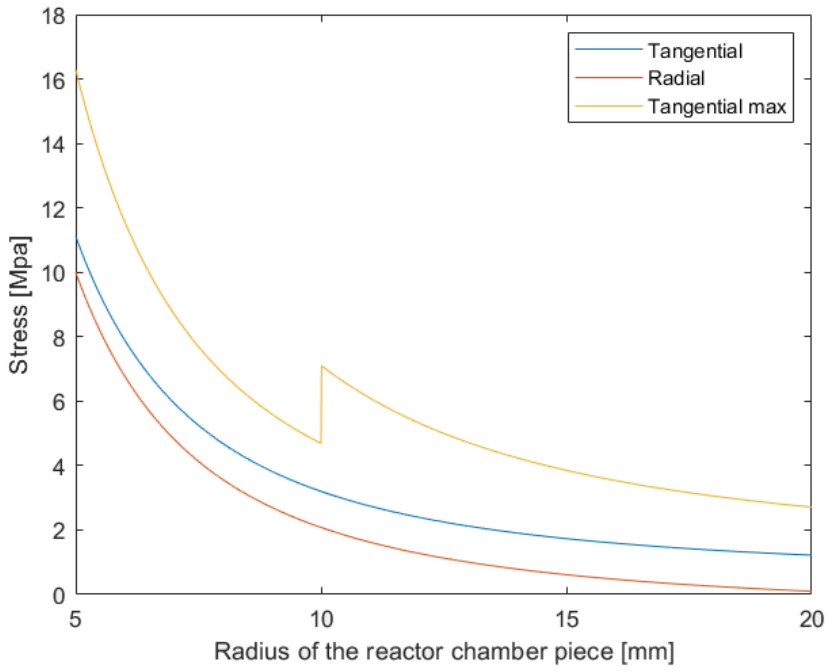

Figure 4.15: A plot of the tangential and radial stress in the reaction chamber due the high pressure inside the reactor.

To see if the material fails with the combined load, the Tresca criteria is applied. The principle stresses are the axial, the tangential and radial stress. The maximum shear stress that the material

undergoes is $26.3MPa$. Note that the axial and radial stresses are compressing, and therefore negative. According to CEP EduPack, the fatigue strength is $28.1 - 41.2MPa$. This implies that a chamber piece can be used for multiple experiments.

$$MAX(|\sigma_1 - \sigma_2|, |\sigma_1 - \sigma_3|, |\sigma_3 - \sigma_2|) = S_y \tag{4.4}$$

Were σ_x is the principle stress in the x direction and S_y is the yield stress.

With equations 4.1, 4.2 and 4.3, the different maximum stresses as function the inner radius and inside pressure of the cylinder can be calculated. If an adaptation is needed in the chamber, it is essential to know what happens to the stress when one alters the inner diameter. The results can be seen in figures 4.16 and 4.17. Increasing the inner diameter with the current outer diameter a few mm should be revisited with the specific material properties and calculations, because the current material stress is near the fatigue strength.

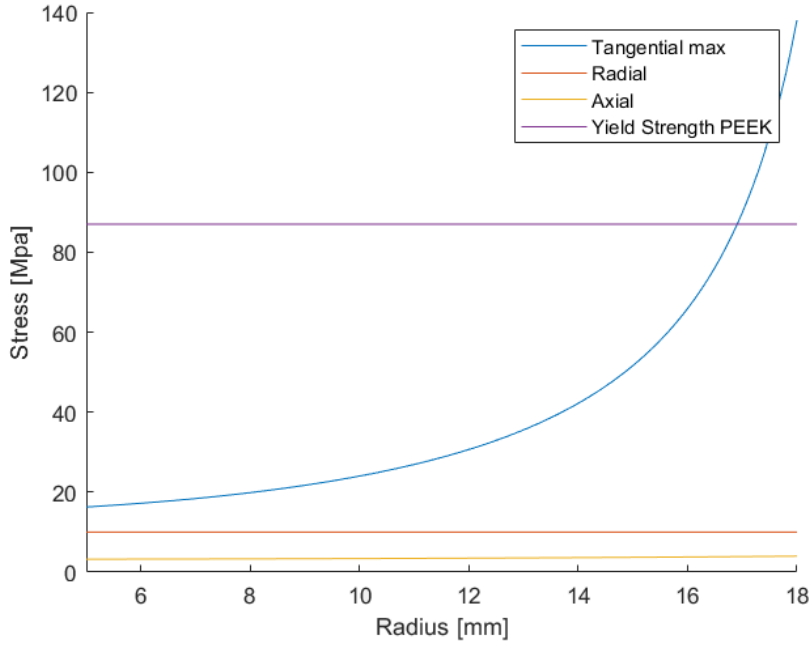

Figure 4.16: A plot of the tangential and radial stress in the reaction chamber due the high pressure inside the reactor

4.3.8. Stress on the frame

Just as the reactor stack, the supporting frame will be subject to the force exerted by the clamp. The frame will be subject to a force that will stretch it and to a moment that will bend it. The stress on the frame will be calculated, without the support of the beams it is attached to, to see what happens to the frame outside the setup.

The weakest point in the frame is next to the block mounting holes. There the holes make the frame the most thin. At the weakest point the frame consist of two beams of $12.5mm$ wide and $10mm$ high. Each of these beams has a hole in it of 6mm in diameter. The two beams will be simplified to a single beam of $13mm$ wide and $10mm$ high.

The lever of the moment applied by the clamp is the distance from the center of the reaction stack to the middle of the frame plate.This distance is $31.1mm$ The moment that is exerted by the clam is $224.4Nm$. The inertia of the profile is $2.34 * 10^{-7} M = m^4$.

The axial stress in the beam is calculated using equation 4.5 and is $30.8Mpa$. The stress caused by the bending moment will be $574.2Mpa$. Because of the orientation of the stress vectors the stress

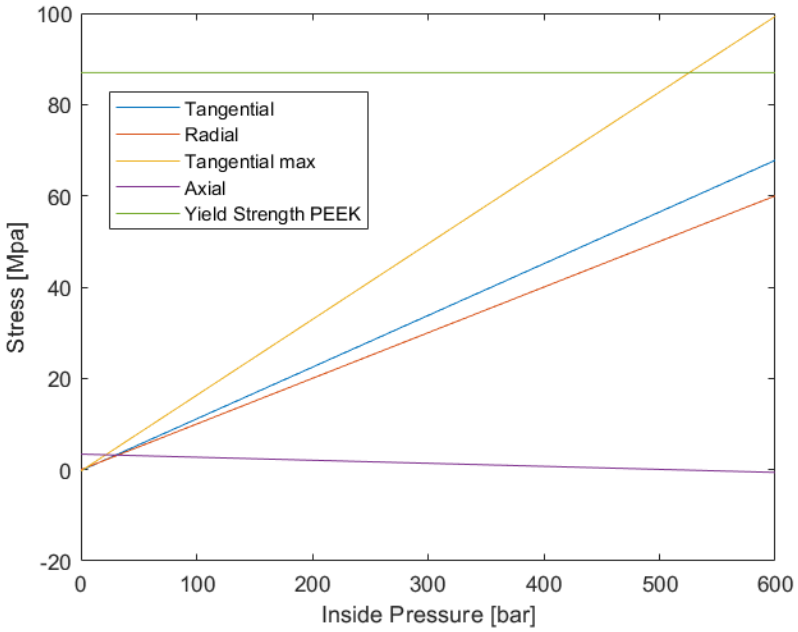

Figure 4.17: A plot of the stresses in the reaction chamber as function of the inside chamber pressure

needs to summed at the top of the profile and the axial stress need to be subtracted from the stress of the bending moment. This gives a maximum stress of $605Mpa$.

$$\sigma_{stretch} = \frac{F_{clamp}}{A_{square}} \tag{4.5}$$

$$\sigma_{moment} = \frac{M_{clamp} * h_{profile}/2}{I_{profile}} \tag{4.6}$$

Where σ_x is the tension of type x, F is the applied force perpendicular to the surface A, M is the bending moment, h is the maximum distance from the profiles mid line and I is the moment of inertia.

The Yield stress of the aluminium 5083 alloy has a yield strength of $228Mpa$ and a ultimate tensile strength of $317MPa$. According to this the frame will yield and fail when it is used outside the setup and the clamp exerts its maximum force on the stack. When this happens the stack will fall apart as well. This means that the stack can not be operated safely without the supporting beams.

4.4. The Reservoir

The second main component is is treated is the reservoir. The reservoir must contain electrolyte and dissolve the CO2 into the electrolyte. The electrolyte has to flow to the pump and reactor and thus the reservoir requires several connections. This section will cover the design choices of the reservoir.

The most influential design perimeter is the need for adaptability. With a small volume of electrolyte in the system, changes in electrolyte composition due to the operation of a set reactor will be faster than with a big volume of electrolyte in the system. Operators of experiments must be able to configure the volume according to if they want the composition to change more or less. Several options to change to volume are presented below.

- **Adjustable pistons**
- **Different reservoir containers**

- **Several filler pieces to occupy volume**

The piston design will be used, because it requires the least amount of material and is seemingly the most flexible. For the volume to change the position of one of these piston's must be able to be altered between experiments. The other can remain on one of the ends of the system.

4.4.1. The cylinder

A maximum volume of about 200 ml is desired. With this volume the concentration of the product will be 3 mM if a current density is applied of 100 mA/cm^2 producing a product that consumes two electrons and is produced with 100% FE over a time span of eight hours.

The cylinder would become relatively long if the diameter was as small as practically possible. This would be a major inconvenience in the fume hood. A large cylinder diameter would result in large forces and the need for much material to contain it. The outer diameter will be 50mm. With this as diameter the length of the cylinder becomes 150 mm. This can easily be fitted in a fume hood.

The requirements for the cylinder material were that it is resistant to acids, alkali and organic solvents. Furthermore the material must be as stiff as possible while being available in the required shape for a decent price. A stainless steel 316 alloy meets these requirements the best, because other materials with a comparable Young's modulus were much more expensive. The Young's modulus and prices were plotted against each other in figure 4.18.

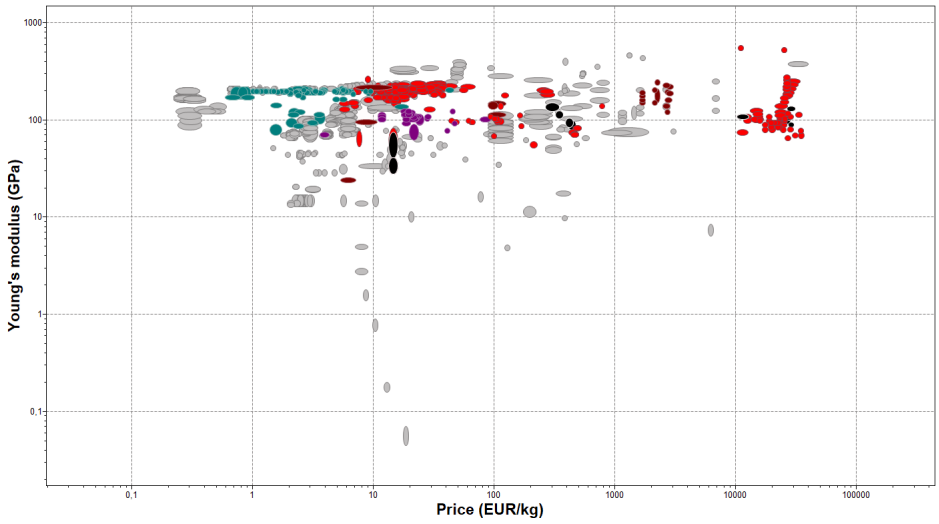

Figure 4.18: A graph displaying materials plotted using CES EduPack in a graph with their price on the X-axis and their Young's modulus on the Y-axis. Materials indicated in grey did not pass the durability filter mentioned in the report. The stainless steel alloys are displayed in teal.

The thickness of the wall is 5.08 mm. This was the size that could be supplied that would not have welding strip across the length of the tube. A welding strip negatively influences the roundness of the cylinder. The piston needs a round fit in order to properly slide through and have a good sealing. An additional reason for the thick wall is the option to weld on nipples. In case the design is not functioning as expected, the material can be used for a different configuration. The cylinders do not have to move often. Therefore, the inside of the cylinder will not be honed. A technical drawing of the cylinder can be found in appendix G figure G.3.

The cylinder is considered to be thick walled and equations 4.2 and 4.3 were applied to calculate the stress. The cylinder has a open shape, so no axial stress are present. The maximum shear stress according to the Tresca criteria is $52.3MPa$. The fatigue strength at 10^7 cycles is $228 - 252MPa$, so this cylinder can safely be used for these experiments. The stress was calculated using the matlab script in appendix D.8 and the result can be seen in figure 4.19.

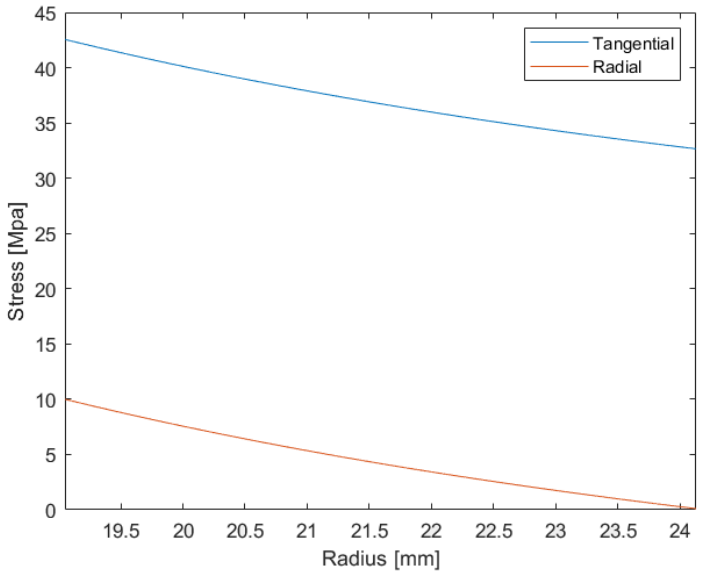

Figure 4.19: A graph displaying stress in the reservoir cylinder as function of the radius of the cylinder

4.4.2. The pistons

The pistons has to remain static during the experiments, but is designed to be dissembled multiple times. The most important aspect of the piston is the sealing. It was decided to have a O-ring for the seal. A backup ring was added to prevent rolling of the O-ring.

Because of the frequent disassembling, the piston is considered to be dynamic for sealing purposed. According to the ERIKS calculator the difference in diameter between the cylinder should be $0.05mm$ The internal diameter of the Cylinder is $38.1mm$, so the piston diameter will be $38.05mm$.

To avoid movement of the cylinder, a pin will go through the cylinder and the piston. This will be the static piston. This will be a quick release pin to provide quick disassemble times. Both the pistons can be seen in figure 4.20 and technical drawings of the pistons can be found in appendix G figure G.4 and G.5.

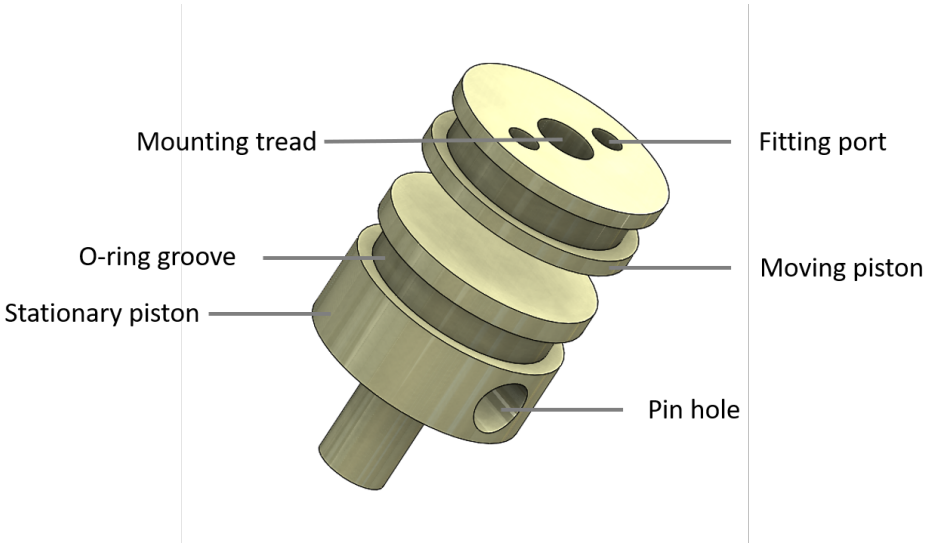

Figure 4.20: The design of the stationary and moving position

The hardness of the piston is preferably lower than that of the cylinder to prevent scratching of the cylinder. Scratches in the cylinder could cause leaks which are not beneficial for performance and

safety. The chemical resistance of the piston material should be the same as the resistance of the cylinder. Because there is already PEEK available in a cylindrical rod, that will also be used for the reaction chamber, PEEK will also be the material for the piston. It meets all the requirements.

The piston is assumed to be under axial stress only. Pressure inside is 100 bars, so that is $10MPa$ of stress on the piston. The static piston has a reduced surface around the hole for the pin. Both scenarios are below the 10^7 cycle strength of PEEK, so it its acceptable. However at the outside a rod of 12mm in diameter will push against the piston. The stress underneath the rod will be $100.8MPa$. This will cause the PEEK piston to fail.

The force of the bolt has to spread over more surface of the piston. A threaded hole was added to the piston design. The thread was simplified to a flat wall for the area calculation. The contract surface between the piston and this piece is $834mm^2$. The stress in the material there for will be $13.6MPa$. This is well below the 10^7 cycle strength of PEEK.

Two versions of the moving piston were made. One version will have port holes for the IDEX fittings and the other will have tube glued to the piston. The relative small size and little required machining makes this an ideal component to experiment on.

4.4.3. The reservoir frame

The pressure inside the cylinder will push the cylinders out. To prevent this from happening a frame is connected to the pistons. The frame will be cut out of an aluminium 5083 plate. This frame also allows for different piston positions. This in turn provides the cylinder with different capacity possibilities for all options to vary the volume of the reservoir.

The bottom piston is supported by a block connected to the frame at the bottom. The top piston will be held by M12 screw thread that runs through a different block connected to the frame. The top of the screw tread will be supplied with a rotary knob. With this knob, the user can change the length of the rod, and with that the capacity of the cylinder without tools.

The bottom block can be bolted to the frame, because it is not necessary to disassemble for cleaning the cylinder. But the top block has to be able to come of the frame for cleaning. So the top block is held in position with quick release pins. The cylinder will also be kept in place with a safety connecting it to the bottom piston.

Because of the design the the frame is not subject to a moment, but only to an axial tension in the length direction of the piston. The high pressure electrolyte will push against the pistons with $11.4KN$.

The thinnest part of the frame is next to the holes were the top block can be mounted. The cross area on that part is $600mm^2$. The tension in the cross section is therefore $19MPa$ is the stress is divided homogeneously. The yield strength of the material is $228Mpa$ as mentioned before. Therefore, the frame will not yield. The technical drawing of the frame can be found in appendix G figure G.9.

4.4.4. The blocks

The blocks hold the stationary piston and the rod pushing against the moving piston in place. The blocks can be seen in the reservoir setup in figure 4.21. Because the same force is applied to the blocks and the block's profile is thicker than that of the frame, it is assumed that the blocks will not yield. The material of the blocks is an aluminium 5083 alloy.

The bottom block with secured in place with two M10 bolts and nuts and bolts. this block can stay permanently on the frame, because the bottom piston can be taken off the block. The top block has to be taken of the frame during disassembly. To do this fast, the block is secured with two safety pins. Both pins are rated for $60kn$, so they will not yield. The technical drawing of the blocks can be found in appendix G figure G.10.

4.4.5. The fittings

The reservoir is connected with with the gas bottle, the pump and with the reactor. This can be seen in figure 4.1. Electrolyte needs to exit and enter the reservoir continuously while the electrolyte needs to be saturated with incoming CO_2. Two options were considered:

- **several pass-through through the piston**
- **Welding nipples on the cylinder with male or female fittings**

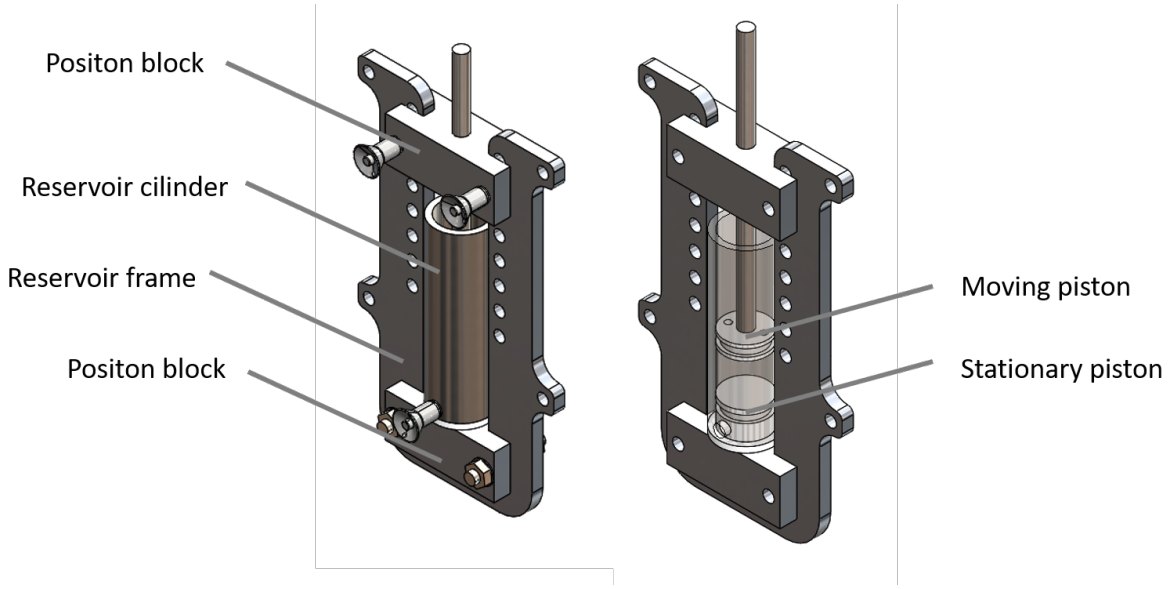

Figure 4.21: Two reservoir setups rendered in Solid Works. On the left is the normal version and on the right is a version with a transparent cylinder.

Several pass-throughs through the piston will be used. The pass-trough requires the an IDEX fitting port in the piston. A nipple welded on the outside is permanent in its position and the weld itself could deform the cylinder. This could make the sealing of the piston unreliable.

By placing the cylinder in a vertical orientation and placing all the pass-throughs through the bottom piston, all the electrolyte will be on the bottom of the cylinder with a gas pocket on top. A schematic of the configuration is displayed in figure 4.22.

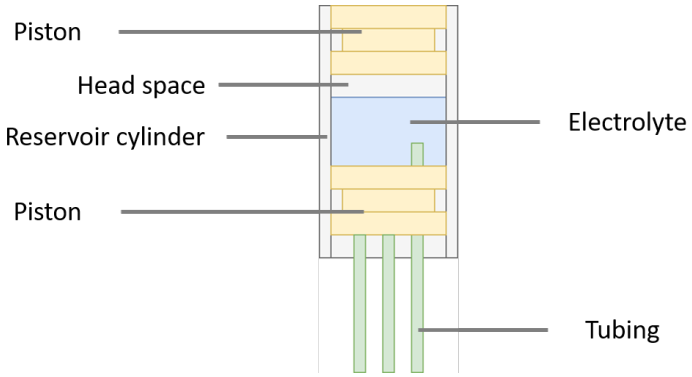

Figure 4.22: A schematic overview of the cross section of the reservoir cylinder.

This ensures that electrolyte keeps flowing to the reactor even with low liquid levels and incoming electrolyte can make extra contact with the gas. Incoming electrolyte has been through the reactor so it will have a lower concentration of CO_2. entering at the top of the reservoir the electrolyte can make contact with CO_2 to dissolve it.

4.5. The pump and the tubing

All the main component of the setup have been designed. To transport the electrolyte to the components, a pump and tubing is needed. A commercially available pump will be used. To facilitate a wide ranges of pumps and preserve adaptability, the design will be based on a pump with a high flow rate. Pumps with a lower flow-rate will and similar head will not encounter difficulties when operating in the setup by designing the setup in this manner.

The GAH series pump of microfluid will be used to function as high flow-rate pump to base the design on, because the characteristics of this pump match to required by the characteristics setup. The characteristics of the pump are displayed in table 4.2. The pump is a good standard for the setup. The characteristics that make this a good research pump are:

- **Small size** - This makes it ideal for implementing in the limited space of a fume hood environments.
- **Fluid path integrity** - The pump design ensures that the fluid passing through does not become contaminated and keeps the fluid inside. This makes analyzing results more easy and straight forward.
- **Smooth pulseless delivery** - Consistent fluid transport makes mass transport experiments more easy to processed and predicted with models.
- **Multiple operating RPM's** - Multiple flow rate can facilitate more different kinds of experiments.

Table 4.2: Characteristics of the GAH series of MICROPUMPS

Maximum flow rate	506 [ml/min]
Max rated differential pressure	5.2 [bar]
Max rated system pressure	345 [bar]
Temperature range	-46 to 177 C
Vicosity range	0.5 to 1500 cps
Maximum recomended speed	5500 rpm

To see if the pump is a good fit for the selected tubing, the pump characteristics and the pressure drop in the loop are needed. The pump characteristics are displayed in figure 4.23.

The pressure drop as function of volumetric flow rate was modeled and plotted using MATLAB. The setup was considered to be a square circuit with two tanks and 4 corners with a total length of 1 meter of 1/8" IDEX tube containing water. The plot can be seen in figure 4.24. The code and determination of friction factors can be found in the appendix D.3.

It can be seen in figure 4.24 that the operating of the pump crosses the line of the pressure drop of the system. This means that the pump will work in this scenario at the intersection. In practice the components and features will have different dimensions. However, for safety reasons, the resistance will be overestimated to be within acceptable safety margins.

4.6. Power

The power supply is used to apply a potential to the cathode and the anode by running a current through the system. This is essential in the CO_2 reduction. Most performed experiments do not exceed 500 mA/cm^2 and do not go below a cathode potential of -5V [83]. With electrodes of 1 cm^2, a power supply of that has maximum current output of 1 A and maximum potential of 20 V should be able facilitate most experiments. For the power supply there are two options that will be considered to provide a potential to the reactor stack:

- **Power supply** - This can alter the potential difference of and current running through the the system. This system only needs two electrodes.
- **Potentiostat** - This maintains the potential of the working electrode in respect to the reference electrode by altering the current. In CO2 reduction this is usually the cathode. As a result, this system needs an additional reference electrode.

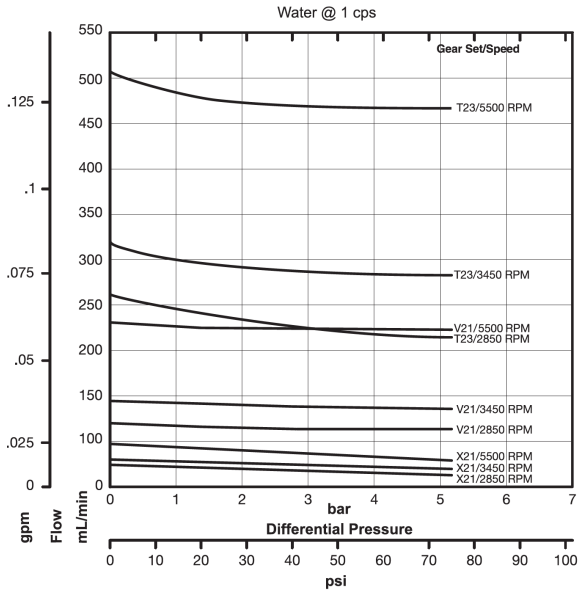

Figure 4.23: The flow rate as function of the pressure drop of the setup circuit and the operation line of the GAH series of MICROPUMPS

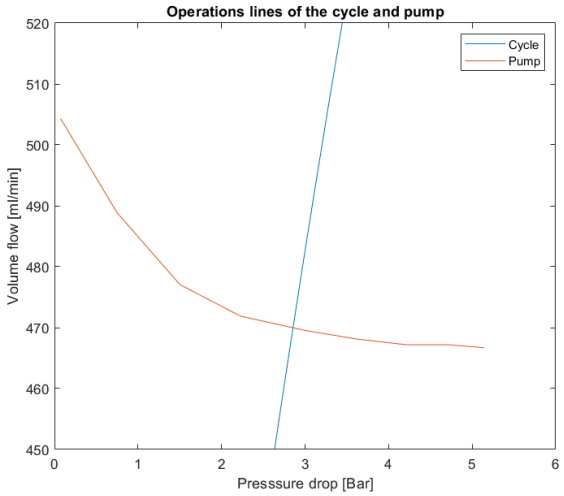

Figure 4.24: The flowrate as function of the pressure drop of the setup circuit and the opperation line of NAME PUMP

Regular power supplies are more readily available than potentiostats. However, potentiostats provide the operator with information on the absolute potential of each electrode, instead of only the potential difference given by the power supply. For that reason, a potentiostat is preferred to use during experimental work.

4.7. The main frame

All components have to be kept organised in a certain space. This will allow the operator to handle the setup more easily. An ITEM frame will be used, because these components are commercially available and they can easily fit transparent safety panels. ITEM is a nearby company that specialises in frames and devices that utilise mainly aluminium profiles. The standard profile is 40x40 mm.

These are the main characteristics of the ITEM system:

- **Flexible** - All the joints are non permanent.
- **Strong** - The joints and profiles are rated for high loads.
- **Good availability** - The company is a few minutes away from the university and there are several ITEM components in storage of the university.
- **Corrosion resistance** - The aluminium is anodized, so will have decent corrosion resistance.
- **Costly** - The frame is relatively expensive.

The main frame must be able to facilitate experiments in and out of the fume hood. A box setup was the best option for outside the fume hood, because it can house both the instruments and panels to protect the operators. The reactor will be housed on the horizontal bottom plane of the frame and the the reservoir on the back of the frame. The main frame can be seen in figure 4.25

The bottom part has two beams that can support the reactor frame. The joint-type allows the beams to change position and be removed with little effort. The profile of the the beams is 40 x 80 mm and makes it ideal to resist the bending moment of the reactor clam and for letting tubing pass underneath. The grooves are rated for 5000 N of tensile strength, so its it safe to assume with the dimension of the reactor frame in mind that the bending moment of the clamp will not yield the ITEM beams.

The back part has two rectangular profiles in the corner and two square profiles in the middle. These allow for multiple reservoirs to be mounted and other components. Example of other components can be e.g. pressure regulators or a pump.

When the reactor is in the fume hood, it does not need to protect the operator during experimentation. The sliding door of the fume hood itself is sufficient in protecting the operators. Therefore, an adapted setup is designed for the frame when it is in the fume hood. This setup is shown in figure 4.25.

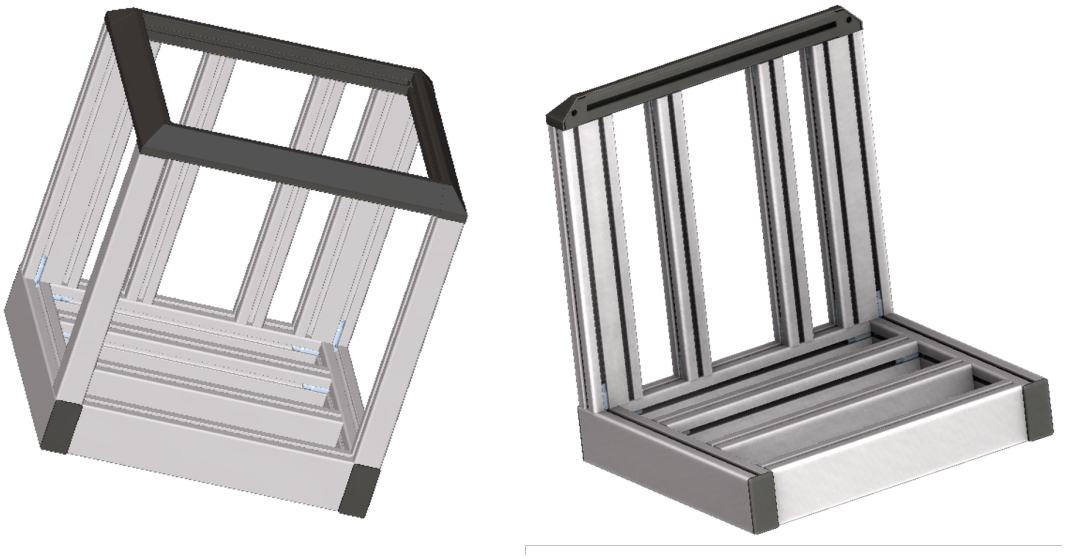

Figure 4.25: On the left, the main frame in the box configuration is shown. On the right, the main frame in the lab configuration is shown.

4.8. Summary

This section summarizes the design of the CO_2 reduction reactor system. The goal was to make an easy reactor system design that can be scaled up, which is eligible for different configurations and convenient for small scale experiments while conforming to the design parameters specified in chapter 3. All the design choices of the components have been listed in table 4.3.

Table 4.3: An overview of the design choices made with reasoning in this chapter

Component	Design choice	Reasoning
Reactor	Stack Configuration	- simple to design, easy to upscale, eligible for different configurations and convenient for small scale experiments
	PEEK reaction chamber	- Simple design due to non-conductivity
	Stainless steel electrode casing	- Simple design due to conductivity
	Female fittings	- Reliable and simple manufacturing
	Kalrez or EPDM O-ring seals	- Good corrosion resistance
	Ring terminal electrical contacts	- Stable electrical connection
	Clamp holding the stack together	- Simple, compact, no tools needed and cheap
	Bolt with star knob for adjusting clamp force	- Simple, compact, no tools needed and cheap
	Aluminium plate frame on beams	- Different configurations possible
	bolts through the reactor	- Option to run and test reactor outside setup
The reservoir	Cylinder with piston configuration	- Variable volume of the reservoir
	Stainless steel thick walled cylinder	- Good dimension, good corrosion resistance and can house different configurations
	PEEK piston	- Good corrosion resistance, material already available and will not scratch the inside of the cylinder
	Kalrez or EPDM O-ring seals	- Good corrosion resistance
	Female fittings in the moving pistion	- Reliable and simple manufacturing
	Addtional piston with alternative fitting	- Reliable and simple manufacturing and ability to test additional design choice
	Aluminium plate frame	- Different configurations possible and supports the use of the moving piston
	Aluminium placement blocks	- Different configurations possible and supports the use of the moving piston
Pump	The GAH series pump of microfluid	- Pump with good qualities
Tubing	IDEX 1/8” PEEK tubing	- Good corrosion resistance,low pressure drops and a wide variety of products
Power supply	Potentiostat	- Option to control the absolute potential of the working electrode
Main Frame	ITEM aluminium profile frame	- Good availability, light weight and easy to adjust and add components

5

Experimental

Several test are needed to validate the design and its characteristics. The most important reason to test is to see if the reactor can safely hold the pressure inside. The second most important reason to test is to see if the reactor can facilitate the CO2 reduction reaction. The system must provide these while being easy to assemble and operate. This chapter will go over the tests conducted.

First, tests will be performed on a small scale to see if these are successful. Afterwards, the complexity and scale of the reactor will be increased. With this approach, the individual components can be reviewed and individual flaws will not hinder the system functioning. The main characteristics the components and system will be reviewed on include:

- **Pressure containment** - Do the components contain the desired pressure
- **Handling** - Does the component/system takes a lot of time to setup/adjust
- **Material-chemical capability** Is there unwanted corrosion on the components
- **Safety** - Can operating the setup harm the user or environment
- **Adaptable** - How easy can the components be replaced or can additional components be attached
- **Location** - Can the setup perform on the designated locations
- **Effectiveness** - Does the component/system accomplish its function
- **Reliability** Is there damage to the components that is not supposed to happen

5.1. Reactor pressure tests

To review the reactor stack and its supporting components, 50 bars of pressure was applied to the stack in multiple settings. The reactor was first constructed from the ground up, then pressurized in these settings and finally disassembled and cleaned.. The pressure is facilitated by a manual pump that will pressurise a mixture of water and air inside the reactor. If the pressure is reached the pressure is maintained for one hour. The setup is shown in figure 5.1.

These different settings of pressure tests were conducted :

- Holding the stack together with bolts and no O-ring at the fittings
- Holding the stack together with bolts and a O-ring at the fittings
- Holding the stack with a modified reactor chamber together with bolts and a O-ring at the fittings
- Holding the stack together with the clamp and a O-ring at the fittings
- Holding the stack together with the clamp mounted on the main frame and a O-ring at the fittings

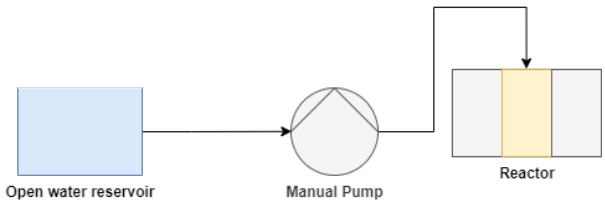

Figure 5.1: The schematic of the setup used for the pressure test.

5.2. Reactor electrical continuity tests

To test if the reactor design would give a potential to the electrodes if a power source was connected, a few continuity tests were conducted. By performing these test before operation, possibility of a fault electrical connection was ruled out. The tests were done with a Mastech MS8302D digital multi-meter. The multi-meter was set on test mode(200 ohm). When there is continuity and the resistance is lower than 20 ohm, the multi-meter would give a sound signal.

These different settings of continuity tests were conducted :

- Electrode casing with a folded aluminium electrode in the casing
- Electrode casing with a tin electrode in the casing
- Electrode casing with a Graphite electrode in the casing
- Electrode casing with a tin electrode in the casing while the reactor chamber was mounted on the casing
- Electrode casing with a Graphite electrode in the casing while the reactor chamber was mounted on the casing
- The full reactor stack held together with both the bolts and the clamp

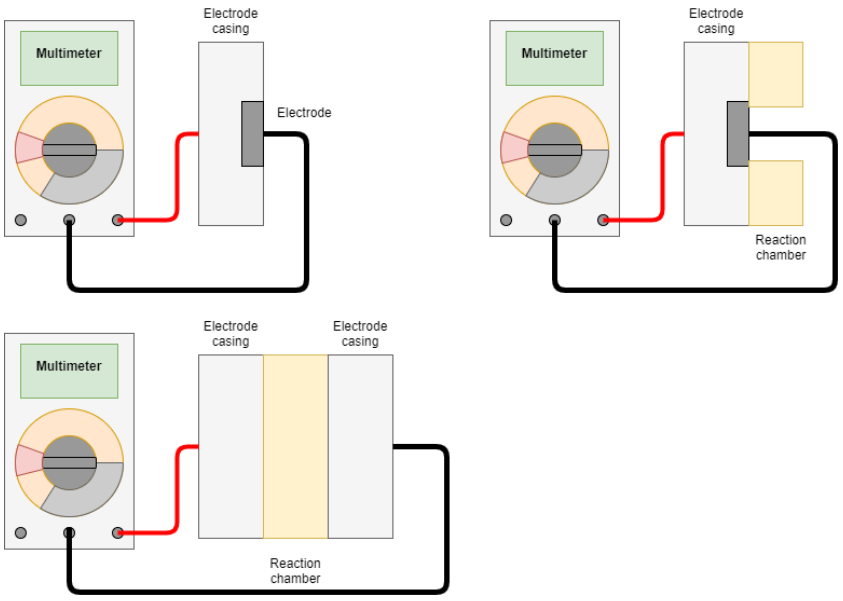

Figure 5.2: Schematics of the continuity tests conducted.

5.3. Reservoir pressure test

To review the reservoir, 50 bars of pressure was applied to the reservoir in multiple settings. The reservoir was first constructed from the ground up, then pressurized in multiple internal volumes and finally disassembled and cleaned. The pressure is facilitated by a manual pump that will pressurise a mixture of water and air inside the reservoir. If the pressure is reached the pressure is maintained for one hour. The setup is shown in figure 5.3.

These different settings of pressure tests were conducted :

- High internal volume
- medium internal volume
- low internal volume
- A medium internal volume with a greased cylinder wall
- A alternative piston with glued tubes
- Modified Cylinder with smoothed edges

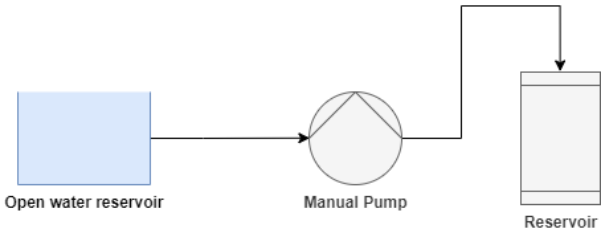

Figure 5.3: Schematic of the setup used for pressure testing the reservoir

5.4. System pressure test

The setup was tested without a pump cycling water in the system and a water pump was used for pressurizing the setup. This was a single test to see if the setup will again contain the pressure as a whole. The system was assembled and pressurized up to 50 bars and monitored for one hour. The test setup can be seen in figure 5.4.

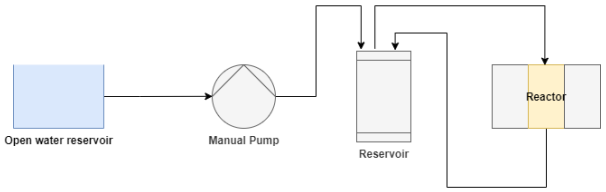

Figure 5.4: Schematic of the setup used for pressure testing the system

5.5. Pump tests

The system was tested with a running pump that pumped electrolyte through the system while pressurized. Since the pump designed for the setup was not available, a Varian Prostar 210 stainless steel pump head with a 10 ml/min max flow rate was used. In this configuration the pump delivered the maximum volume flow of 10 ml/min based on the specs of the machine.

The tubing was different from the design as well. The pump and the gas bottle had swagelock 1/16” and 6mm tubing and fittings. These tubes were connected via adapters to the tubing of the design. The ferule that was present in the pump was unknown and some adapters that were used were intended for 3mm tubing instead of 1/8”(3.175mm) tubing. Therefore, the tests were not operated at the design pressures.

The fluid in the setup was a 0.5 M solution of sodium sulfate in water. To ensure that air was out of the pump, the manual valve was opened and pressure was applied on the piston in the reservoir until was came out the tube connected to the manual valve. The piston was lifted after the flush to create head space in the reservoir.

The manual valve was slightly opened at the beginning of the test to validate the flow of electrolyte. After the validation the manual valve was closed. The setup could then be pressurized. A CO2 gas bottle was opened and the gas was allowed to flow in the cycle via a regulator. The regulator was set to 2 bar. The pump ran for 30 minutes after the system was pressurized. There was approximately 75 ml of electrolyte in the system. This allowed the CO2 to dissolve into the fluid. The setup can be seen in figure 5.5.

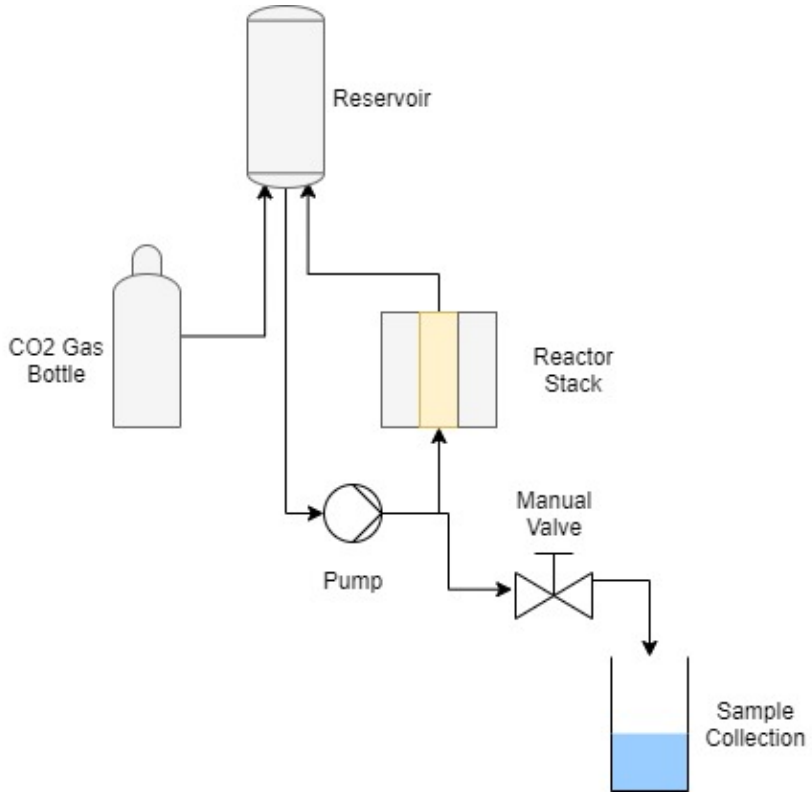

Figure 5.5: Schematic of the setup used for pump testing

5.6. Operation test

The operation test was conducted by adding a VOLTCRAFT LPS 1305 as power source to the setup. A cell potential of 3.5V +/- 5mV was applied to the stack a current of initially 10 mA. The test was run for 45 minutes at the 2 bars of CO_2 pressure and the pump was set to 10 ml/min. During the test the current increased from 10 mA to 20mA. After 45 minutes the pressure was increased to 5 bar by altering the regulator of the gas bottle. This was run for again 45 minutes at with the same potential and 20mA of current. The setup can be seen in figure 5.6.

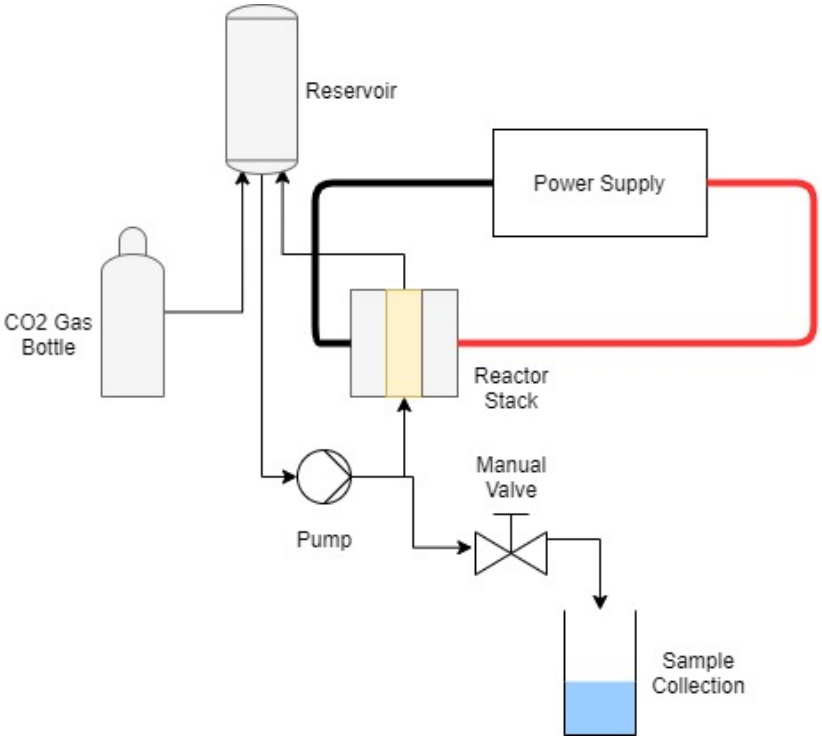

Figure 5.6: Schematic of the setup used for the operation test

During the operation test, samples were taken after the 2 bar and 5 bar operation. Samples were taken by opening the manual valve and letting 30 ml into a beaker. The beaker was stored in the lab to let any particles settle on the bottom of the beaker. The samples were analysed by HPLC.

5.7. Operation test with a reference electrode

A reference electrode (leakless Ag/AgCl) was added to the chamber of the reactor. 65 +/- 10 ml of a 0.5 M solution of sodium sulfate in water was used as electrolyte. A pressure of 5 bars was applied by letting CO_2 flow in the reactor. the regulator was set at 5 bars of pressure. The pump was turned on at 10 ml/min for 25 minutes to mix the electrolyte and let the CO2 gas dissolve. A current was applied on the reactor of 70 mA.

The electrode were made differently than the operating test without reference electrode. A mold provided tailor-made lines on the material. The electrodes were then cut to size with a Stanley knife. During the cutting process, the electrodes were constantly fitted in the casing to check size. When the electrodes had the correct fitting, they were abrased by a fine sanding pad.

During the operation the potential of the cathode was was measured every few minutes. This was done by measuring the potential over the reference electrode and the cathode. All the electrolytes was drained from the system into a beaker. The beaker was stored in the lab to let any particles settle on the bottom of the beaker. A sample of the beaker is then analysed by the HPLC.

6

Results and Discussion

In this chapter, the results of the tests are discussed. The test were performed to test the design on the parameters and to see if the reactor processes a CO_2 reduction reaction product. The results of all the pressure tests combined are reviewed first. After that the results of the continuity tests will be reviewed. Finally the results of the pump and operation test are discussed in the final chapter.

6.1. Pressure tests

In this section the components and the setup are reviewed according the relevant characteristics of the previous chapter:

- **Pressure containment** - Almost no leaks were detected in all the test and pressure was maintained in almost all tests. The leeks that did occur, were between the fittings and the machined peek components. The leeks were not present when a O-ring was present. The surfaces of the machined components were rough compared to the PEEK staff and IDEX parts. This suggests that PEEK parts that are machined are not suitable for high pressure flat-bottom fittings without O-rings. Additional polishing of the bottom of the port could reduce the roughness to an extent that O-rings are not necessary for a sealing.
- **Handling** - In the test, all the components were easy to assemble and took little time except for the reservoir pistons. The pistons were difficult to position in the cylinder in both the dry and greased tests. The use of grease will contaminate the electrolyte, but the grease was used to determine of the friction was due to material choice. Both tests where hard to assemble, so it was not the material choice, but presumably the roundness of the cylinder. It was also hard to control the amount of electrolyte in the system and getting it in without spilling electrolyte in the environment. The current piston design for the reservoir is therefor not suitable for easy handling.
- **Material-chemical capability** - There was no visible corrosion.
- **Safety** - When leaks occurred the liquid did not spray out the system or components. The liquid dripped out, because the leaks were not occurring on the surface of the component or setup.
- **Adaptable** - The components could be modified easily and still perform well. In appendix A figure A.12 is a picture of the modified piston on top of the reservoir setup.
- **Location** The components and setup had good mobility and performed well in all locations. The tests were done on multiple locations and sometimes moved from one to an other. Pictures of the Assembly and operation can be seen in appendix A figures A.6,A.8,A.9 and A.11.
- **Reliability** - Several O-rings were damaged in the pressure tests, but all other components were not affected. These O-rings were all damaged in the reservoir cylinder. This was presumably cause by the sharp edges of the cylinder. Tests with the smoothed edges did not have damaged O-rings. A O-ring damaged by the cylinder can be seen in appendix A figure A.17.

6.2. Continuity tests

In this section the reactor stack, the electrodes and frame are reviewed according the relevant characteristics of the previous chapter :

- **Handling** - The electrodes were hard to get into the correct shape. Its was intended to get a tight fit in the casing. The materials properties and shaping methods were a mismatch.
- **Adaptable** - The electrodes were made quickly to fit in the casing
- **Location** - Because the reactor was small the tests could mostly conducted in a office. This was ideal for documenting the results.
- **Effectiveness** - All the electrodes had the intended continuity and resistance of less than 20 ohm except for the graphite electrode. When the multi-meter was connected to the electrode and casing, the signal was less constant than with the tin and aluminium electrode. With the reaction chamber was mounted on the casing the signal of the multi-meter was consistent. The inconsistent continuity was probably caused by the shape of the layered electrode. Around the edges the electrode was de-laminated, so it could be that the pressure of the chamber pushed those layers together.

6.3. Pump and operation test

In this section the system in operation is reviewed according the relevant characteristics of the previous chapter :

- **Pressure containment** - The components did not have leaks during the operation
- **Handling** - The setup was easy to build, because the tubing was of different companies and various diameters of tubes, a lot of time went into connecting and checking tubing. The piston design was beneficial for manually pressing the electrolyte through the system, but was not easy to fill up with liquid. Mounting the reservoir was difficult to do without damaging the tubing or spilling the electrolyte.
- **Material-chemical capability** - At the cathode casing there was a orange deposit around the tin electrode. This was presumably the iron of the casing that was oxidized. The casing and the electrodes have to be designed or/and assembled to stop excess current from getting through the steel rather than through the cathode. A picture of the oxidation is in appendix A figure A.14
- **Safety** - The poor handling of the reservoir could be a hazard if a operator was doing experiments with corrosive chemicals. The absence of leaks was good for the safety of the environment.
- **Location** - The test was done with outside the lab and it did not affect the process negatively.
- **Effectiveness** - The HPLC analysis showed that there was possibility of 0.03 mM of formate present in both samples taken from the subsequent operation tests. The analysis graph can be seen in appendix B figure B.1. The efficiency of the first operation test was therefor 1.0 +/- 0.8 % and the second was 0 % efficient. However the corresponding peak had a retention time of 24 min instead of the formate calibration time of 26 min. There are several explanations for these measurements:
  - Equilibrium was reached between reduction into formate at the cathode and oxidation of formate at the anode.
  - The graphite anode was giving off black particles that could have adsorbed the formate.
  - The measured peak was something else and no formate was produced
  - The corrosion on the steel casing represented the entire current and no current flowed through the tin electrode, hence no formate was formed.

  The last possibility is the least likely because a Sn based CO_2 reduction reaction is well understood and formate is the main product [83]. The first two possibilities are more likely to have happened. The most likely scenario is that the first two possibilities both happened simultaneously.

- **Reliability** - There was no visible damage to the system except for oxidation, so in general the design handled the tests well.

6.4. Operation test with reference electrode

In this section the system in operation is reviewed according the relevant characteristics of the previous chapter. This test was similar in results in multiple aspects, so the pressure containment, handling, safety location and reliability were left out:

- **Material-chemical capability** - The better fitting tin electrode did not have rust on the edges on the casing. Because of the better fit, excess current from getting through the steel rather than through the cathode. The design will need some modifications to be more reliable. The electrode casing without rust can be seen in appendix A figure A.1
- **Adaptable** - The reference electrode was added and the modification of the reaction chamber only took 1 hour and was done by someone with limited experience in machining. This was because the material is easy to work with and the shape makes is possible to have a large tolerance. Pictures of the modification process are in appendix A figure A.4.
- **Effectiveness** - The HPLC analysis gave two peaks at retention times 24 min and 26 min. The 26 min peak correspond well with the formate calibration retention time of 25.83 minutes. The peak at 24 minutes corresponds to 0.057 mM(0.3 +/- 0.3 % FE) and the second peak at 26 minutes corresponds to 0.188 mM (1.1 +/- 0.04 % FE) of formic acid. The HPLC data can be seen in appendix B in figures B.2 and B.3. In this test thee graphite electrode giving off more black particles than the first test. Pictures of the reactor with the black particles are shown in appendix A figure A.5 and A.10. Comparing these results with the previous test shows :
  - The first two tests may not have been producing formate, because this test had a peak at a different retention time closer to the calibration time and better electrode surface quality.
  - The black particles had limited influence on the concentration of formate. All tests had comparable (potential) formate concentration , but there were significantly more particles in the last test.
  - Formate produced at the cathode was being consumed at the anode. This effectively limited the concentration.

7

Conclusion

A literature study on electrolysis cells and the electrochemical reduction of CO_2 was carried out. The conclusions from this study have been used to formulate design parameters for the design of a new CO_2 reduction reactor system. From these design parameters, it is clear that such a reactor system should be an easy to handle, adaptable and a safe tool, which is able to conduct high pressure experiments with corrosive electrolyte. The reactor system should be usable both inside and out of the lab environment.

With these design parameters in mind, a CO_2 reduction reactor system has been designed and constructed. With this reactor, experimental tests have been conducted to identify whether the reactor system functions as intended, and what the advantages and possible weaknesses of the reactor design are. Below, each design parameter is reviewed based on the conducted experimental tests.

High pressure

The reactor could withstand all pressure tests. The reactor only leaked without O-rings, because the tolerances of the fitting port could not be met. The design itself was not flawed, but the manufacturing of the fitting port was not suitable. Moreover, the O-rings in the casing and chamber piece provided a reliable sealing. With the modifications the system can reliably handle the required high pressures, , but the design goal of minimizing parts was somewhat sacrificed

Chemical Resistance

The only instance of corrosion occurred at the cathode casing with an electrode with a poor fit in the pocket. The corrosion was likely due to excess current going through the steel casing. To make the design more reliable the fit of the electrode must be tight. Overall the material choices matched the requirements of the parameters.

Fast assembly and disassembly

The system was quick to assemble with every test despite the design of the reservoir. All test setup were build within the hour. When the correct tubing for the design is available for the operators, the setup time will be even less. If the reservoir design is modified the setup can reach its potential and can perform to the desired standards.

Adaptability

The piston fitting, electrode manufacturing and reactor chamber design could all be modified and replaced withing a few hours. The simple design of many parts lends itself to adaptations and the cylindrical staff design choice allows for quick and cheap replacements. The systems adaptability performs according the parameters.

Location

The setup had all of its test out side the lab during testing of the design. Only 4 bolts are needed to change the frame to the lab setup, so the same performance can be expected in the lab without much tinkering. The design is therefor well suited for both locations.

Safety

The reservoir was hard to work with in a precise and clean manner due to the difficult assembly of the reservoir. The whole setup leak-less and reliable during operation. When the operation method or design on the reservoir is improved, the design meets the safety goals.

In conclusion, the majority of the design choices were able to provide the desired characteristics of the reactor system. The design choices that did not deliver the desired results, gave important additional insights in what is important in designing a CO_2 reduction reactor system. This shows that trying the unconventional designs is important in gathering knowledge. Overall, this thesis is a step for furthering the design of CO_2 reduction reactors for research, which will in turn facilitate important further research into the electrochemical reduction of CO_2.

8

Recommendations

The design and construction of the CO_2 reactor system gave insight in what can be modified to improve the design. The current system is not yet at its peak potential. For the safety of the operators and for accumulation of knowledge, it is important that the setup is improved. Therefore, recommendations for improving the the design are focused on the handling and the reliability of the system. All the recommendations that require a new design have been worked out, or an example is presented in appendix C.

Below is a list with proposed improvements:

- **Grooves and holes for the fitting port O-rings** - The O-rings function the best when they are placed in a hole or groove with the right dimensions. O-rings are not supposed to seal two flat surfaces. By adding grooves/holes for the O-rings in the fitting ports, the handling and reliability will increase. The concept is shown in appendix C.2.
- **Research achieving a smooth bottom of the fitting port** - Using the IDEX fitting as intended would be a major benefit for the handling and reliability. This solution is only viable if it requires less effort than making holes/grooves for the O-ring.
- **Smaller non-metallic bolts** - The bolts proved useful for the assembly and transport of the stack. To make them more design orientated, the can be made thinner and from polymers materials. This frees up room in the stack and eliminates the need for electrical insulation.
- **Add additional valves to the setup around the reservoir** - The problem in handling the reservoir was the spilling the electrolyte, potentially causing hazardous situations. If valves are added, the tubing can be connected later while the filler reservoir is mounted. IDEX have a PEEK shutoff valve in their product range that seems the be the best fit. This was added to a concept setup in appendix C.1.
- **Hone the inside of the of the cylinder** - One of the reasons the piston had a lot of trouble going the tube, was the roundness of the tube. By honing the tube handling will improve.
- **Holes trough the reservoir frame blocks** - The blocks are in the path of the tubing. To eliminate this problem holes can be drilled trough the blocks to facilitate a clear path. The concept design of the blocks can be seen in appendix C.3.
- **Additional components to fill the reservoir and flush the system** - With the current setup the filling and flushing of the system is not easy and inaccurate. By adding several components to the setup, the handling can be greatly improved. This was added to a concept setup in appendix C.1.

A

Pictures of the components and setup

Figure A.1: The reactor casing with tin electrode and O-ring after operation.

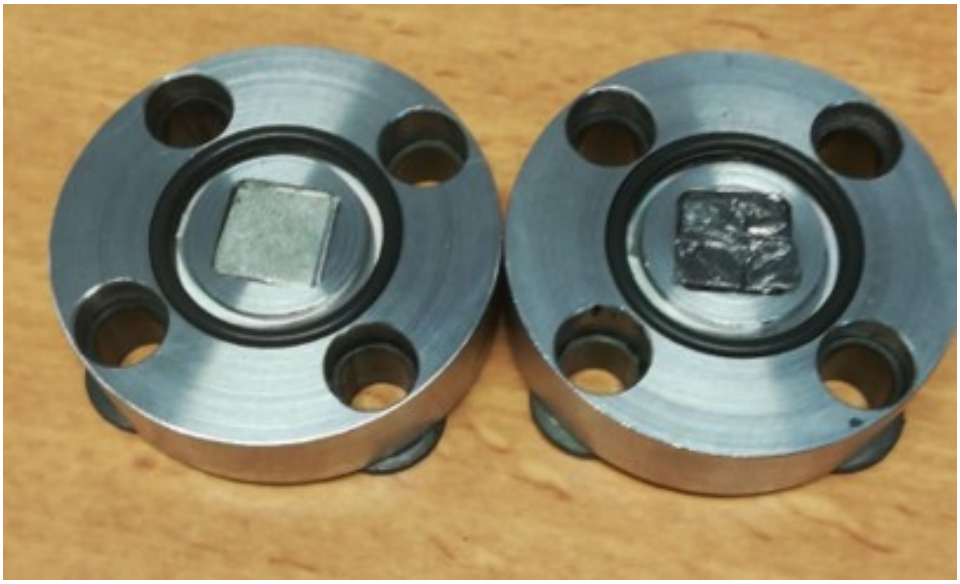

Figure A.2: The electrode casings with Electrodes and O-rings before operation.

Figure A.3: Reactor chamber with added reference electrode.

Figure A.4: Machining the existing reactor chamber

Figure A.5: Disassembled reactor stack after the operation test with reference electrode.

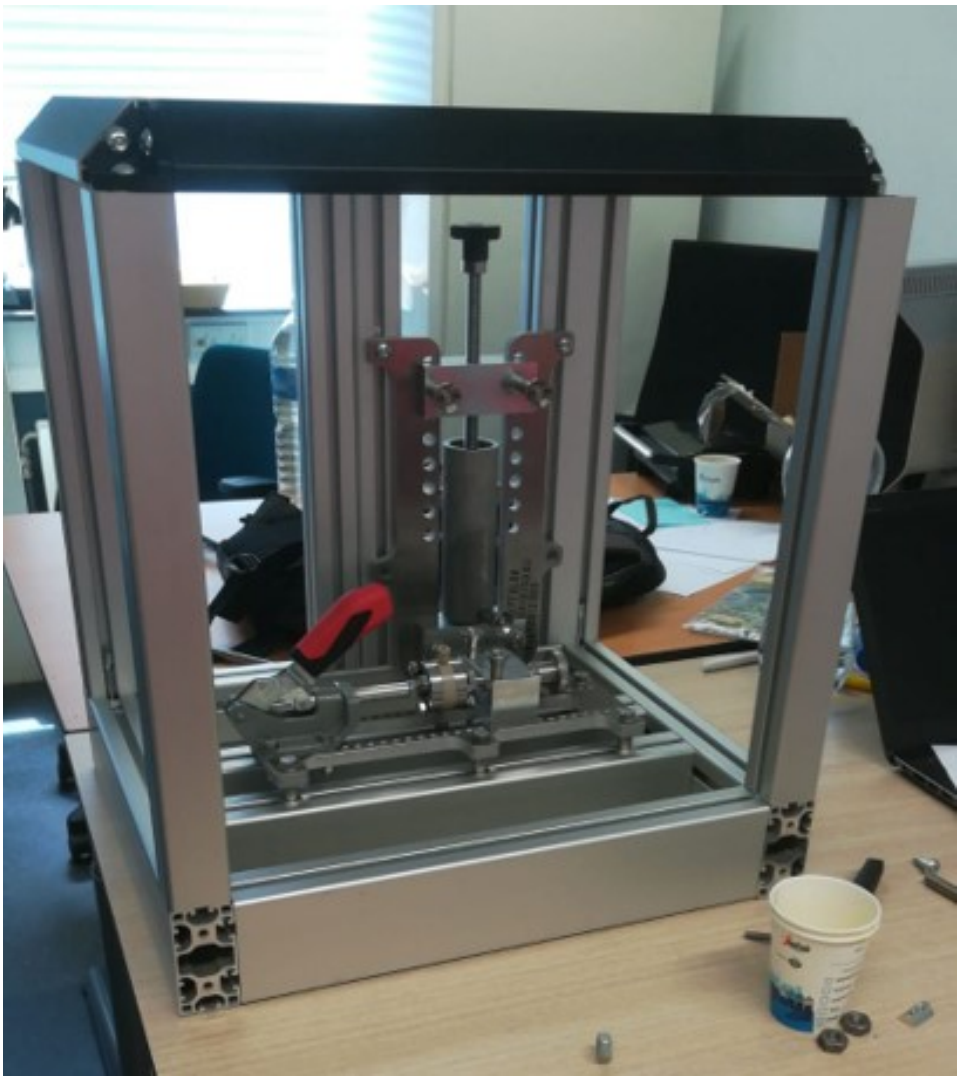

Figure A.6: The main frame with reactor stack and the reservoir mounted.

Figure A.7: The piston after an operation test

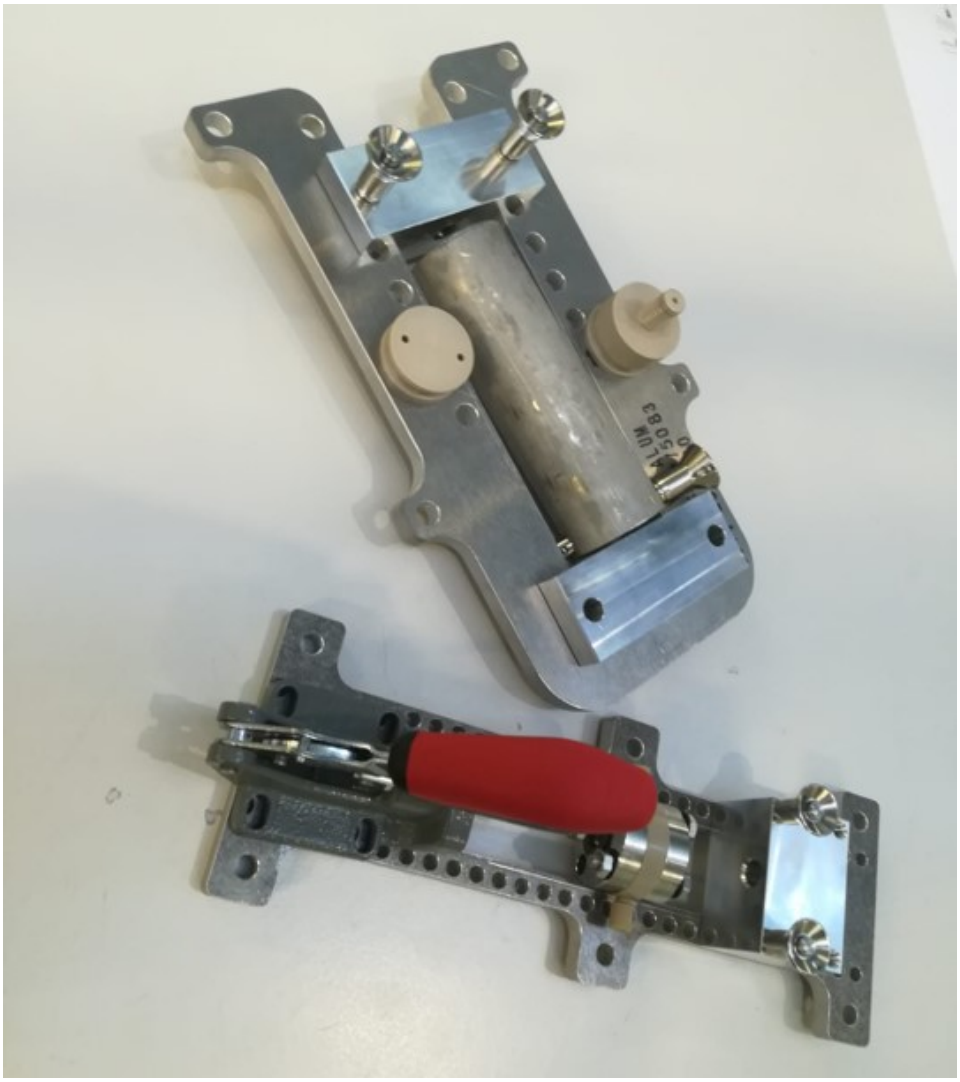

Figure A.8: The reservoir and reactor stack in their frames

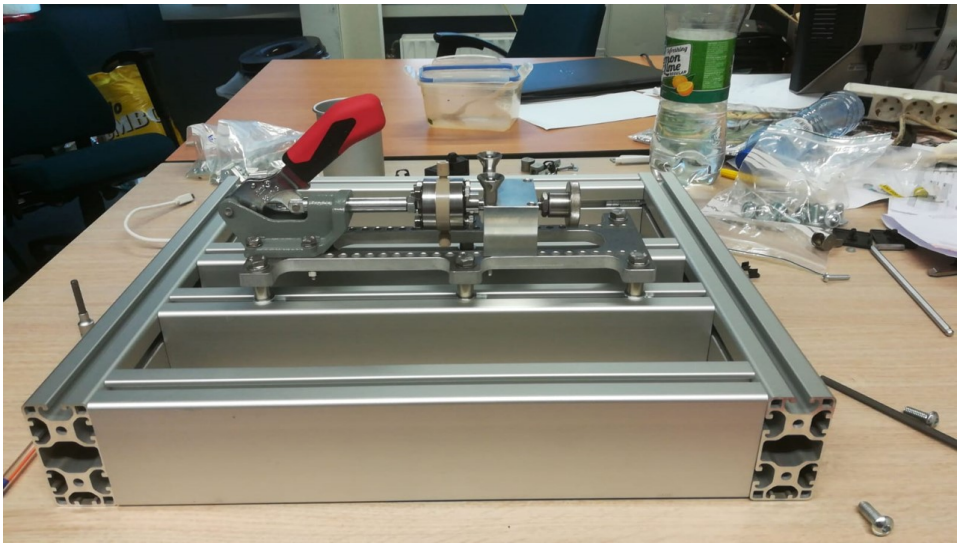

Figure A.9: The reactor stack system mounted on the bottom of the mainframe.

Figure A.10: reactor stack after the operation test with reference electrode.

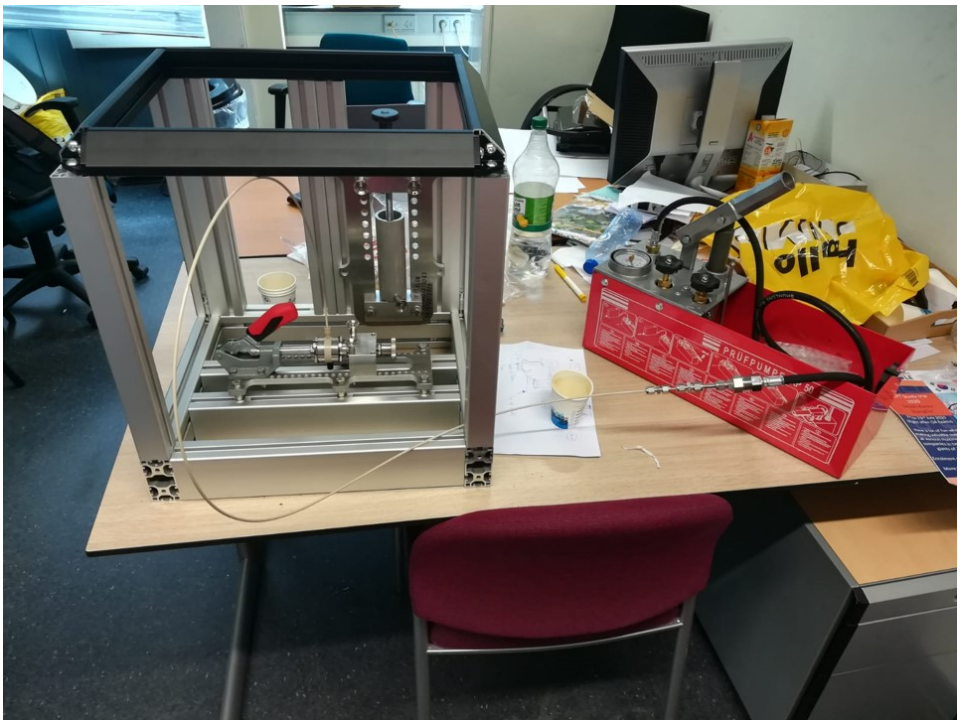

Figure A.11: Assembly of the reactor pressure test in the office.

Figure A.12: The reservoir in its frame with the modified piston on top.

Figure A.13: Samples in the make for the HPLC

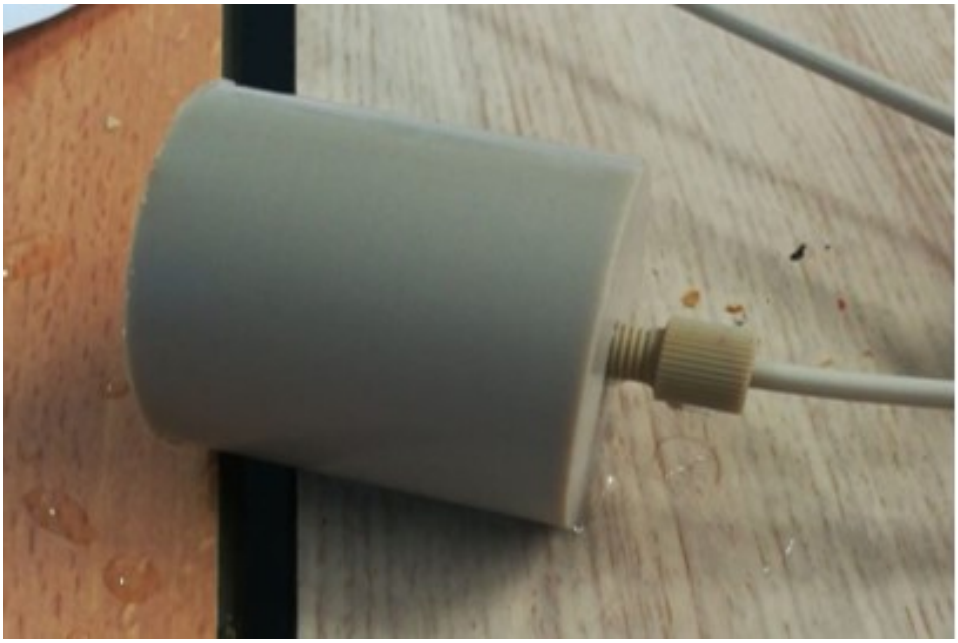

Figure A.14: The fitting tester with tubing attached.

Figure A.15: Tubing with a ferule and an O-ring.

Figure A.16: The electrode casings after the operation test without reference electrode.

Figure A.17: A damaged O-ring

B

Data from the HPLC analysis

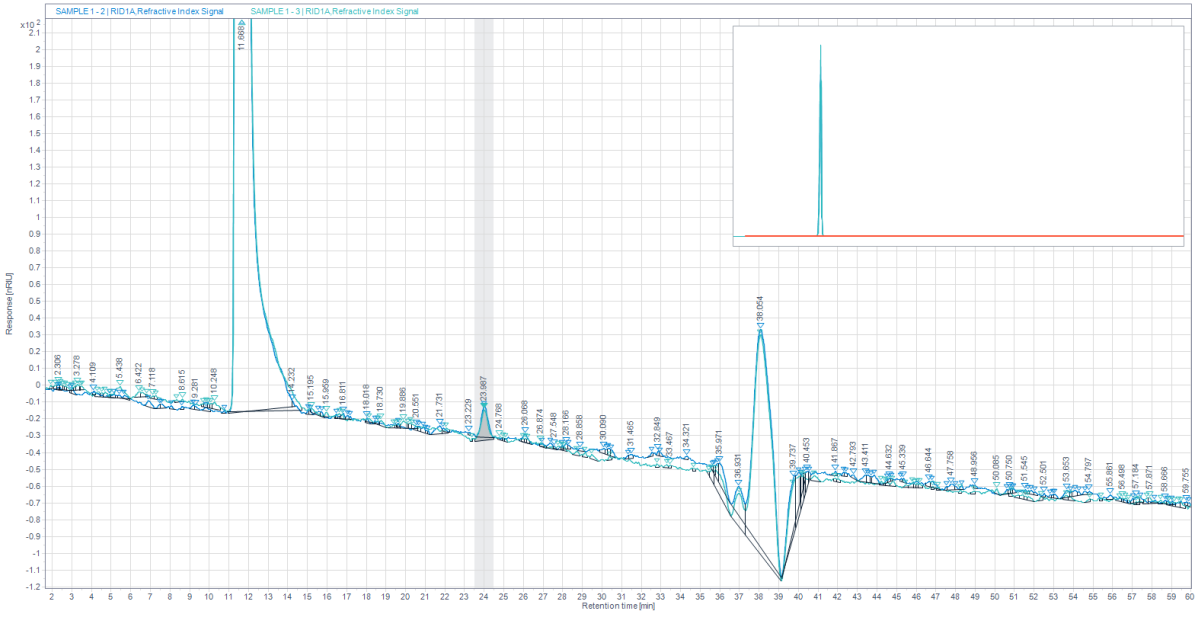

Figure B.1: The HPLC analysis data of the operation tests without reference electrode

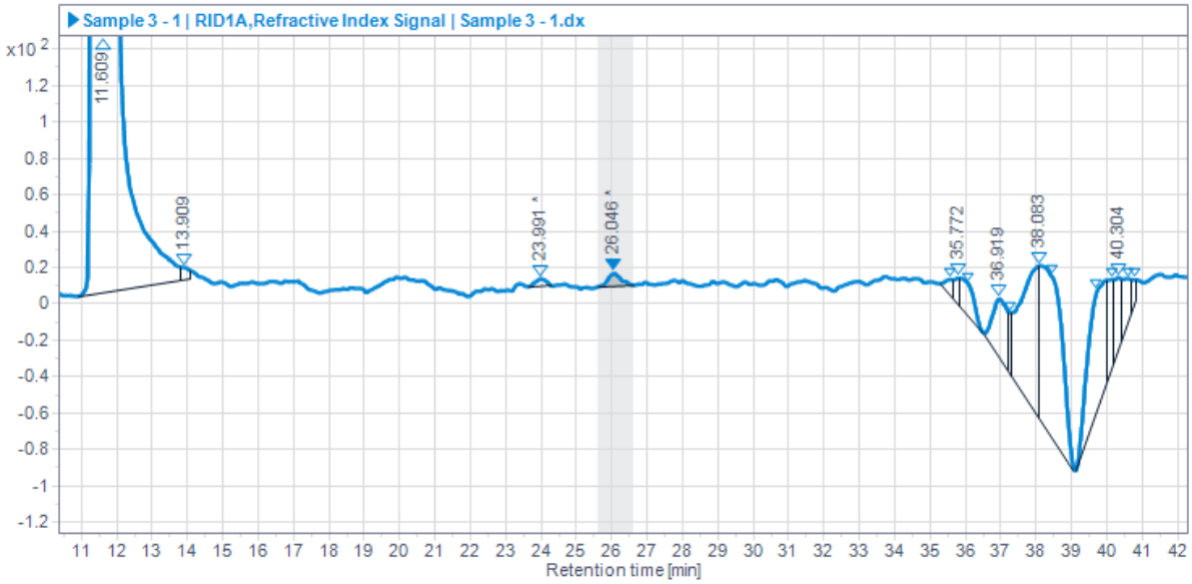

Figure B.2: The HPLC analysis data of the operation tests with reference electrode

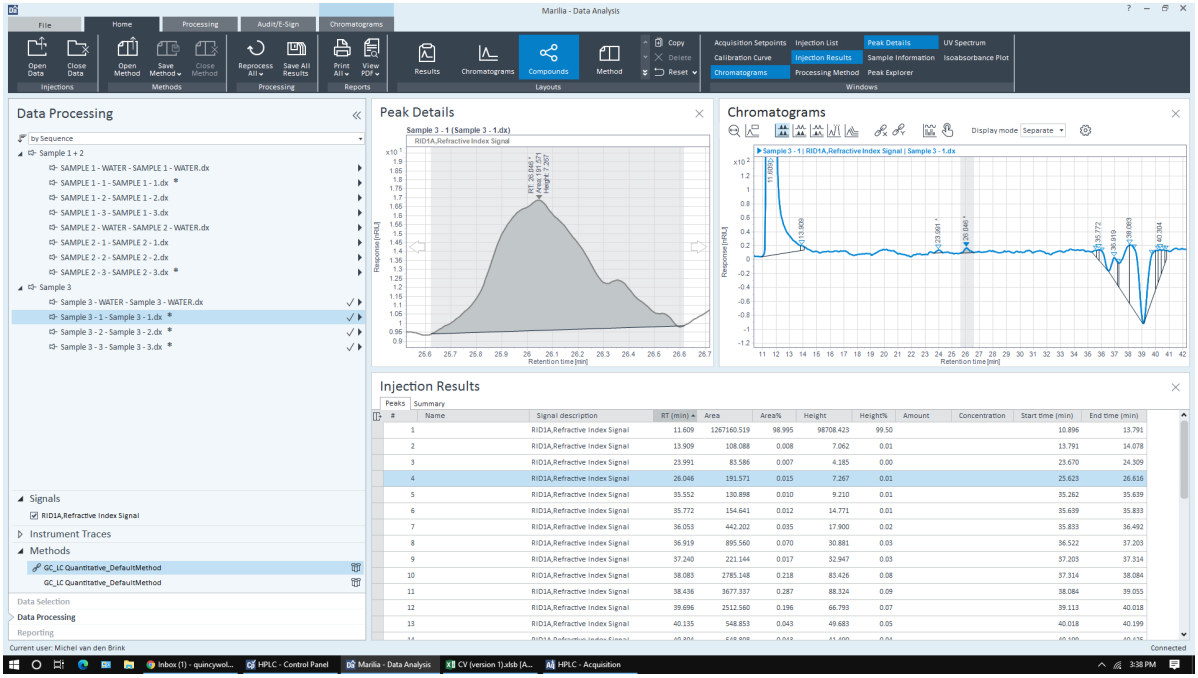

Figure B.3: The screenshot of the HPLC analysis data of the operation tests with reference electrode with additional information

C

Recommendation concepts

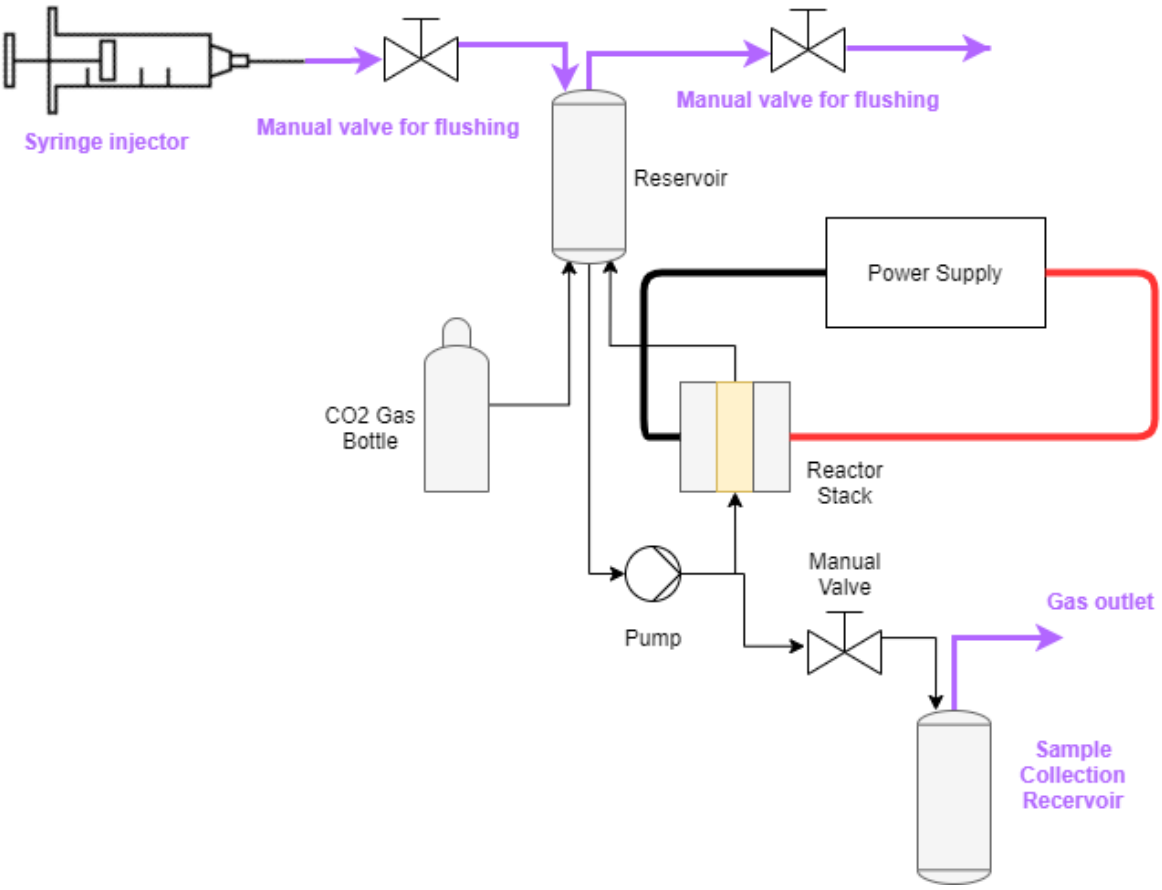

Figure C.1: Concept setup that includes the additional components of the recommendation. Purple lines are added tubes and components with purple description are added components

,

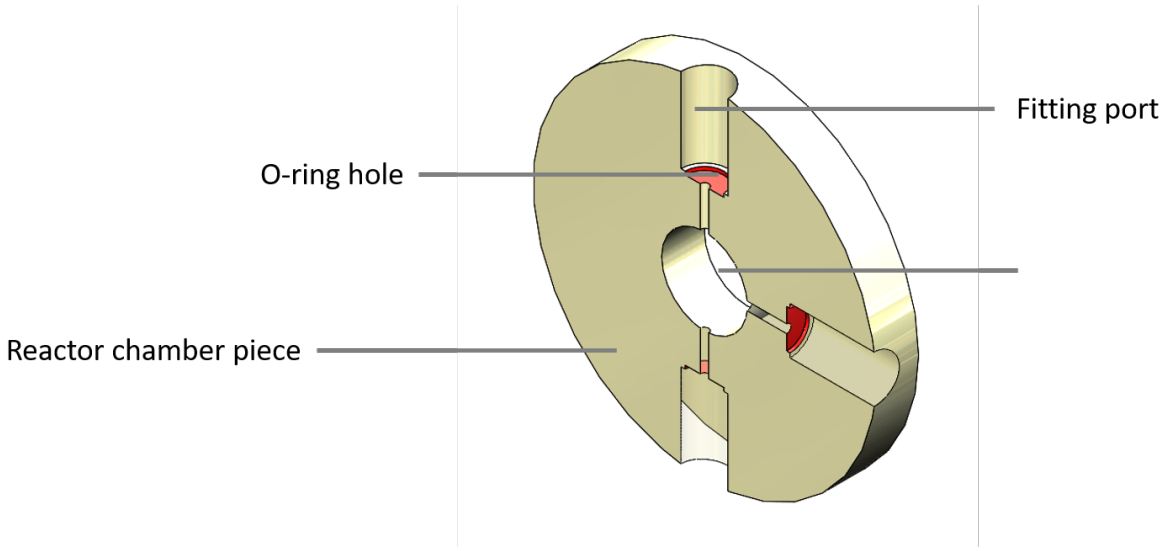

Figure C.2: A concept of a more reliable reactor chamber piece based on the recommendations

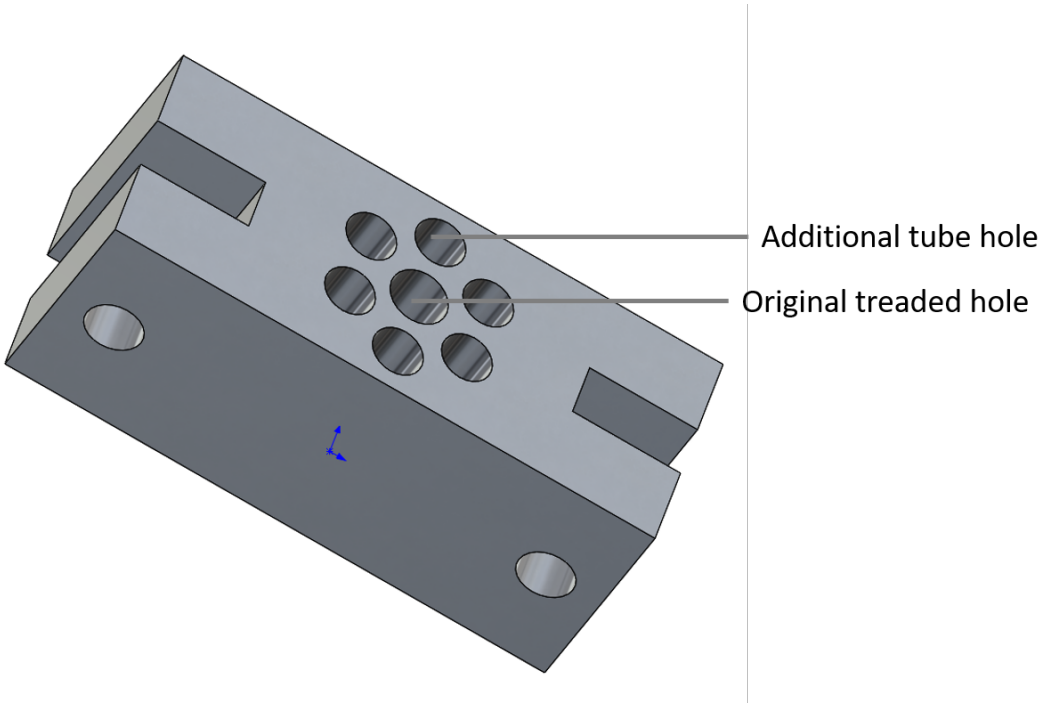

Figure C.3: A concept of a more easy to handle block piece for the reservoir setup based on the recommendations

D

Matlab code used

D.1. Calculating cell efficiency

```
F = 96500;                                  %fardeic constant
I = 0.07;                                   %A
t = 60*45;                                  %s
V = 0.055;                                  %L
max_moles = I*t/(2*F);                      %moles

Concentration_sample = 0.1*10^-3;           %moles/l
Amount_sample        = Concentration_sample*V;  %moles
Efficiency           = Amount_sample/max_moles  %FE
```

D.2. Calculation the pressure drop over the setup cycle

```
%% Window exterminator
clc
close all

%% Pump Function (T23 @5500rpm)

Dp_pump =[0.071230342
0.751156337
1.502312673
2.227567068
3.004625347
3.62627197
4.222016651
4.727104533
5.141535615];

Q_pump =[504.3529412
488.8235294
477.0588235
471.8823529
469.5294118
468.1176471
467.1764706
467.1764706
466.7058824];
plot(Dp_pump,Q_pump)

%% Tubing Functions

```

```
% Flow

Q_electrolyte = [450:520];                    %ml/min
Q_electrolyte = Q_electrolyte.*10^-6./60;     %M3/s

% Electrolyte is water(pure substance)

Rho_electrolyte = 1000;                       %kg/m3
Mu_electrolyte  = 1.00016*10^-3;              %pa/s

% Tube dimensions and other charasteristics

L_tube      = 1;                              %M
D_tube      = 1/16;                           %inch
D_tube      = D_tube*0.0254;                  %M
A_tube      = D_tube^2*pi/4;                  %M2
V_tube      = Q_electrolyte./A_tube;           %m/s
Re_tube     = Rho_electrolyte.*V_tube.*D_tube./Mu_electrolyte;

%Pressure drop tube from figure 19.24 from chemical engineering design

Re      = [3002.043103
4030.458676
5041.858101
5911.255491
6930.568212
7936.332545
9088.107376
9986.551072
19897.80248
29879.52061
40116.35675
50480.3445
58837.53576
69801.57356
79462.43312
90460.93706
99404.42959];

Fr      = [0.006701137
0.006111435
0.005747512
0.005505746
0.005274149
0.005052226
0.004869508
0.004751393
0.003976558
0.003626853
0.003390098
0.003227708
0.003111007
0.002998556
0.002907936
0.002837459
0.002785719];
```

```
86
87 % interpolation, plots and checks
88
89 loglog(Re,Fr)
90 title('Friction factor of a tube')
91 xlabel('Reynold number ')
92 ylabel('Friction factor')
93 ft       = fittype('a +b*log(x)+c/x^2');
94 f        =fit(Re,Fr,ft,'StartPoint',[1 1 1]);
95 figure
96 plot(Re,Fr,'o')
97 hold on
98 plot(f)
99 title('Friction factor of a tube')
100 xlabel('Reynold number ')
101 ylabel('Friction factor')
102 legend({'Data from figure','Fitted function'})
103 Check    = (f(Re(6))-Fr(6))/Fr(6);
104
105 % Pressure drop calculation
106
107 Fr_tube = f(Re_tube);
108 Fr_tube = Fr_tube.';
109 DeltaP_tube = 8.*Fr_tube.*(L_tube./D_tube).*Rho_electrolyte.*V_tube.^2./2;
      %Pa
110 DeltaP_tube = DeltaP_tube.*10^-5; %bar
111
112 % miscellaneous pressure losses from table 20.4 from chemical engineering
      design
113
114 %velocity heads in numbers K of several components
115
116 Head_bend    = 0.8;
117 N_bend       = 4;
118 Head_tank    = 1.5;
119 N_tank       = 2;
120
121 % Total head
122
123 Head         = Head_bend*N_bend + Head_tank*N_tank;
124
125 Head_loss    = V_tube.^2./(2*9.81).*Head;
126 DeltaP_misc = Head_loss.*Rho_electrolyte.*9.81;
127 DeltaP_misc = DeltaP_misc.*10^-5;
128
129 % Total pressure loss
130 Cv           = 0.07;
131 DeltaP_reg   = ((Q_electrolyte*15850.3231)./Cv).^2./14.503773779685869;
                                        %bar
132 DeltaP       = DeltaP_misc+DeltaP_tube+DeltaP_reg;%bar
133 Part_tube    = DeltaP_tube./DeltaP;
134 Part_misc    = (DeltaP_misc+DeltaP_reg)./DeltaP;
135
136 %% Plot results and find the flow
137 Q_electrolyte = [450:520];
138 figure
```

```
plot(DeltaP,Q_electrolyte)
hold on
plot(Dp_pump,Q_pump)
title('Operations lines of the cycle and pump')
xlabel('Presssure drop [Bar]')
ylabel('Volume flow [ml/min]')
legend({'Cycle','Pump'})

Found_Flow = 470; %ml/min found on figure by user
```

D.3. Model of a perfect mixed CO_2 reduction reactor tank

```
%% Mass flows of the tank

close all
clc

%% Dimensions

r = 0.005;                  %m
h = 0.011;                  %m
V = pi*r^2*h;               %m^3
A = pi*r^2;                 %m^2

%% Solubility of gasses in water
% Assuming it doesn't change with increasing concentration of formaldehyde

P = [ 1; 5; 10; 50; 100; 200]; %bar

%CO2 at 303.15

sol_CO2 = [ 0.0286; 0.1442; 0.2809; 1.0811; 1.3611; 1.4889]; %Mol/kg water
plot(P,sol_CO2,'o')
f       =fit(P,sol_CO2,'smoothingspline');
hold on
plot(f)
xlabel('Pressure [bar]')
ylabel('CO2 solubility (mol/kg water) in water')

%O2

sol_O2      = [ 0.001152; 0.006089; 0.01228; 0.059419; 0.11151; 0.19674];
   %Mol/kg water
figure
plot(P,sol_O2,'o')
g           =fit(P,sol_O2,'smoothingspline');
hold on
plot(g)
xlabel('Pressure [bar]')
ylabel('O2 solubility (mol/kg water) in water')

%H2
P2              = [ 1; 5; 25; 50; 100; 200]; %bar
sol_H2          = [ 0.35/25; 0.350/5; 0.350; 0.696; 1.386; 2.720]; %Mol/kg
     water
sol_H2          = sol_H2./1000;
figure
```

```
44 plot(P2,sol_H2,'o')
45 h            =fit(P2,sol_H2,'smoothingspline');
46 hold on
47 plot(h)
48 xlabel('Pressure [bar]')
49 ylabel('H2 solubility (mol/kg water) in water')
50
51 % All together
52
53 figure
54 hold on
55 plot(P,sol_CO2,'o')
56 plot(f)
57 plot(P,sol_O2,'o')
58 plot(g)
59 plot(P2,sol_H2,'o')
60 plot(h)
61 xlabel('Pressure [bar]')
62 ylabel('Solubility (mol/kg water) in water')
63
64 sol_CH4      = (0.0023/0.0043).*sol_O2;
65 i            =fit(P2,sol_CH4,'poly2');
66 figure
67 hold on
68 plot(P,sol_CH4,'o')
69 plot(i)
70 xlabel('Pressure [bar]')
71 ylabel('CH4 Solubility (mol/kg water) in water')
72
73 sol_CO      = (0.0028/0.0043).*sol_O2;
74 j            =fit(P2,sol_CO,'poly2');
75 figure
76 hold on
77 plot(P,sol_CO,'o')
78 plot(i)
79 xlabel('Pressure [bar]')
80 ylabel('CO Solubility (mol/kg water) in water')
81
82
83
84
85 %% Fluid properties
86
87 % Water
88
89 rho_W        = 996;              %kg/m^3 is incompressible
90 m_mass_W     = 0.001801528;      %kg/mol
91
92 % Formaldehyde
93
94 rho_F        = 815;              %kg/m^3 is incompressible
95 m_mass_F     = 0.0030031;        %kg/mol
96
97 % Formic Acid
98
99 rho_Acid     = 1220;             %kg/m3 is incompressible
```

```
100 m_mass_Acid = 0.004603;        %kg/mol
101
102 %CO2
103 P3          = [ 1; 2; 5; 10; 20; 30; 40; 50; 75; 100; 125; 150; 175; 200;
        ]; %bar
104 rho_CO2     = [ 1.7543; 3.5254; 8.9437; 18.352; 38.837; 62.211; 89.759;
        124.02; 661.10; 771.50; 816.35; 846.98; 870.79; 890.50; ];
105 %rho_CO2     = [ 1.7543; 8.9437; 18.352; 124.02; 771.50; 890.50; ]; %kg/m3
        from REFPROP using 'P' as input at 303.15 k
106 m_mass_CO2  = 0.004401; %kg/mol
107 f2          =fit(P3,rho_CO2,'smoothingspline');
108
109 %O2
110
111 rho_O2      = [ 1.2703; 6.3663; 12.769; 65.179; 132.77; 266.31; ]; %kg/m3
        from REFPROP using 'P' as input at 303.15 k
112 m_mass_O2  = 0.0015999; %kg/mol
113 g2          =fit(P,rho_O2,'smoothingspline');
114
115 %H2
116
117 rho_H2      = [ 0.079932; 0.39873; 0.79516; 3.8849; 7.5493; 14.263; ]; %kg/
        m3from REFPROP using 'P' as input at 303.15 k
118 m_mass_H2  = 0.00201588; %kg/mol
119 h2          =fit(P,rho_H2,'smoothingspline');
120
121 figure
122 hold on
123 plot(P3,rho_CO2)
124 plot(P,rho_O2)
125 plot(P,rho_H2)
126 plot(f2)
127 plot(g2)
128 plot(h2)
129 xlabel('Pressure [bar]')
130 ylabel('Density [kg/m3]')
131
132 %% Electrolisys production
133 % Reactrions :
134 % 2H20              -> O2 + 4H+ +4e-
135 % 4H+ + 4e-         -> 2H2
136 % CO2 + 4H+ + 4e-   -> HCHO + H20
137 %2CO2 + 4H+ + 4e-   -> 2HCOOH
138
139 I           = 30000*A;  %A
140 F           = 96500;
141 eta_H2      = 0.011;
142 eta_F       = 0.74;
143 eta_Acid    = 0.15;
144 eta_O2      = eta_H2+eta_F+eta_Acid;
145
146 %% Initial conditions
147 %only water and CO2, but added O2 and H2 for for-loop calculations
148 P_ini           = 20;               %bar
149
150 %Water
```

```
151
152 V_W              = 0.9*V;                %m3
153 Mass_W           = rho_W*V_W;            %kg
154 Moles_W          = Mass_W/m_mass_W;
155
156 % Formaldehyde
157
158 Moles_F          = 0;
159 Mass_F           = Moles_F*m_mass_F;
160 V_F              = Mass_F*rho_F;
161
162 % Formic Acid
163
164 Moles_Acid       = 0;
165 Mass_Acid        = Moles_Acid*m_mass_Acid;
166 V_Acid           = Mass_Acid*rho_Acid;
167
168 %All liquids
169
170 V_liq            = V_W+V_F+V_Acid;
171
172 %CO2
173
174 V_CO2            = V-V_W;                %m3
175 Mass_CO2_gas     = V_CO2*f2(P_ini);      %kg
176 Moles_CO2_gas    = Mass_CO2_gas/m_mass_CO2;
177 Mass_CO2_liq     = f(P_ini)*Mass_W*m_mass_CO2; %kg
178 Moles_CO2_liq    = f(P_ini)*Mass_W;
179 Moles_CO2        = Moles_CO2_gas+Moles_CO2_liq;
180
181 %O2
182
183 Moles_O2         = 0;
184 Moles_O2_liq     = min(Moles_O2,g(P_ini)*Mass_W);
185 Mass_O2_liq      = Moles_O2_liq*m_mass_O2;
186 Moles_O2_gas     = max(Moles_O2-Moles_O2_liq,0);
187 Mass_O2_gas      = Moles_O2_gas*m_mass_O2;
188
189 %H2
190
191 Moles_H2         = 0;
192 Moles_H2_liq     = min(Moles_H2,h(P_ini)*Mass_W);
193 Mass_H2_liq      = Moles_H2_liq*m_mass_H2;
194 Moles_H2_gas     = max(Moles_H2-Moles_H2_liq,0);
195 Mass_H2_gas      = Moles_H2_gas*m_mass_H2;
196
197 %all gasses
198
199 Moles_gas        = Moles_H2_gas+Moles_O2_gas+Moles_CO2_gas;
200
201 %% Simulation
202
203 t = 100; %s
204 t = 1:t;
205
206 %Begin vectors
```

```
207
208 %liquids
209
210 Vec_Moles_W                 = zeros(1,length(t));
211 Vec_Moles_F                 = zeros(1,length(t));
212 Vec_Moles_Acid              = zeros(1,length(t));
213 Vec_V_liq                   = zeros(1,length(t));
214
215 %gasses
216 Vec_Moles_CO2               = zeros(1,length(t));
217 Vec_Moles_CO2_gas           = zeros(1,length(t));
218 Vec_Moles_CO2_liq           = zeros(1,length(t));
219 Vec_Moles_O2                = zeros(1,length(t));
220 Vec_Moles_O2_gas            = zeros(1,length(t));
221 Vec_Moles_O2_liq            = zeros(1,length(t));
222 Vec_Moles_H2                = zeros(1,length(t));
223 Vec_Moles_H2_gas            = zeros(1,length(t));
224 Vec_Moles_H2_liq            = zeros(1,length(t));
225 Vec_Moles_gas               = zeros(1,length(t));
226
227 %pressure
228 Vec_P                       = zeros(1,length(t));
229
230 for i=1:length(t)
231     %Water
232     Moles_W                 = Moles_W+(I*(eta_F-2*eta_O2))/(4*F);
233     Vec_Moles_W(i)          = Moles_W;
234     V_W                     = Moles_W*m_mass_W/rho_W;
235     %Formaldehyde
236     Moles_F                 = Moles_F+(I*eta_F)/(4*F);
237     Vec_Moles_F(i)          = Moles_F;
238     V_F                     = Moles_F*m_mass_F/rho_F;
239     %Formic Acid
240     Moles_Acid              = Moles_Acid+(2*I*eta_Acid)/(4*F);
241     Vec_Moles_Acid(i)       = Moles_Acid;
242     V_Acid                  = Moles_Acid*m_mass_Acid/rho_Acid;
243     %Liquid Volume
244     Vec_V_liq(i)            = V_W+V_F+V_Acid;
245     %CO2
246     Moles_CO2               = Moles_CO2-(I*(eta_F+2*eta_Acid))/(4*F);
247     Vec_Moles_CO2(i)        = Moles_CO2;
248     Moles_CO2_liq           = min(Moles_CO2,f(P_ini)*Mass_W);
249     Vec_Moles_CO2_liq(i)    = Moles_CO2_liq;
250     Moles_CO2_gas           = max(Moles_CO2-Moles_CO2_liq,0);
251     Vec_Moles_CO2_gas(i)    = Moles_CO2_gas;
252     %O2
253     Moles_O2                = Moles_O2+(I*eta_O2)/(4*F);
254     Vec_Moles_O2(i)         = Moles_O2;
255     Moles_O2_liq            = min(Moles_O2,g(P_ini)*Mass_W);
256     Vec_Moles_O2_liq(i)     = Moles_O2_liq;
257     Moles_O2_gas            = max(Moles_O2-Moles_O2_liq,0);
258     Vec_Moles_O2_gas(i)     = Moles_O2_gas;
259     %H2
260     Moles_H2                = Moles_H2+2*(I*eta_H2)/(4*F);
261     Vec_Moles_H2(i)         = Moles_H2;
262     Moles_H2_liq            = min(Moles_H2,h(P_ini)*Mass_W);
```

```
263         Vec_Moles_H2_liq(i)       = Moles_H2_liq;
264         Moles_H2_gas              = max(Moles_H2-Moles_H2_liq,0);
265         Vec_Moles_H2_gas(i)       = Moles_H2_gas;
266         %Total gas
267         Vec_Moles_gas(i)          = Moles_H2_gas+Moles_O2_gas+Moles_CO2_gas;
268         Vec_V_gas(i)              = V-(V_W+V_F+V_Acid);
269         %Pressure
270         Vec_P(i)                  =P_ini*(Vec_Moles_gas(i)/Moles_gas)*(V-V_liq)/
                Vec_V_gas(i);
271
272
273 end
274 %%% Grafieken
275 % close all
276 % plot(Vec_Moles_CO2)
277 % hold on
278 % plot(Vec_Moles_O2)
279 % plot(Vec_Moles_H2)
280 % figure
281 % plot(Vec_P)
```

D.4. Calculation of the force on a bolt as result of pressure in a tank/reactor and potting it against bolt strength standards

```
1  %% To calculate the force in the bolt that will compres the recervoir/
       stack
2  close all
3  clc
4
5  % Tank
6  P        = 50*10^5;          %Pa
7  D_r      = 0.03;             %M
8  A_r      = 1/4*pi*D_r^2;     %m2
9  F        = P*A_r             %N
10 F_s      = 1;                %Safety factor
11 F        = F*F_s             %N
12 D_b      = 0.014;            %M
13 A_b      = 1/4*pi*D_b^2;     %m2
14 Sigma    = F/A_b*10^-6       %Mpa
15
16 %strength klas 8.8
17 M = [3; 4; 5; 6; 7; 8; 10; 12; 14; 16; 18; 20; 22; 24; 27; 30; 33; 36;
       39;];
18 Pf= [2290; 5100; 8230; 11600; 16800; 21200; 33700; 48900; 66700; 91000;
       115000; 147000; 182000; 212000; 275000; 337000; 416000; 490000;
       586000;];
19 plot(M,Pf,'o')
20 hold on
21 plot(M,Pf)
22 plot([0,39],[F,F])
```

D.5. Calculation of the groove dimensions

```
1  %% O-Ring Calculation
2  clear all
3  clc
```

```

% Tube and piston dimensions
D_tube      = 38.1;  % [mm]
D_piston    = 38.05; % [mm]

%O-ring and groove calculations
Squeeze  = 0.16;                % (W_o-W_c)/W_o = squeeze CHOSEN
W_o      = 3.53;                % Thickness O-ring [mm] CHOSEN
W_c      = -1*(Squeeze*W_o-W_o);% Distance groove and tube [mm]
D_ring   = 34.52;               % mm CHOSEN

D_groove = D_tube-2*W_c;

Stretch_min = 0.01; % (D_groove-D_ring)/D_ring = Stretch
Stretch_max = 0.05; % (D_groove-D_ring)/D_ring = Stretch

%  D_groove - D_ring = Stretch * D_ring
%  D_Groove = (1+Stretch) * D_ring

D_ring_max = D_groove/(Stretch_min+1);
D_ring_min = D_groove/(Stretch_max+1);

Fill_groove_min     = 0.6;
Fill_groove_max     = 0.85;
A_oring             = W_o^2*pi/4;                       % mm^2
t_bring             = 3;                                % mm CHOSEN
A_bring             = (D_tube-D_groove)*t_bring;        % mm^2
A_groove_min        = (A_oring+A_bring)/Fill_groove_max; % mm^2
A_groove_max        = (A_oring+A_bring)/Fill_groove_min; % mm^2
T_Groove_min        = A_groove_min/(D_tube-D_groove);   % mm
T_Groove_max        = A_groove_max/(D_tube-D_groove);   % mm

%Results
O_ring       = [ D_ring W_o ]
Backupring   = [ D_groove D_tube t_bring ]
Groove       = [ D_groove D_tube T_Groove_min T_Groove_max ]
```

D.6. Oxidation calculation of formaldehyde

```
%% Oxidation Rate Formaldehyde
clear all
clc

T    = 290; %degrees kelvin
R    = 8.314; %J/(mol K)
C_O2 = 0.059419; %mol/kg water @ 50 bar
%E, activation energy

E1 = 169*10^3; %J/mol
E2 = 43*10^3; %j/mol
E3 = 71*10^3; %j/mol

%A, preexponential factor

A1 = 1.6*10^19; %[(L/mol)^n*(1/min)]
A2 = 3.38*10^5; %[(L/mol)^n*(1/min)]
A3 = 2.57*10^6; %[(L/mol)^n*(1/min)]
```

```
19
20 %n, order with respect to the concentration of oxygen
21
22 n1 = 1.27;
23 n2 = 1.41;
24 n3 = 0.08;
25
26 %k, reaction rate constant
27
28 k1 = A1*exp(-E1/(R*T));
29 k2 = A2*exp(-E2/(R*T));
30 k3 = A3*exp(-E3/(R*T));
31
32 K1 = k1*C_O2^n1;
33 K2 = k2*C_O2^n2;
34 K3 = k3*C_O2^n3;
35
36 %Change in total organic concentration normalized
37 t    = 0
38 DCDT = ((-K1+K2)*(K1-K3))/(K1+K2-K3)*exp(-(K1+K2)*t)+(-K3*K2)/(K1+K2-K3)*
       exp(-K3*t)
39
40 %this is very low and in compliance with literature and estimations
```

D.7. Calculating stress on the 2 plate frames

```
1 %% Stress and moment
2 clear
3 clc
4 close all
5
6 h       = 0.015;          %m
7 b       = 0.013;          %m
8 F       = 4000;           %n
9 L       = 0.0261+h/2;     %m
10 A      = b*h;            %m2
11 I      = (b*h^3)/12;     %m4
12 M      = F*L;            %nm
13 Sigma_a = F/A;           %n/m2
14 Sigma_a = Sigma_a/(10^6);%Mpa
15 Sigma_m = M*(h/2)/I;     %n/m2
16 Sigma_m = Sigma_m/(10^6);%Mpa
```

D.8. Calculating stress in the thick-walled container and application of Tresca

```
1 %% Thickwalled stress
2 clear
3 clc
4 close all
5
6 Pi = 100;       %Bar
7 Pi = Pi*100000;%N/m2
8 Po = 1;         %Bar
9 Po = Po*100000;%N/m2
10 ri = 0.01/2;     %m
```

```
ro = 0.04/2;      %m

r       = [ri:0.00001:ro];
Sigma_t = (Pi.*ri.^2-Po.*ro.^2)./(ro.^2-ri.^2) + (ri.^2.*ro.^2.*(Pi-Po))
    ./(r.^2.*(ro.^2-ri.^2));
Sigma_t = Sigma_t./(10^6);
Sigma_r = (Pi.*ri.^2-Po.*ro.^2)./(ro.^2-ri.^2) - (ri.^2.*ro.^2.*(Pi-Po))
    ./(r.^2.*(ro.^2-ri.^2));
Sigma_r = abs(Sigma_r)./(10^6);
r       = r.*1000;
plot(r,Sigma_t)
hold on
plot(r,Sigma_r)

D_tube      = 0.003175;
D_fitting   = 0.0055;
t           = 0.01;
mul1        = t/(t-D_tube);
mul2        = t/(t-D_fitting);
Multo       = [ones(1,501).*mul1 ones(1,1000).*mul2];
Sigma_t2    = Sigma_t.*Multo;
plot(r,Sigma_t2)
ylabel('Stress [Mpa]')
xlabel('Radius [mm]')
legend('Tangential','Radial','Tangential max')

ri2             = [ri:0.0001:ro-0.002];
Sigma_t3        = (Pi.*ri2.^2-Po.*ro.^2)./(ro.^2-ri2.^2) + (ri2.^2.*ro
    .^2.*(Pi-Po))./(ri2.^2.*(ro.^2-ri2.^2));
Sigma_t3        = Sigma_t3./(10^6).*(Sigma_t2(1)/Sigma_t(1));
figure
hold on
Sigma_r2        = (Pi.*ri2.^2-Po.*ro.^2)./(ro.^2-ri2.^2) - (ri2.^2.*ro
    .^2.*(Pi-Po))./(ri2.^2.*(ro.^2-ri2.^2));
Sigma_r2         = abs(Sigma_r2)./(10^6);
Sigma_axial     = 4000./(pi.*((0.04.^2./4)-(0.01.^2./4)));
Sigma_axial     = Sigma_axial./10^6;

ri2 = ri2.*1000;
plot(ri2,Sigma_t3)
plot(ri2,Sigma_r2)
plot(ri2,Sigma_axial)
plot([5 18],[87 87])
ylabel('Stress [Mpa]')
xlabel('Radius [mm]')
legend('Tangential max','Radial','Axial','Yield Strength PEEK')
xlim([5 18])

s               = [Sigma_t2(1) -Sigma_r(1) -Sigma_axial(1)]
Tresca          = max([abs(s(1)-s(2)),abs(s(1)-s(3)),abs(s(2)-s(3))])
```

E

Pressure Equipment Directive

The pressure equipment directive is applicable to pressure equipment with a maximum allowable pressure greater than 0.5 barg. It is a measure to ensure that pressure equipment is safely used in the European Economic Area.

The first step of the pressure equipment directive is to identify the category of a particular piece of equipment. The two relevant categories are piping and vessel. In the pressure equipment directive, piping is defined as components intended for the transport of fluids when connected together for integration into a pressure system. Vessels are defined as a housing designed and built to contain fluids under pressure.

The second step is to define the state of the fluid. If the fluid has a vapour pressure at the maximum allowable temperature of the equipment of greater than 0.5 bar above normal atmospheric pressure, it is treated as a gas, otherwise it is treated as a liquid. Gasses include liquefied gasses and gasses dissolved under pressure.

The third step in determining the Pressure Equipment Directive category is to decide whether the fluid contained within the equipment is classified as a Group 1 fluid or a Group 2 fluid. In general, a fluid belongs to group 2 if it does not belong to group 1. Group 1 fluids are classified, according to the EC Directive on the classification of dangerous substances as:

- explosive
- extremely flammable
- highly flammable
- flammable (where the maximum allowable temperature is above flashpoint)
- very toxic
- toxic
- oxidizing

The fourth step is to determine the Pressure Equipment Directive category of the component by using the appropriate classification chart based on the previous steps. The charts deemed relevant for this report are displayed below.

Once the category of the equipment piece is determined by using figure E.1 the assessments in the design and production stage can be determined as well. The categories with the corresponding modules are shown in table E.1. The modules with corresponding assessments are displayed in table E.2.

Table E.1: The categories with the corresponding modules

PED Category	Module
SEP	Sound engineering practice
I	A
II	A1, D1, E1
III	B1+D, B1+F, B+E, B+C1, H
IV	B+D, B+F, G, H1

Table E.2: The modules with corresponding assessments

Module	Design Stage Assessment	Production Stage Assessment
SEP	No specific requirements	No specific requirements
A	Technical documentation	Internal production control
A1	Technical documentation	Internal production control with monitoring of the final assessment
B	Type examination	No specific requirements
B1	Design examination	No specific requirements
C1	No specific requirements	Monitoring of final assessment
D	No specific requirements	Quality assurance for production, final inspection and test
D1	Technical documentation	Quality assurance for production, final inspection and test
E	No specific requirements	Quality assurance for final inspection and test
E1	Technical documentation	Quality assurance for final inspection and test
F	No specific requirements	Product verification
G	Unit verification	Unit verification
H	Quality assurance for design	Quality assurance for manufacture, final inspection and test
H1	Quality assurance for design with design examination	Quality assurance for manufacture, final inspection, test and monitoring of final assessment

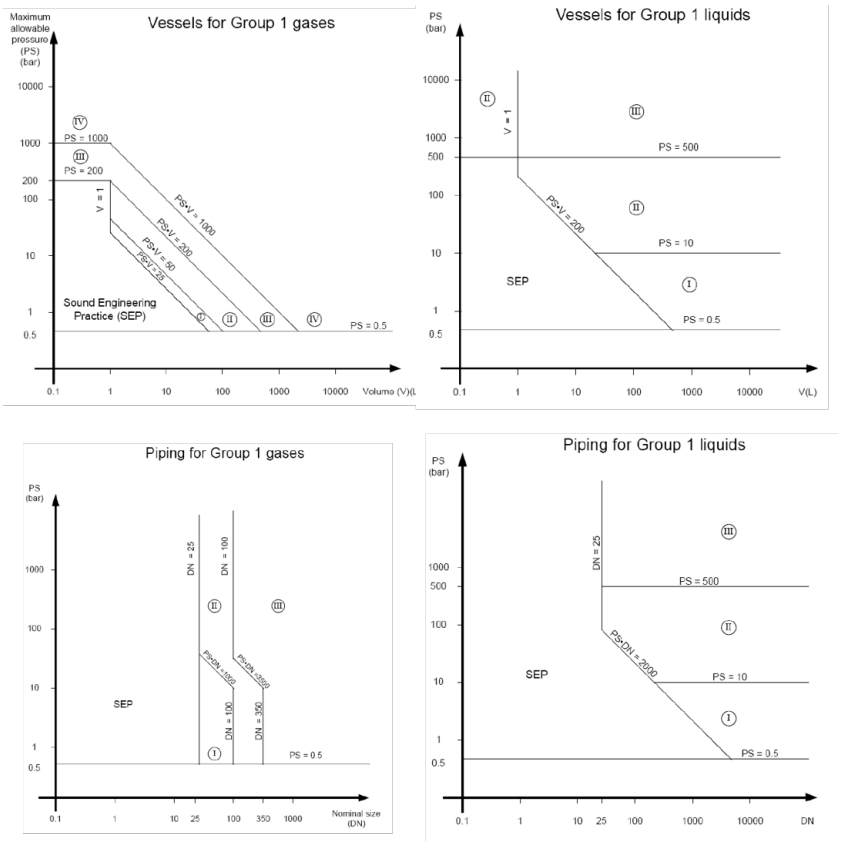

Figure E.1: Different liquid groups with PED categories based on pressure and volume/diameter.

F

Modeling the flow in the inner reactor

As mentioned before the model's validity is very depend on the composition of the electrolyte. It is therefor decided to use the simulation for a global flow behaviour study. Global behaviour of the flow inside the cell can help with predicting and explaining results from experiments done with the reactor stack.

It can be seen that the inside of the reactor has a cylindrical shape with a inlet and outlet at the bottom and top. This is shown in figure F.1. The simulation of the flow inside the reactor is done by using COMSOL.

A 3D model was used, because a 2D models was not representative of the situation. At the inlet of the model a volume flow of 500 ml/min and at the outlet a pressure of 50 bars was set. The Reynolds number in the inlet tube was calculated to be 3413, so solvers for turbulent flow were used.

The grid was chosen to be very coarse. The reasons were that the computing time was reduced drastically, the simulation could not be used for a precise quantitative analysis and finer grids had more chance of not converging.

The result of the simulation can be seen below. It can be seen that most of the flow trough the reactor will simply pass straight trough the reactor. There is some flow that flows over the area that will house the electrodes, but it is relatively little.

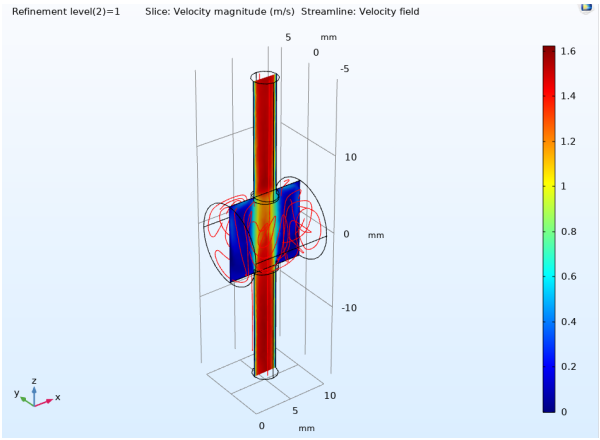

Figure F.1: A simulation using COMSOL of a flow of water trough a cylinder with cylindrical inlet and outlet that will approach the flow inside the CO2 reduction reactor.

It can be expected that the reactor will not very effective in CO2 mass transport with the current characteristics, because of the low velocity at the electrode surface. Another issue that may come up with shorter tests is that the product is not homogeneously distributed over the whole electrolyte. This is likely to be even more so at lower volume flows, but this a acceptable trade of because the design is easy to manufacture and the lack of mixing can be mitigated by pumping the electrolyte through the system longer.

G

Drawings

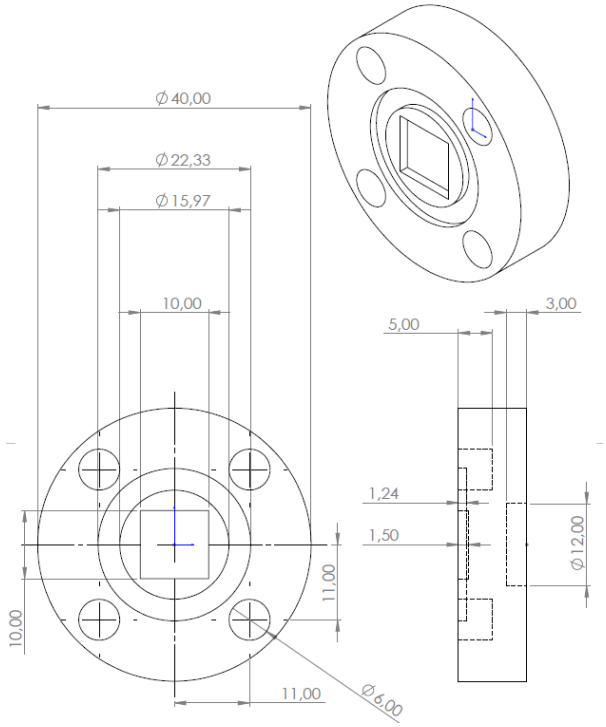

Figure G.1: Technical drawing in mm's of the electrode casing.

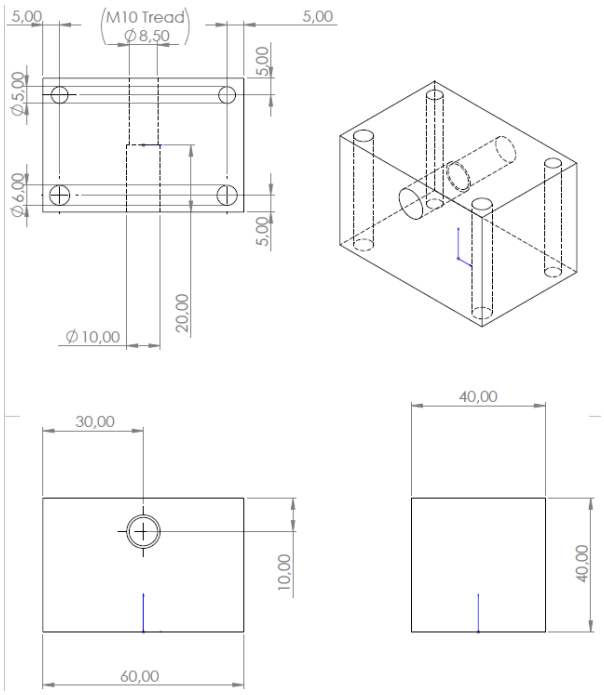

Figure G.2: Technical drawing in mm's of the correction block.

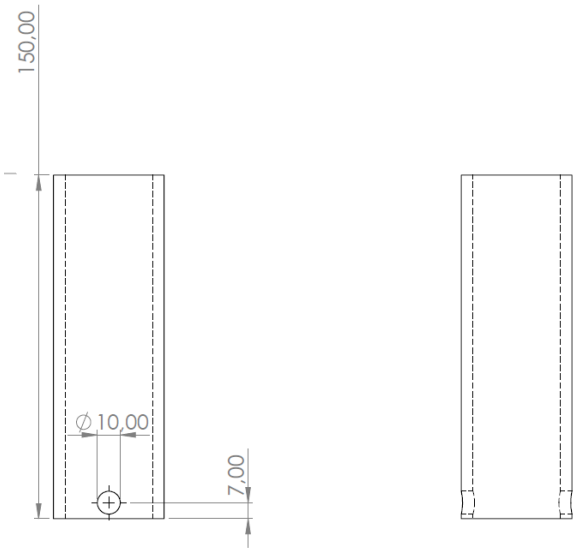

Figure G.3: Technical drawing in mm's of the reservoir cylinder.

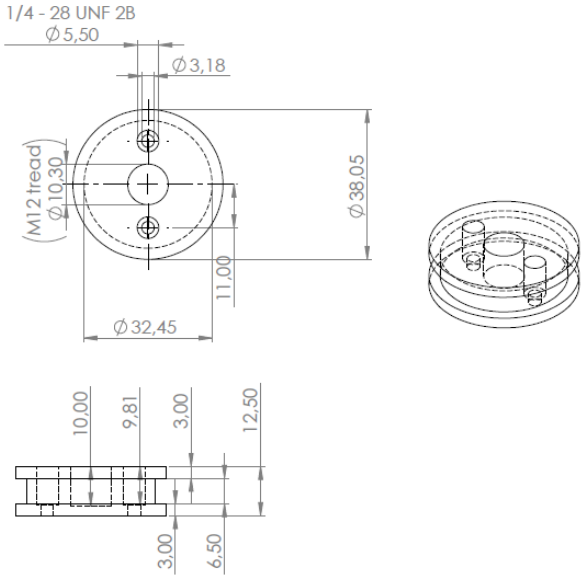

Figure G.4: Technical drawing in mm's of the moving piston.

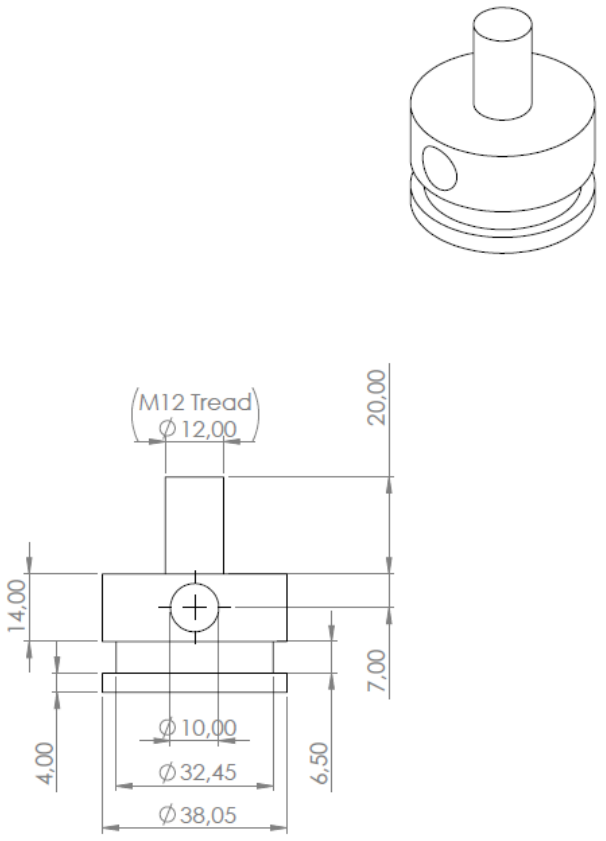

Figure G.5: Technical drawing in mm's of the stationary piston

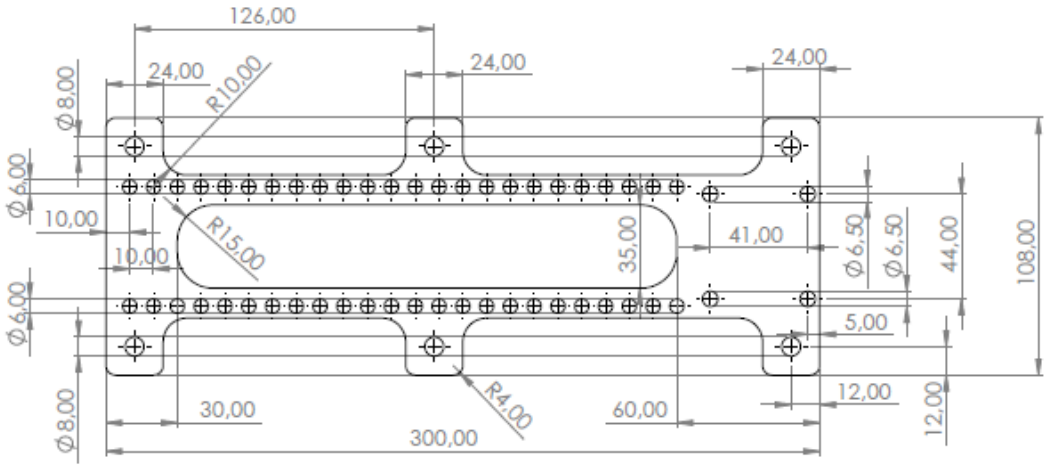

Figure G.6: Technical drawing in mm's of the plate frame of the reactor.

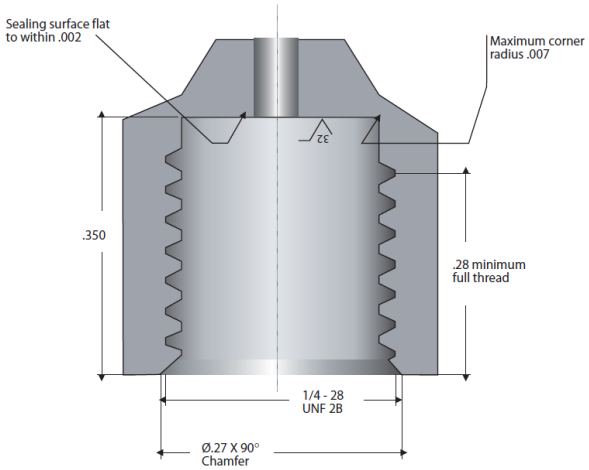

Figure G.7: Technical drawing in inches of the fitting port.

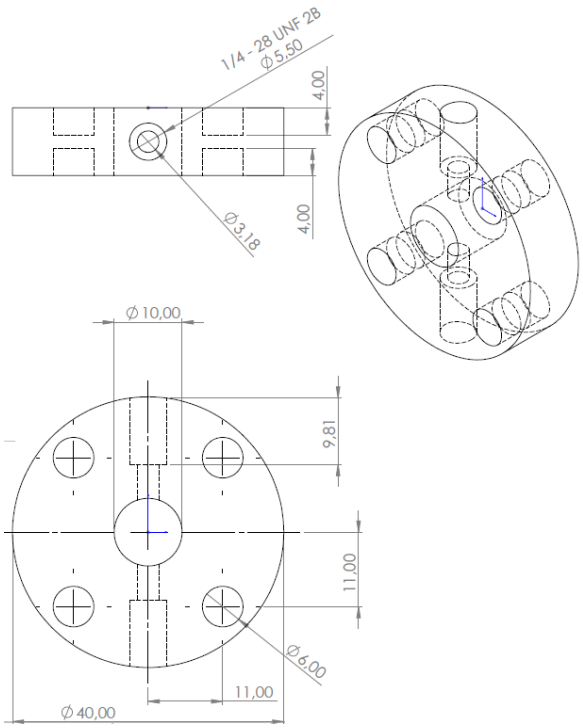

Figure G.8: Technical drawing in mm's of the reactor chamber piece.

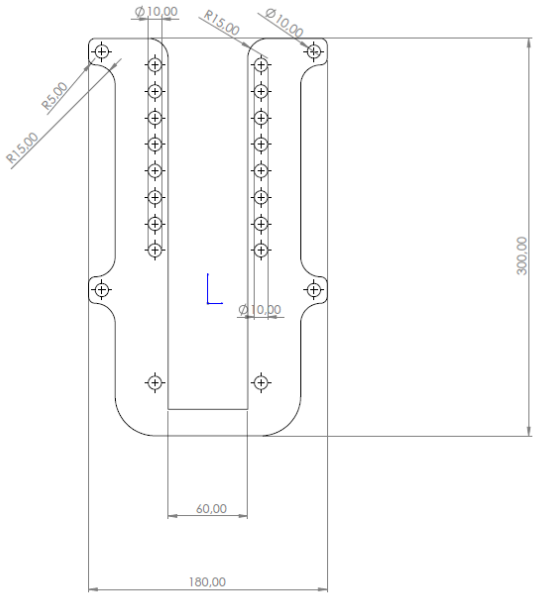

Figure G.9: Technical drawing in mm's of the plate frame of the reservoir.

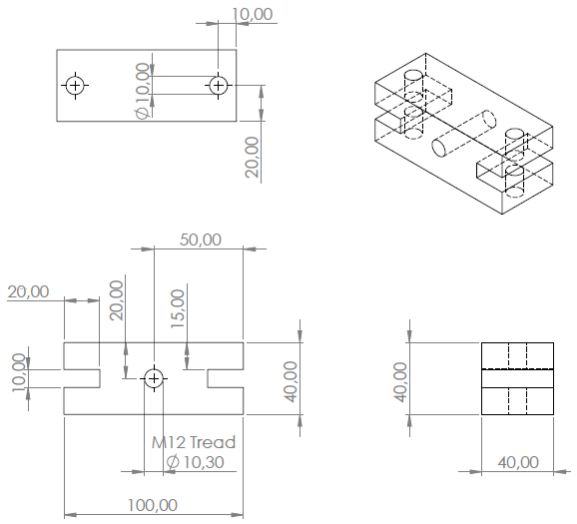

Figure G.10: Technical drawing in mm's of the reservoir frame block.

H

Options of table 4.1

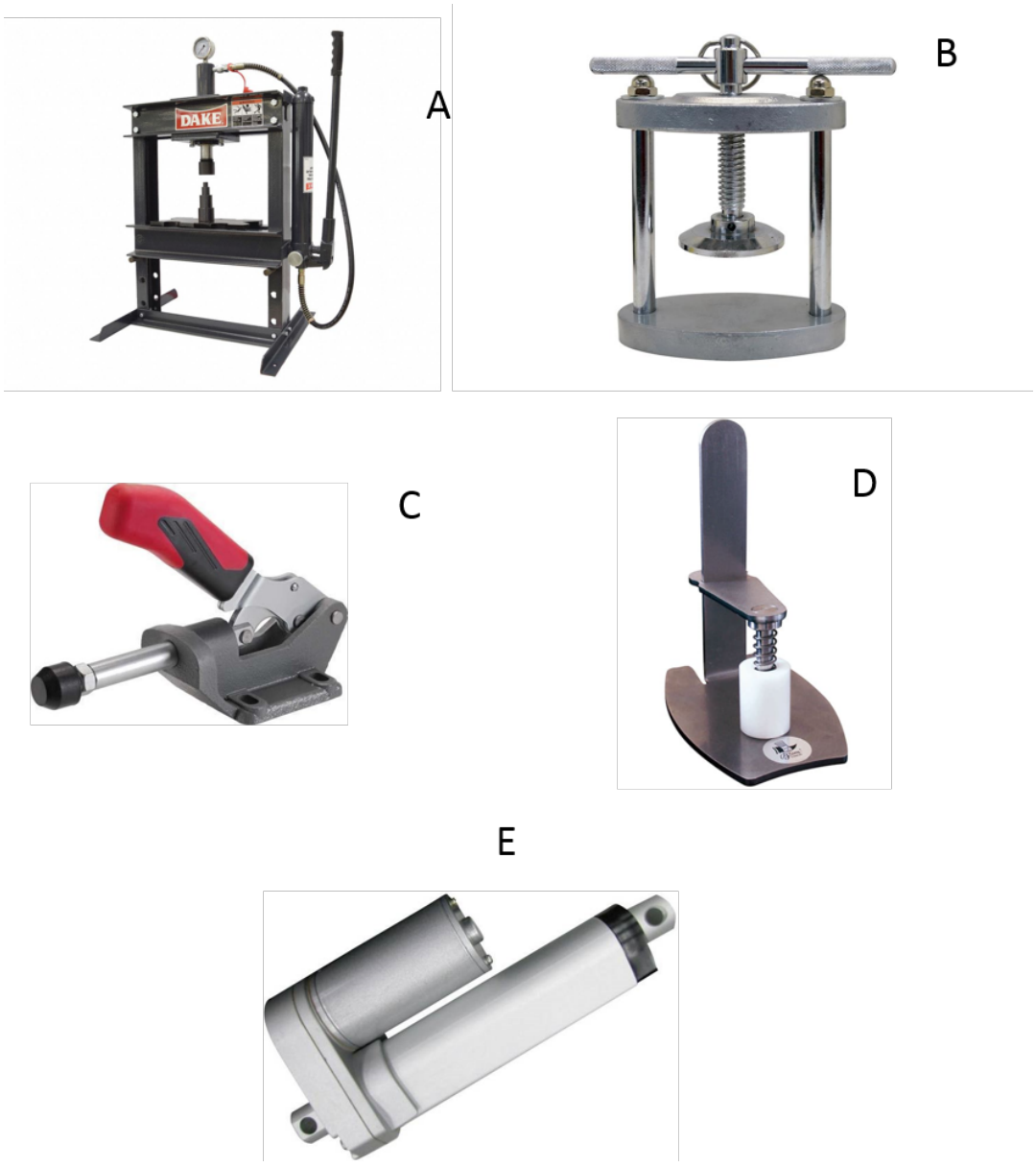

Figure H.1: A - Hydraulic press, B - Screw clamp, C - Clamp, D - Spring clamp, E - Linear actuator

Bibliography

[1] J. Houghton, *Global Warming: The Complete Briefing*. Cambridge University Press, 2009.

[2] T. H. Oliver and M. D. Morecroft, "Interactions between climate change and land use change on biodiversity: attribution problems, risks, and opportunities," *Wiley Interdisciplinary Reviews: Climate Change*, vol. 5, no. 3, pp. 317–335, 2014.

[3] J. Lipponen, "Climate change: a rational choice politics view," *Energy Procedia*, 2017.

[4] A. Demirbas, "Global renewable energy projections," *Energy Sources*, 2009.

[5] I. R. E. Agency, "Renewable power generation costs in 2018," 2019.

[6] G. Aneiros, "Short-term forecast of daily curves of electricity demand and price," *Electrical Power and Energy Systems*, 2016.

[7] Y. Yang, "Battery energy storage system size determination in renewable energy systems: A review," *Renewable and Sustainable Energy Reviews*, 2018.

[8] B. Kumar, J. P. Brian, V. Atla, S. Kumari, K. A. Bertram, R. T. White, and J. M. Spurgeon, "New trends in the development of heterogeneous catalysts for electrochemical co2 reduction," *Catalysis today*, vol. 270, pp. 19–30, 2016.

[9] Q. Lu and F. Jiao, "Electrochemical co2 reduction: Electrocatalyst, reaction mechanism, and process engineering," *Nano Energy*, vol. 29, pp. 439–456, 2016.

[10] M. Bailera, "Power to gas projects review: Lab, pilot and demo plants for storingrenewable energy and co2," *Renewable and Sustainable Energy Reviews*, sep 2017.

[11] M. Jouny, W. Luc, and F. Jiao, "General techno-economic analysis of co2 electrolysis systems," *Industrial & Engineering Chemistry Research*, vol. 57, no. 6, pp. 2165–2177, 2018.

[12] B. Kumar, "New trends in the development of heterogeneous catalysts for electrochemical co2 reduction," *Catalysis Today*, 2016.

[13] M. Todoroki, "Electrochemical reduction of high pressure co 2 at pb, hg and in electrodes in an aqueous khco 3 solution," *Journal of Electroanalytical Chemistry*, 1995.

[14] X. Zhu and Y. Li, "Review of two-dimensional materials for electrochemical co2 reduction from a theoretical perspective," *Wiley Interdisciplinary Reviews: Computational Molecular Science*, vol. 9, no. 6, p. e1416, 2019.

[15] D. R. Kauffman, J. Thakkar, R. Siva, C. Matranga, P. R. Ohodnicki, C. Zeng, and R. Jin, "Efficient electrochemical co2 conversion powered by renewable energy," *Applied material and interfaces*, 2015.

[16] Q. Lu, "Electrochemical co2 reduction: Electrocatalyst, reaction mechanism, and process engineering," *Nano Energy*, 2016.

[17] D. A. Tryk and A. Fujishima, "Electrochemists enlisted in war the carbon dioxide reduction battle," *The Electrochemical Society Interface*, 2001.

[18] M. R. Singh, J. D. Goodpaster, A. Z. Weber, M. Head-Gordon, and A. T. Bell, "Mechanistic insights into electrochemical reduction of co2 over ag using density functional theory and transport models," *Proceedings of the National Academy of Sciences*, vol. 114, no. 42, pp. E8812–E8821, 2017.

[19] K. Hara, “Large current density co2 reduction under high pressure using gas diffusion electrodes,” *The Chemical Society of Japan*, 1996.

[20] F. Proietto, “Electrochemical conversion of co2 to hcooh at tin cathode: Development of a theoretical model and comparison with experimental results,” *ChemElectroChem*, 2019.

[21] K. Hara, “Electrochemical reduction of c02 on a cu electrode under high pressure,” *Journal of the Electrochemical Society*, 1994.

[22] F. Proietto, “Electrochemical conversion of co2 to hcooh at tin cathode in a pressurized undivided filter-press cell,” *Electrochimica Acta*, 2018.

[23] M. Mench, *Fuel cell engines*. John Wiley and Sons, 2008.

[24] A. links open overlay panelMyung JunKim, “Accelerating electrochemistry with metal nanowires,” *Current Opinion in Electrochemistry*, vol. Volume 16, pp. Pages 19–27, aug 2019.

[25] B. Łosiewicz, G. Dercz, and M. Popczyk, “Electrode materials,” in *Solid State Phenomena*, vol. 228, pp. 3–15, Trans Tech Publ, 2015.

[26] W. Zhang, “Progress and perspective of electrocatalytic co2 reduction for renewable carbonaceous fuels and chemicals,” *Renewable Fuels*, 2017.

[27] C. H. Lee and M. W. Kanan, “Controlling h+ vs co2 reduction selectivity on pb electrodes,” *Acs Catalysis*, vol. 5, no. 1, pp. 465–469, 2015.

[28] R. L. Borup, J. R. Davey, F. H. Garzon, D. L. Wood, and M. A. Inbody, “Pem fuel cell electrocatalyst durability measurements,” *Journal of Power Sources*, vol. 163, no. 1, pp. 76–81, 2006.

[29] T. Burdyny and W. A. Smith, “Co 2 reduction on gas-diffusion electrodes and why catalytic performance must be assessed at commercially-relevant conditions,” *Energy & Environmental Science*, vol. 12, no. 5, pp. 1442–1453, 2019.

[30] B. Wallen and G. Wranglen, “Influence of ph and sulphate content of the solution on the corrosion of graphite anodes in alkali chloride electrolysis,” *Electrochimica Acta*, vol. 10, no. 1, pp. 43–48, 1965.

[31] J. Brauns and T. Turek, “Alkaline water electrolysis powered by renewable energy: A review,” *Processes*, vol. 8, no. 2, p. 248, 2020.

[32] H. Vogt, “Superposition of microconvective and macroconvective mass transfer at gas-evolving electrodes—a theoretical attempt,” *Electrochimica acta*, vol. 32, no. 4, pp. 633–636, 1987.

[33] R. Phillips and C. W. Dunnill, “Zero gap alkaline electrolysis cell design for renewable energy storage as hydrogen gas,” *RSC advances*, vol. 6, no. 102, pp. 100643–100651, 2016.

[34] R. Cameron, “Effects of on-board hho and water injection in a diesel generator,” *University of Southern Queensland*, 2012.

[35] J. Cheng, C. Wang, and S. Zhang, “Methods to determine the mine gas explosibility–an overview,” *Journal of Loss Prevention in the Process Industries*, vol. 25, no. 3, pp. 425–435, 2012.

[36] O. G. Sánchez, Y. Y. Birdja, M. Bulut, J. Vaes, T. Breugelmans, and D. Pant, “Recent advances in industrial co2 electroreduction,” *Current Opinion in Green and Sustainable Chemistry*, vol. 16, pp. 47–56, 2019.

[37] V. S. K. Yadav, “Synthesis of pb2o electrocatalyst and its application in the electrochemical reduction of co2 to hcooh in various electrolytes,” *RSC Advances*, 2015.

[38] Emerson, *Conductance Data For Commonly Used Chemicals*, dec 2010.

[39] M. JITARU, “Electrochemical reduction of carbon dioxide on ¯at metallic cathodes,” *JOURNAL OF APPLIED ELECTROCHEMISTRY*, 1997.

[40] J.-P. Jones, “Electrochemical co2 reduction: Recent advances and current trends,” *Israel Journal of Chemistry*, 2014.

[41] M. Todoroki, K. Hara, A. Kudo, and T. Sakata, “Electrochemical reduction of high pressure co2 at pb, hg and in electrodes in an aqueous khco3 solution,” *Journal of Electroanalytical Chemistry*, vol. 394, no. 1-2, pp. 199–203, 1995.

[42] S. Ikeda, T. Takagi, and K. Ito, “Selective formation of formic acid, oxalic acid, and carbon monoxide by electrochemical reduction of carbon dioxide,” *Bulletin of the Chemical Society of Japan*, vol. 60, no. 7, pp. 2517–2522, 1987.

[43] K. Hara, A. Kudo, and T. Sakata, “Electrochemical reduction of carbon dioxide under high pressure on various electrodes in an aqueous electrolyte,” *Journal of Electroanalytical Chemistry*, vol. 391, no. 1-2, pp. 141–147, 1995.

[44] S. Kaneco, K. Iiba, H. Katsumata, T. Suzuki, and K. Ohta, “Electrochemical reduction of high pressure co2 at a cu electrode in cold methanol,” *Electrochimica Acta*, vol. 51, no. 23, pp. 4880–4885, 2006.

[45] K. Hara and T. Sakata, “Large current density co2 reduction under high pressure using gas diffusion electrodes,” *Bulletin of the chemical Society of Japan*, vol. 70, no. 3, pp. 571–576, 1997.

[46] B. A. Rosen, A. Salehi-Khojin, M. R. Thorson, W. Zhu, D. T. Whipple, P. J. Kenis, and R. I. Masel, “Ionic liquid–mediated selective conversion of co2 to co at low overpotentials,” *Science*, vol. 334, no. 6056, pp. 643–644, 2011.

[47] D. Canfield and K. Frese Jr, “Reduction of carbon dioxide to methanol on n-and p-gaas and p-inp. effect of crystal face, electrolyte and current density,” *Journal of the Electrochemical Society*, vol. 130, no. 8, pp. 1772–1773, 1983.

[48] K. Hirota, D. A. Tryk, T. Yamamoto, K. Hashimoto, M. Okawa, and A. Fujishima, “Photoelectrochemical reduction of co2 in a high-pressure co2+ methanol medium at p-type semiconductor electrodes,” *The Journal of Physical Chemistry B*, vol. 102, no. 49, pp. 9834–9843, 1998.

[49] R. Renaud and R. LeRoy, “Separator materials for use in alkaline water electrolysers,” *International Journal of Hydrogen Energy*, vol. 7, no. 2, pp. 155–166, 1982.

[50] M. Ramdin, “High pressure electrochemical reduction of co2 to formic acid/ formate: A comparison between bipolar membranes and cation exchange membranes,” *Industrial & Engineering Chemistry Research*, 2019.

[51] K. Hara, “Electrochemical reduction of carbon dioxide under high pressure on various electrodes in an aqueous electrolyte,” *Journal of Electroanalytical Chemistry*, 1995.

[52] G. Zhao, “Electrochemical reduction of supercritical carbon dioxide in ionic liquid 1-n-butyl-3-methylimidazolium hexafluorophosphate,” *J. of Supercritical Fluids*, 2004.

[53] F. Köleli, “Reduction of co2 under high pressure and high temperature on pb-granule electrodes in a fixed-bed reactor in aqueous medium,” *Applied Catalysis A: General*, 2004.

[54] R. Aydin, “Electrochemical reduction of co2 on a polyaniline electrode under ambient conditions and at high pressure in methanol,” *Journal of Electroanalytical Chemistry*, 2002.

[55] S. Kaneco, “Electrochemical reduction of high pressure co2 at a cu electrode in cold methanol,” *Electrochimica Acta*, 2006.

[56] F. Proietto, “Electrochemical conversion of co2 to hcooh at tin cathode in a pressurized undivided filter-press cell,” *Electrochimica Acta*, 2018.

[57] S. Ma, M. Sadakiyo, M. Heima, R. Luo, R. T. Haasch, J. I. Gold, M. Yamauchi, and P. J. Kenis, “Electroreduction of carbon dioxide to hydrocarbons using bimetallic cu–pd catalysts with different mixing patterns,” *Journal of the American Chemical Society*, vol. 139, no. 1, pp. 47–50, 2017.

[58] S. Ma, M. Sadakiyo, R. Luo, M. Heima, M. Yamauchi, and P. J. Kenis, “One-step electrosynthesis of ethylene and ethanol from co2 in an alkaline electrolyzer,” *Journal of Power Sources*, vol. 301, pp. 219–228, 2016.

[59] D. Pletcher, “The cathodic reduction of carbon dioxide—what can it realistically achieve? a mini review,” *Electrochemistry Communications*, vol. 61, pp. 97–101, 2015.

[60] S. Ma, P. J. Kenis, *et al.*, “Electrochemical conversion of co2 to useful chemicals: current status, remaining challenges, and future opportunities,” *Current Opinion in Chemical Engineering*, vol. 2, no. 2, pp. 191–199, 2013.

[61] T. Saeki, K. Hashimoto, A. Fujishima, N. Kimura, and K. Omata, “Electrochemical reduction of co2 with high current density in a co2-methanol medium,” *The Journal of Physical Chemistry*, vol. 99, no. 20, pp. 8440–8446, 1995.

[62] T. Saeki, K. Hashimoto, N. Kimura, K. Omata, and A. Fujishima, “Electrochemical reduction of co2 with high current density in a co2+ methanol medium at various metal electrodes,” *Journal of Electroanalytical Chemistry*, vol. 404, no. 2, pp. 299–302, 1996.

[63] K. Nakata, T. Ozaki, C. Terashima, A. Fujishima, and Y. Einaga, “High-yield electrochemical production of formaldehyde from co2 and seawater,” *Angewandte Chemie*, 2014.

[64] M. Albert, B. C. Garcıa, C. Kreiter, and G. M. ´, “Vapor-liquid and chemical equilibria of formaldehyde-water mixtures,” *AIChE Journal*, 1993.

[65] M. Albert, B. C. Garcıa, C. Kuhnert, R. Peschla, and G. Maurer, “Vapor–liquid equilibrium of aqueous solutionsof formaldehyde and methanol,” *AIChE Journal*, 2000.

[66] T. Geissman, “The c annizzaro reaction,” *Organic reactions*, vol. 2, pp. 94–113, 2004.

[67] R. Martin, “The mechanism of the cannizzaro reaction of formaldehyde,” *Australian Journal of Chemistry*, vol. 7, no. 4, pp. 335–347, 1954.

[68] A. M. Silva, R. M. Quinta-Ferreira, and J. Levec, “Catalytic and noncatalytic wet oxidation of formaldehyde. a novel kinetic model,” *Industrial & engineering chemistry research*, vol. 42, no. 21, pp. 5099–5108, 2003.

[69] H. Hidaka, N. Watanabe, T. Shiraki, A. Nagaoka, and A. Kouchi, “Conversion of h2co to ch3oh by reactions of cold atomic hydrogen on ice surfaces below 20 k,” *The Astrophysical Journal*, 2004.

[70] H. Hasse and G. Maurer, “Vapor-liquid equilibrium of formaldehyde-containing mixtures at temperatures below 320 k,” *Fluid Phase Equilibria,*, 1991.

[71] R. E. Zeebe and D. Wolf-Gladrow, *CO2 in seawater: equilibrium, kinetics, isotopes*. Gulf Professional Publishing, 2001.

[72] Z. Duana, “An improved model calculating co2 solubility in pure water and aqueous nacl solutions from 273 to 533 k and from 0 to 2000 bar,” *Chemical Geology*, 2003.

[73] U. J. JÁUREGUI-HAZA, “Solubility of hydrogen and carbon monoxide in water and some organic solvents,” *Latin American Applied Research*, 2004.

[74] M. Geng, “Prediction of oxygen solubility in pure water and brines up to high temperatures and pressures,” *Geochimica et Cosmochimica Acta*, 2010.

[75] I. R. Krichevsky, “Thermodynamical calculations of solubilities of nitrogen and hydrogen in water at high pressures,” *Journal of the American Chemical Society*, 1935.

[76] O. L. Culberson, “The solubility of methane in water at pressures to 10,000 psia,” *PHASE EQUILIBRIA IN HYDROCARBON-WATER SYSTEMS*, 1951.

[77] J. E. McMurry, *Organic Chemistry: With Biological Applications*. Cengage Learning, 2010.

[78] L. M. Harwood, “Introduction to organic spectroscopy,” *Oxford University Press*, 1996.

[79] J. H. Gross, *Mass spectrometry: a textbook*. Springer Science & Business Media, 2006.

[80] NewDealSeals, *The World’s Best O-Ring Handbook*.

[81] ERIKS, *Engineering basis: De gids voor O-ringen*.

[82] M. F. Ashby, H. Shercliff, and D. Cebon, *Materials: engineering, science, processing and design*. Butterworth-Heinemann, 2018.

[83] M.-Y. Lee, K. T. Park, W. Lee, H. Lim, Y. Kwon, and S. Kang, “Current achievements and the future direction of electrochemical co2 reduction: A short review,” *Critical Reviews in Environmental Science and Technology*, vol. 50, no. 8, pp. 769–815, 2020.